January 2018

Improving Aav Transduction Efficiency In Retinal Bipolar Cells For Optogenetic Vision Restoration

Shengjie Cui
Wayne State University, shengjiecui@gmail.com

IMPROVING AAV TRANSDUCTION EFFICIENCY IN RETINAL BIPOLAR CELLS FOR OPTOGENETIC VISION RESTORATION

by

SHENGJIE CUI

DISSERTATION

Submitted to the Graduate School

of Wayne State University,

Detroit, Michigan

in partial fulfillment of the requirements

for the degree of

DOCTOR OF PHILOSOPHY

YEAR: 2018

MAJOR: ANATOMY AND CELL BIOLOGY

Approved By:

_____

Advisor Date

_____

_____

_____

_____

DEDICATION

This work is dedicated to my family and friends who give me selfless support and encouragement. The special dedication goes to my dad Jianling Cui, who inspired me to start my PhD journey, thank you for always standing behind me whenever I had difficulties. To my mom Yanjing Liu, thank you for your unconditional love and encouragement. To my close friend, Xinxin Shi, thank you for your company and support. I owe my deepest gratitude to you; I would not be able to achieve my goal without you.

ACKNOWLEDGMENTS

First and most important, I would like to thank my advisor, Dr. Zhuo-Hua Pan. Thank you for teaching me everything to become a scientist, from critical thinking and experiment design, to presentation and writing skills. You are always open and supportive on new ideas; I truly thank you for allowing me to try different things and giving me time to learn from mistakes. Without your guidance and support, I would never be able to have confidence in doing research independently in the future.

I would like to thank my committee members, Dr. Shunbin Xu, Dr. Rodney Braun, and Dr. Daoqi Zhang, for their patience, valuable suggestions, and continual encouragement in my research.

I would like to thank the graduate program director of Anatomy and Cell Biology, Dr. Susmit Suvas, who has always been nice and supportive.

I would like to thank my colleagues and friends, especially Dr. Qi Lu and Tushar Ganjawala. Dr. Qi Lu, thank you for taking so much time training me virus injection, eye dissection, immunostaining, microscopy imaging techniques, and data analysis, and thank you for always answering my questions patiently, no matter how trivial they are. Tushar Ganjawala, thank you for teaching me the molecular biology techniques step by step and helping me out when I was trying new experiments.

I would like to thank Ronald P. Barrett for helping me with the slit lamp imaging, and training me the cryosectioning, confocal microscopy, and optical coherence tomography.

I also would like to thank Selina Hall, LaTonia Jointer, and Roselle Cooper for providing assistance related my research and graduate studies.

I enjoyed all the time working with you. I would cherish what I have experienced with you forever.

TABLE OF CONTENTS

LIST OF TABLES

LIST OF FIGURES

LIST OF ABBREVIATIONS

AAV	Adeno-associated virus
AMD	Age-related macular degeneration
ANOVA	Analysis of variance
As_2O_3	Arsenic trioxide
Chop2	Channelopsin-2
ChR2	Channelrhodopsin-2
CAG	CMV early enhancer/chicken β actin
CMV	Cytomegalovirus
DAPI	4',6-diamidino-2-phenylindole
dsDNA	Double-stranded DNA
EGFR-PTK	Epidermal growth factor receptor protein tyrosine kinase
FDA	Food and Drug Administration
FGFR1	Fibroblast growth factor receptor 1
FKBP52	FK506-binding protein 52
GCL	Ganglion cell layer
GFP	Green fluorescent protein
hGRK1	Human rhodopsin kinase promoter
HSP90	Heat-shock protein 90
HSPG	Heparin sulfate proteoglycans
IACUC	Institutional Animal Care and Use Committee
ILM	Inner limiting membrane
INL	Inner nuclear layer

IPL	Inner plexiform layer
IRE	Iron regulatory elements
IRP	Iron regulatory proteins
ITR	Inverted terminal repeat
LCA	Leber Congenital Amaurosis
mGluR6	Metabotropic glutamate receptor 6
MTOC	Microtubule-organizing center
NpHR	Halorhodopsin from Natronomonas pharaonic
ONL	Outer nuclear layer;
OPL	Outer plexiform layer;
OS/IS	Outer and inner segments of rods and cones
PB	Phosphate buffer
PKC	Protein kinase C
PP5	Protein phosphatase 5
rAAV	Recombinant adeno-associated virus
RBC	Retinal bipolar cells
RGC	Retinal ganglion cells
ROS	Reactive oxygen species
RP	Retinitis pigmentosa
RPE	Retinal pigment epithelium
RT	Room temperature
scAAV	Self-complementary adeno-associated virus
SD	Standard deviation

ssDNA	Single-stranded DNA
TC-PTP	T-cell protein tyrosine phosphatase

CHAPTER 1: BACKGROUND

1.1 Retinal degenerative diseases

Retinal degenerative diseases are caused by progressive death of the photoreceptor cells, which can lead to vision impairment and even blindness in millions of people. Age-related macular degeneration (AMD) and retinitis pigmentosa (RP) are two leading retinal degenerative diseases. AMD often affects people over 50 years of age and leads to a central field vision loss. The advanced AMD is classified as non-neovascular and neovascular AMD (Jager, 2008). In the US, approximately 13.4% of people over 60 years old have AMD (Parmeggiani et al., 2013) and the 15-year cumulative incidence of late AMD is 8% among AMD patients over 75 years old (Casaroli-Marano et al., 2014). RP is an inherited ocular disease; more than 2 million people are affected in the world, with a prevalence of 1 in 3500-5000 people (Anasagasti et al., 2012). More than 65 genes have been found to be involved in RP (Anasagasti et al., 2012); the onset age of RP patients can range from infancy to late middle age. Typically, rod photoreceptor cells are first affected, resulting in night blindness and peripheral vision loss. As the disease progresses, cone photoreceptor cells are also impaired; consequently patients will have decreased central vision, visual acuity and day vision. In addition, the retinal pigment epithelium (RPE) may also get involved (Phelan and Bok, 2000).

At present, there is no cure for retinal degenerative diseases, yet several vision restoring strategies have been pursued over the past decades. For early stages of retinal degeneration, when all cell types are still alive, gene replacement therapy is recommended. If photoreceptors are already degenerated as in late stages, optogenetic approaches, electronic implants, and stem cell approaches are alternative therapies

currently under development (Ong and da Cruz, 2012; Sahel and Roska, 2013; Stingl and Zrenner, 2013).

1.2 Developing therapies

Gene replacement therapy

Gene therapy has been used to potentially treat recessive hereditary diseases that result from gene mutations in retinal cells. One successful example is the treatment of Leber Congenital Amaurosis (LCA). LCA is an autosomal recessive eye disease that affects approximately 1 in 81,000 of the population (Stone, 2007). Mutation of the RPE65 gene comprises 16% of all LCA cases, which are categorized as type 2 LCA (Morimura et al., 1998). In 2005, Acland et al. restored visual function in LCA dog models by injecting adeno-associated virus 2 (AAV2) vectors carrying RPE65 cDNA. More excitingly, gene therapy trials have also been done on RPE65 deficient patients who were reported to experience a functional improvement in vision (Cideciyan et al., 2008; James W.B. Bainbridge, 2008). Nevertheless, there are several limitations of gene replacement therapy. One concern it requires the presence of viable photoreceptor cells (Scholl et al., 2016). Another concern is that hereditary retinal diseases such as RP are caused by hundreds of mutated genes, while mutations in 30%-35% of RP patients have not been identified to date (Petrs-Silva and Linden, 2013). Moreover, the loading vectors such as AAV, has only a limited capability of ~4.7 kb for transgenes (Sahel and Roska, 2013).

Electronic devices

An electronic method to restore visual function is to put light dependent electric implants in the eye to stimulate the inner retinal layer, substituting for the light sensory function of the degenerated photoreceptor layer. The device usually contains an external

camera and series of stimulating electrodes, and can be fixed epiretinaly, subretinaly, or suprachoroidaly. However, a major limitation lies in converting the electronic image received from the camera into effective electrode stimulations and thus neurological signals. The compatibility of the electrode device and the human eye is another concern (Stingl and Zrenner, 2013).

Stem cell transplantation

Owing to their multipotent capability, stem cells can differentiate into any cells to replace the cell type that has been damaged. In addition, stem cells also secrete neurotrophic factors to support the growth of the neurons. At present human embryonic stem cells have been approved by U.S.FDA to apply in clinical trails for retinal pigment epithelial (RPE) cell development. RPE subretinal transplant in RCS rats has been proved to survive over 220 days (Lu et al., 2009). However, there is a potential risk that the stem cell proliferation could become uncontrollable and a tumor could develop. Immunorejection of heterogenic stem cell transplant can also be a problem (Ong and da Cruz, 2012). The biggest challenge in stem cell transplantation in vision restoration is the synapse connectivity between the transplanted neurons and the local ones (Osakada and Takahashi, 2015).

Optogenetic approach

The optogenetic approach is to genetically target light sensors to retinal cells and make them responsive to light, thus replacing the function of the degenerated photoreceptor cells (Bi et al., 2006). Our lab focuses on this approach for vision restoration, and it is also the focus of my project.

1.3 Optogenetic approaches

1.3.1 Optogenetic tools

One of the most promising optogenetic tools is channelrhodopsin-2 (ChR2), which was found in green algae Chlamydomonas reinhardtii and is formed by channelopsin-2 (Chop2) and a retinal chromophore (Nagel et al., 2003). The ChR2 is a light activated cation channel; upon light stimulation, the channel opens and leads to depolarization of the cell membranes (Bi et al., 2006; Boyden et al., 2005). Another optogenetic tool is the halorhodopsin from the archea Natronomonas pharaonis (NpHR) (Lanyi, 1986); it is a light driven inward chloride pump that can lead to cell membrane hyperpolarization upon light activation (Boyden et al., 2005; Zhang et al., 2009b). This means ChR2 expressing cells can mimic ON cells whereas NpHR expressing cells can mimic OFF cells in the retina. In order to understand the approaches used to implement the optogenetic strategy to restoring vision, I will give a brief introduction on the vision signaling pathways.

1.3.2 Visual signaling pathways

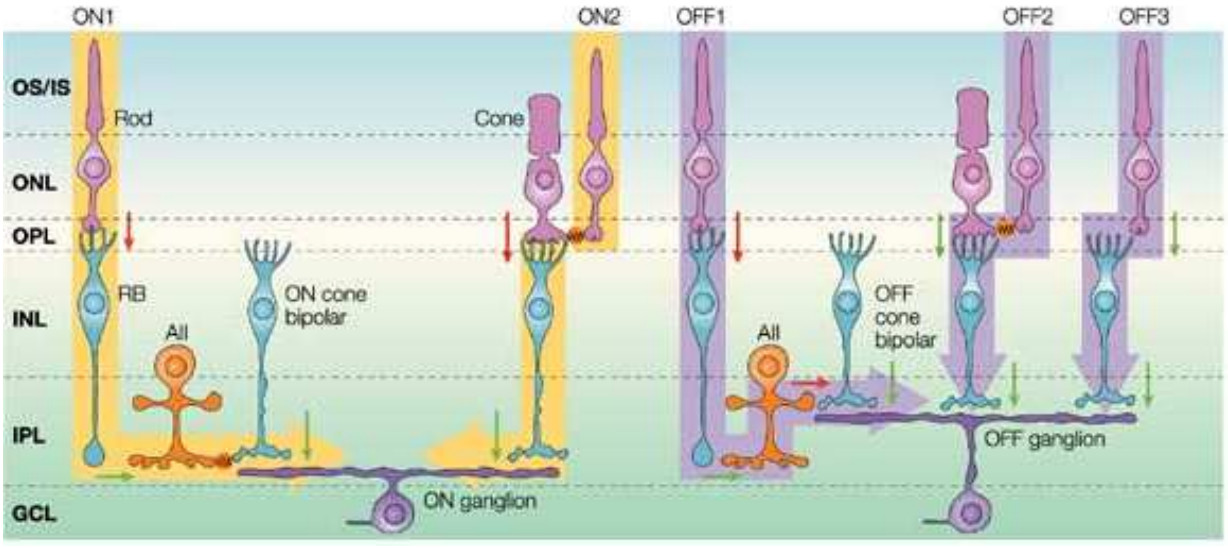

Figure 1: The ON and OFF pathways of the mammalian retina (Wassle, 2004). OS/IS, outer and inner segments of rods and cones; ONL, outer nuclear layer; OPL, outer

plexiform layer; INL, inner nuclear layer; IPL, inner plexiform layer; GCL, ganglion cell layer; RB, rod bipolar cells; AII, AII amacrine cells.

In the mammalian retina, there are three major layers of cells: photoreceptor cells in the outer nuclear layer; bipolar cells, amacrine cells, and horizontal cells in the inner nuclear layer; ganglion cells in the ganglion cell layer. Photoreceptor cells (first order neuron) sense light and transduce the light signal into an electrical signal to depolarize or hyperpolarize the bipolar cells (second order neuron); then the ganglion cells (third order neuron) gather all the signals to send projections to the brain for integrated processing. Both rod and cone photoreceptors depolarize in the dark and hyperpolarize in response to light. Bipolar and ganglion cells are divided into ON and OFF cells that respond to light with depolarization and hyperpolarization, respectively. Rod bipolar cells are ON bipolar cells; signals of the rod pathway feed into the cone pathway through AII amacrine cells. The AII amacrine cells transfer signals to the ON bipolar cells through gap junctions and to the OFF pathway through inhibitory glycinergic synapses (Figure 1). What causes the difference between ON and OFF cells is that ON bipolar cells express the metabotropic glutamate receptors (mGluR6), while the OFF bipolar cells express ionotropic glutamate receptors (Wassle, 2004).

1.3.3 Optogenetic approach by targeting retinal bipolar cells

The light sensors such as ChR2 can be targeted to each order of retinal neurons, from photoreceptor cells to ganglion cells. Surviving cone photoreceptors as the targeting sites have a special advantage because they are the only cell type existing in the fovea, and the aggregation of cones endows this area the highest spatial acuity (Curcio and Hendrickson, 1991). Targeting ChR2 to the rod bipolar cells and AII amacrine cells can stimulate both ON and OFF responses in the downstream ganglion cells (Ivanova and

Pan, 2009). In the condition that photoreceptor death has caused remodeling of the remaining retina, targeting ChR2 to the ganglion cells will be the only option because ganglion cells are the most resistant to remodeling (Jones and Marc, 2005; Kolomiets et al., 2010). The proof-of-concept study for the latter has been demonstrated in animal models (Bi et al., 2006).

My research focuses on the strategy of targeting ChR2 to ON bipolar cells (both rod bipolar cells and ON cone bipolar cells) to restore vision instead of photoreceptors and ganglion cells for the following reasons: 1) In patients who have retinal degenerative diseases, their cone photoreceptors may already be severely damaged before application of this optogenetic therapy; 2) targeting ON bipolar cells may preserve more of the visual processing pathways compared to targeting ganglion cells, which would result in higher vision acuity when applied in patients. However, a big challenge is to achieve AAV-mediated high specificity and high efficiency of ChR2 expression in bipolar cells. Even though our lab has developed an optimized bipolar cell specific promoter (Lu et al., 2016), the AAV transduction efficiency to bipolar cells is still low. Our lab also reported recently that the bipolar cell targeting is less efficient than ganglion cell targeting (Lu et al., 2018). The low AAV transduction efficiency in retinal bipolar cells could be due to factors such as physical barrier of the retina, AAV intracellular trafficking and capsid tropisms. My goal is to address this problem and potentially make the vision restoration more efficient.

1.3.4 Adeno-associated virus as a vehicle

Adeno-associated virus (AAV) has been the most widely used and effective gene delivery vehicle in retinal gene therapy (Buch et al., 2008; Dalkara and Sahel, 2014; Vandenberghe and Auricchio, 2012); it is a nonpathogenic virus that contains a single stranded DNA genome up to 4.7-kb and an outer capsid (composed of VP1, VP2, VP3

structural protein). There are at least 12 serotypes of AAV that have been described, with serotype 2 most widely used (Watanabe et al., 2013). The recombinant AAV2 was first made by Hermonat and Muzyczka (1984), with a SV40 promoter driving the neo resistance gene. This construct was successfully brought into cultured mammalian cells, which proved the availability of foreign DNA sequence being introduced via AAV vectors (Hermonat and Muzyczka, 1984). On December 19th, 2017, LUXTURNA (an AAV2-based gene therapy for patients with RPE65 mutation-associated retinal disease) was approved by FDA; it is the first AAV-based gene therapy approved in the US. Two methods have been used for delivering AAV vectors to the retina in vivo; one is intravitreal injection, and the other is subretinal injection. Subretinal injection has been widely used given its advantage of avoiding the inner limiting membrane as well as its easier access to photoreceptors (Surace and Auricchio, 2003). However, the fact that it can cause retinal detachment and other damage cannot be ignored; besides, it only transduces AAV vectors to a limited region of the retina (Dalkara et al., 2009a). In contrast, intravitreal injection is less invasive and enables AAV transduction to any retinal cell type despite differences in their efficiencies (Dalkara, 2013).

1.3.5 Adeno-associated virus-mediated targeting to retinal bipolar cells

Promoters are critical for cell-targeted specificity and efficiency because they initiate particular gene transcription. CMV and CAG are ubiquitous promoters; Bi et al. (2006) delivered AAV2 vectors in mouse retinas with a CMV enhancer/chicken β-actin (CAG) promoter, leading to transgene expression in various cell types: mostly ganglion cells, some amacrine/horizontal cells, and few bipolar cells. My project focuses on targeting ChR2 to ON bipolar cells; therefore, a selective promoter for ON bipolar cells is required. Since metabotropic glutamate receptors (mGluR6) are specifically expressed in ON

bipolar cells (Brandstatter et al., 1998) and the Grm6 gene encodes the mGluR6, delivering the gene under the control of regulatory elements intraocularly should target ON bipolar cells in particular. It was reported that targeted expression of transgene in ON bipolar cells can be achieved by using the SV40 eukaryotic promoter fused with the 200-base pair enhancer sequence of the Grm6 gene (Grm6En) (Cronin et al., 2014; Doroudchi et al., 2011; Lagali et al., 2008; Mace et al., 2015). However, AAV vectors containing this 200bp enhancer and SV40 promoter have relatively low expression efficiency in bipolar cells (Lu et al., 2016). In addition, the light intensity required for activating ChR2 (10^{14} photons cm^{-2} s^{-1}) is much higher than that of the opsins from rod (10^{6} photons cm^{-2} s^{-1}) and cone (10^{10} photons cm^{-2} s^{-1}) photoreceptors (Mace et al., 2015). In order to enhance the light responsiveness of the bipolar cells, the expression level of ChR2 must be increased. Our lab has developed an optimized mGluR6 promoter construct (In4s+In3-Grm6En-mGluR500P) which replaces the mSV40 promoter (mSV40P) by the 500 bp mGluR6 promoter and adds a shortened intron 4 and an intron 3 (In4s-In3) enhancer sequence (Lu et al., 2016). This leads to a marked enhancement in AAV transduction efficiency in retinal bipolar cells as well as a reduction in off targeting (Figure 2). Moreover, the optimized mGluR6 promoter construct was found to mainly target rod bipolar cells (Figure 3).

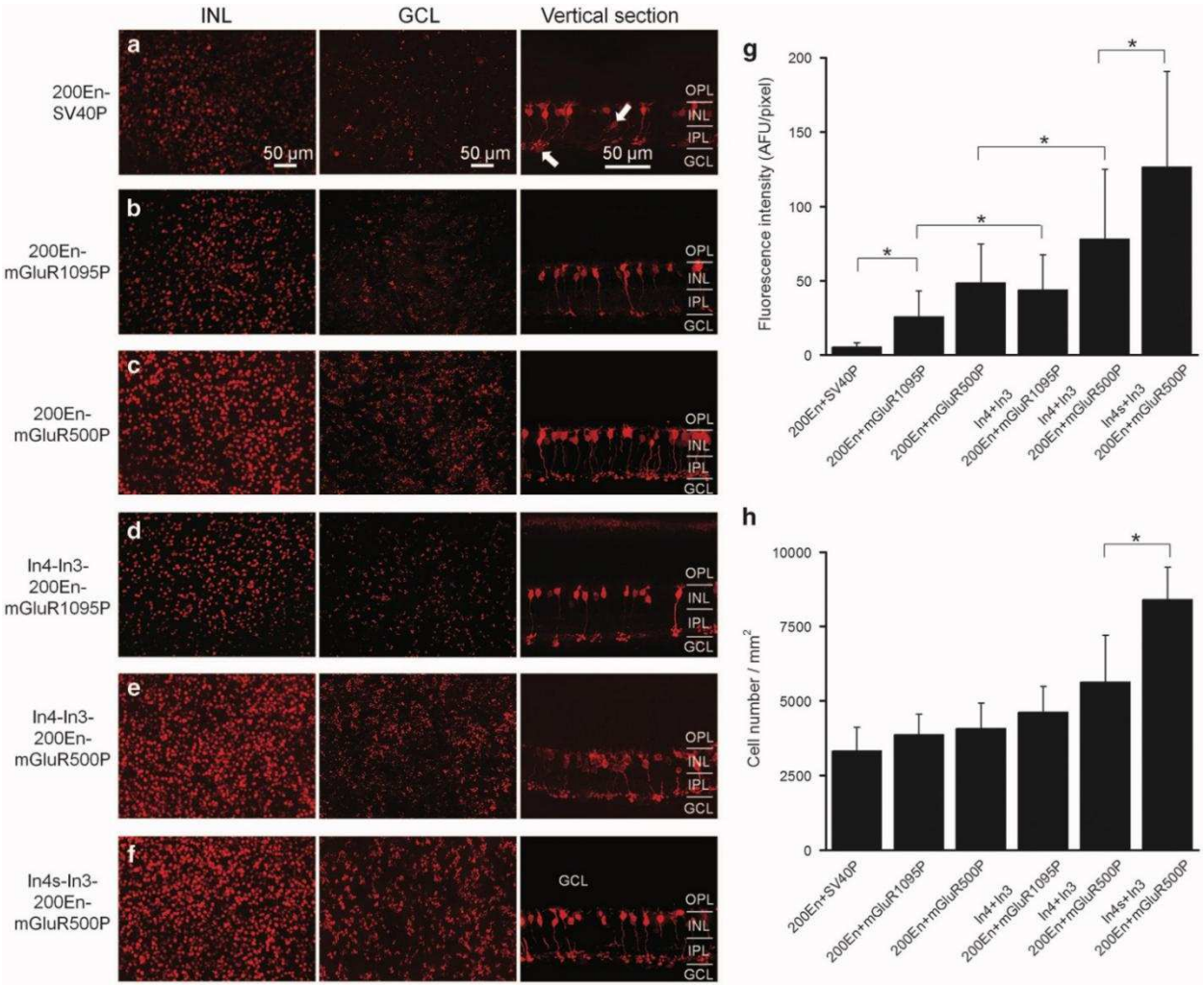

Figure 2: Comparison of AAV-mediated mCherry expression with different mGluR6 promoter constructs in the mouse retinas (Lu et al., 2016). (a-f) Left/middle panels: whole-mount fluorescence images acquired at the inner nuclear layer (left panels) and ganglion cell layer (middle panels). Right panels: fluorescence images of retinal vertical sections after immunolabeling with anti-mCherry antibody. (g) Comparison of mCherry fluorescence intensities with different mGluR6 promoter constructs. (h) Comparison of cell densities of the mCherry-expressing bipolar cells with different mGluR6 promoter constructs. The data are shown as mean ± SD. The asterisk indicates statistically significant differences at $p<0.05$ (one-way analysis of variance).

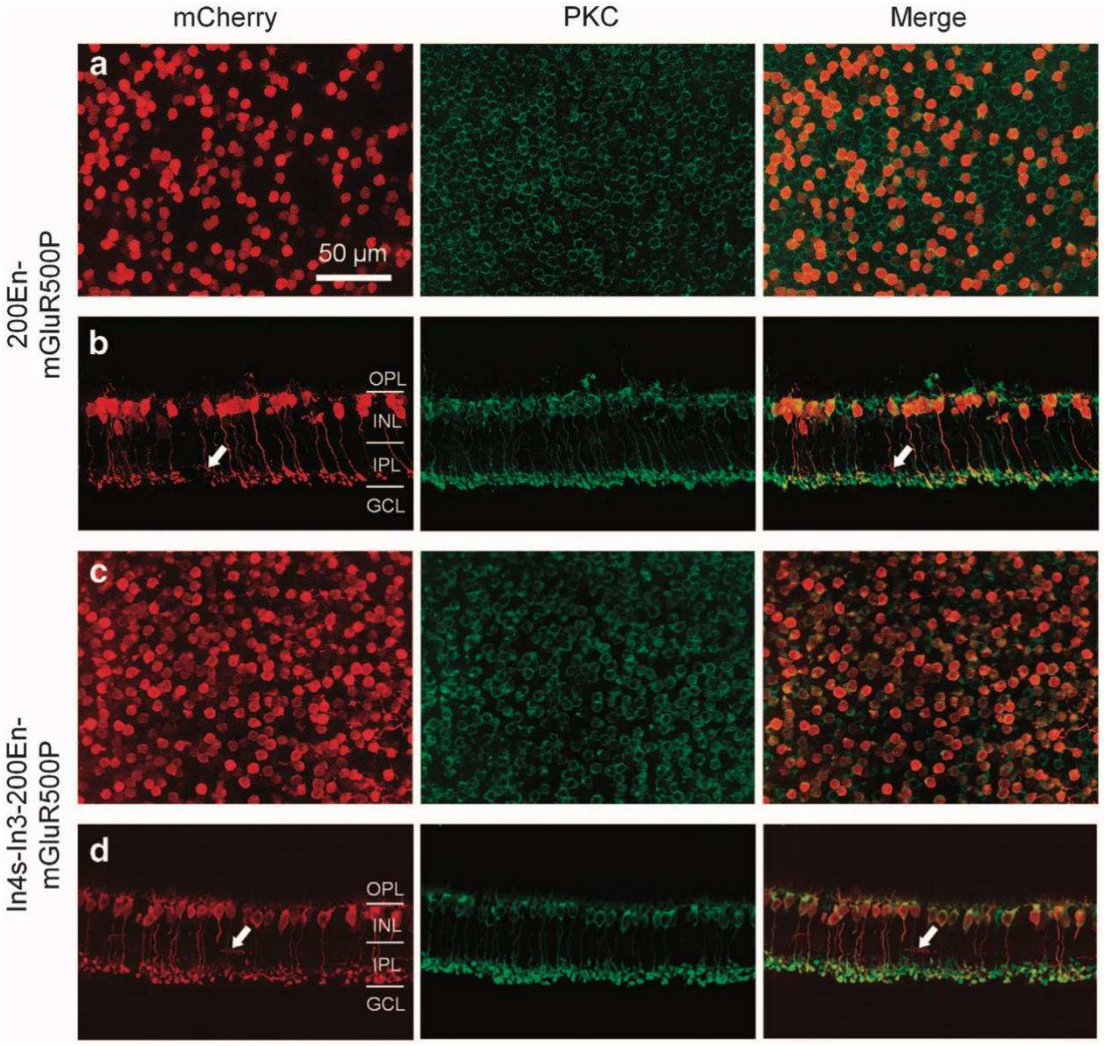

Figure 3: Immunostaining of mCherry-expressing bipolar cells transduced by the virus vectors containing modified mGluR6 promoter constructs. The mCherry expression was driven by the promoter construct of 200E-mGluR500P (a-b) and In4s-In3-200En-mGluR500P (c-d). Retinal whole-mount (a,c) and vertical section (b,d) were colabeled for mCherry and PKC (rod bipolar cell marker) (Lu et al., 2016).

1.3.6 Factors that affect the AAV transduction in the retina

Physical barriers and inner limiting membrane

First of all, the bipolar cell layer is located in the middle of the retina, which means that it is difficult for viruses to access bipolar cells with either intravitreal or subretinal delivery. For our purpose, we prefer to inject virus through the vitreous space; hence the second barrier shows up: the inner limiting membrane. The inner limiting membrane (ILM)

is a basement membrane that resides between the vitreous body and the retina as a boundary. Functionally, it is a layer that facilitates the attachment between the neuroretina and the vitreous body. Under a high resolution electron microscope, the ILM consists of two thin layers of lamina lucidas with a layer of lamina densa in between (Halfter et al., 2008). Under a conventional light microscope, like a surgical microscope, the ILM appears to be a transparent layer covering the neuroretina. Nowadays, peeling off the ILM layer has been an option for many retinal surgical conditions, like macular hole. It is believed that by peeling off the ILM, traction from the vitreous body against the macula is released and since the ILM is more or less functionally dispensable, getting rid of the ILM for better medical outcome appears to be extremely appealing (Mester and Kuhn, 2000). The composition of the inner limiting membrane contains 10 types of high-molecular weight extracellular matrix proteins, including nidogen1 and 2 (laminin), collagen II, and heparin sulfate proteoglycans (HSPG), agrin, perlecan and collagen IV (Halfter et al., 2008). This is of importance because it explains how the ILM affects the diffusion of different serotypes of AAV. For example, AAV2 binds to the HSPG and laminin, which facilitates its accumulation at the ILM and further access to the ganglion cell layer, while AAV5 doesn't have a binding site at the vitreoretinal junction. Interestingly, a robust expression of AAV5 in various retinal cell types can be achieved following intravitreal co-injection with a proteolytic enzyme Pronase E, suggesting the ILM may constitute a barrier for AAV penetration into the retina (Dalkara et al., 2009a).

Although the ILM is relatively thin in rodents, larger mammals possess a much thicker ILM that differs in thicknesses from region to region of the retina. In primates and human, the ILM is thinnest in the fovea and thickest around the fovea; the ILM above the retinal

vessels is thinner than in the surroundings (Matsumoto et al., 1984). Accordingly, AAV2 transduction in marmoset retinas is best in the fovea and above retinal vessels, almost absent near the fovea, and modest in peripheral areas (Ivanova et al., 2010). Therefore, enzymatic treatment of the ILM is necessary for the future application of the optogenetic approach clinically. Microplasmin has been demonstrated to disrupt the border between the ILM and vitreous body in macaque, resulting in an increased transduction similar to the effect of pronase E on rodents (Yin et al., 2011). Plasmin is a trypsin-like serine protease; it can dissolve laminin and fibronectin in ILM, as well as facilitate extracellular matrix degradation (Liotta et al., 1981). In this study, I examined the effect of plasmin in improving AAV-mediated transgene expression in the retinal bipolar cells. The results are presented in Chapter 4.

AAV serotypes

Hybrid AAV serotypes

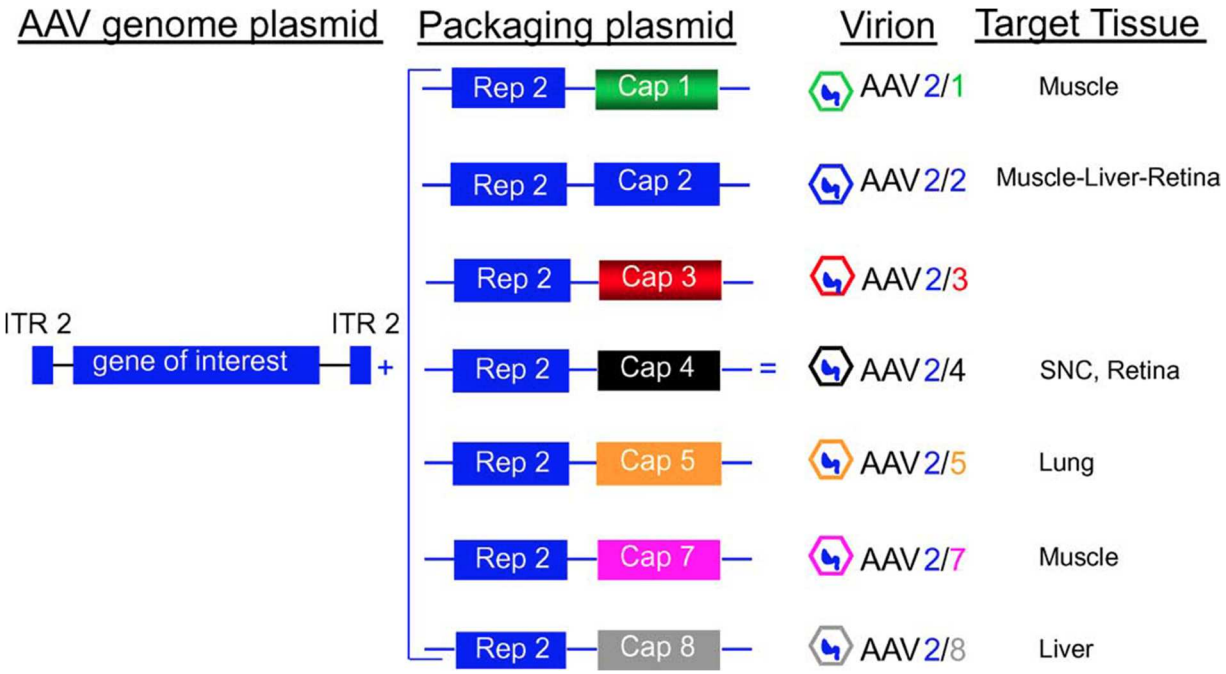

Figure 4: Schematic representation of hybrid AAV production and targeting (Auricchio, 2003).

AAV has tropisms towards various tissue types, and tissue specificity is due to different AAV capsid serotypes. Numerous serotypes of AAV have been described, with serotype 2 most extensively studied. The recombinant AAV2 (rAAV2) genome contains a therapeutic gene sequence with one ITR (inverted terminal repeat) sequence on each end, followed by two opening reading frames: rep and cap. The rep2 gene codes for proteins that are necessary to maintain the AAV2 life cycle (replication); the cap2 gene codes for the AAV2 capsid protein that determines the AAV2 tropism. By packaging AAV2 genome with capsids of other serotypes, hybrid AAV vectors are produced (Figure 4). These pseudotyped AAVs possess advantages over the original ones in their ability to avoid the pre-existing immunity, as well as gaining a variety of tissue tropisms according to the different outer capsids (Auricchio, 2003). Intravitreal application of rAAV2/2 and rAAV2/8 particularly transduced to retinal ganglion cells (RGCs), while subretinal injection of rAAV2/5, rAAV2/8 and rAAV2/9 resulted in transduction of cone photoreceptors (McClements and MacLaren, 2013). In addition, AAV2/8 vectors driven by the mGluR6 promoter can get a strong and stable transgene expression in the mouse retinal ON bipolar cells by subretinal injection (Doroudchi et al., 2011). However, no one has tested the AAV2/8 vector with mGluR6 promoter through intravitreal injection. In my preliminary work, I did intravitreal injection of the virus construct, but the result showed barely any transgene expression on bipolar cells (data not shown).

Single capsid mutation

Since the phosphorylation of surface-exposed tyrosine residues on AAV capsids acts as a signal for ubiquitination, mutations on tyrosine can help the AAV vectors escape the

proteasome degradation process (Zhong et al., 2008a; Zhong et al., 2008b). There are all together seven surface-exposed tyrosine residues in the VP3 common region of the capsid, Y252, Y272, Y444, Y500, Y700, Y704, and Y730 (Zhong et al., 2008b). AAV2 with an original capsid has been proved to target mainly ganglion cells, frequently horizontal cells and amacrine cells, and occasionally bipolar cells following intravitreal injection in mouse eyes (Bi et al., 2006). Petrs-Silva et al. (2009) made tyrosine to phenylalanine single point mutations (Y444F and Y730F) on the AAV2 capsid and reported that both of them showed enhanced RGC transduction after intravitreal injection. Moreover, Y444F mutation made on rAAV2/2 vectors showed photoreceptor transduction after intravitreal injection and RGC transduction following subretinal injection, indicating an improved ability to penetrate throughout the retinal layers (McClements and MacLaren, 2013). In our lab, we have demonstrated that AAV2 vectors with the Y444F mutation could significantly increase the transduction efficiency in both ganglion cells and bipolar cells (under ubiquitous CMV promoter) via intravitreal injection; while without this mutation, the AAV2 vectors could only reach the ganglion cell layer (Lu et al., 2013). Therefore, our current AAV2 vectors with the mGluR6 promoter are all made with the Y444F mutation, resulting in good expression restricted to bipolar cells.

Multiple capsid mutations

Multiple combinations of Y-F mutations (from double to septuple) on AAV2 vectors have been tried on the mouse retinas through vitreous delivery (Petrs-Silva et al., 2011). All mutants showed similar reporter gene expression pattern from ganglion cell layer through the photoreceptor layer, with the quadruple (Y272,444,500,730F) and pentuple (Y272,444,500,704,730F) mutant even extending to the RPE layer. In addition to tyrosine

to phenylalanine mutations, threonine (T) to valine (V) mutations (T-V mutations) have also been tested. Both the Y-F and T-V/A mutations enhance AAV transduction by blocking the capsid residue phosphorylation; therefore, the capsids can avoid ubiquitination and subsequent proteasome degradation (Aslanidi et al., 2013; Petrs-Silva et al., 2009). Among 17 surface-exposed threonine residues on the AAV capsid, four of them were shown to increase AAV transduction efficiencies in human HEK293 cells after T-V mutation (T455V,T491V,T550V,T659V), with the T491V the best-performing one. The T491V mutation was then combined with the triple mutant Y444,500,730F to form the quadruple mutant Y444,500,730F+T491V, which was demonstrated to transduce mouse hepatocytes efficiently both in vivo and in vitro (Aslanidi et al., 2013). Shannon Boye's group gained robust photoreceptor expression in mouse retinas by using a quintuple AAV2 mutant (Y272,444,500,730F+T491V) driven by the human rhodopsin kinase promoter (hGRK1) via intraviteal delivery (Kay et al., 2013).

In vivo-directed evolution approach

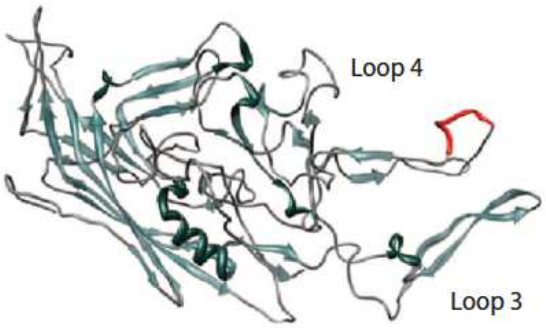

Figure 5: Molecular model of AAV2 with the insertion LALGETTRP (shown in orange). The interactions between the inserted loop and the other surface loops of the capsid likely play a role in the novel properties of the virus (Dalkara, 2013).

Another method to increase the AAV diffusion capability by altering their capsid protein is the in vivo-directed evolution approach (Figure 5). In 2013, Dalkara et al. modified the AAV2 capsid by making a ^{588}LALGETTRP insertion (7mer insertion), leading

to a lower binding ability to its primary receptor, thus a higher possibility of penetration through the retinal layers as well as the inner limiting membrane. The 7mer insertion works by impacting arginine residues in loop 4 within the HSPG binding domain of the AAV2 capsid, therefore the affinity between AAV2 and its primary receptor is lowered. This AAV2 variant with 7mer insertion is called 7m8, which has shown higher infection rates than AAV2 in cultured cells. They further applied 7m8 carrying GFP sequence driven by a ubiquitous CAG promoter to the mouse retinas by intravitreal injection, getting a result of a pan-retinal gene expression. More excitingly, they also targeted photoreceptor cells specifically by replacing the CAG promoter with a rhodopsin promoter (Dalkara, 2013). The transduction ability of 7m8 will make it a potent tool for targeting any retinal cell types of interest, including bipolar cells, after intravitreal administration. Therefore, I hypothesize that, together with our optimized mGluR6 promoter, the 7m8 vector will dramatically increase the ChR2 expression in RBCs. In my preliminary data, one month after intravitreal injection, ChR2-GFP expression in bipolar cells driven by 7m8 vector with In4s+In3-Grm6En-mGluR500P promoter construct can be clearly seen (data not shown), while that by original AAV2 is very weak without staining. This suggests the 7m8 works better than AAV2 in targeting RBCs.

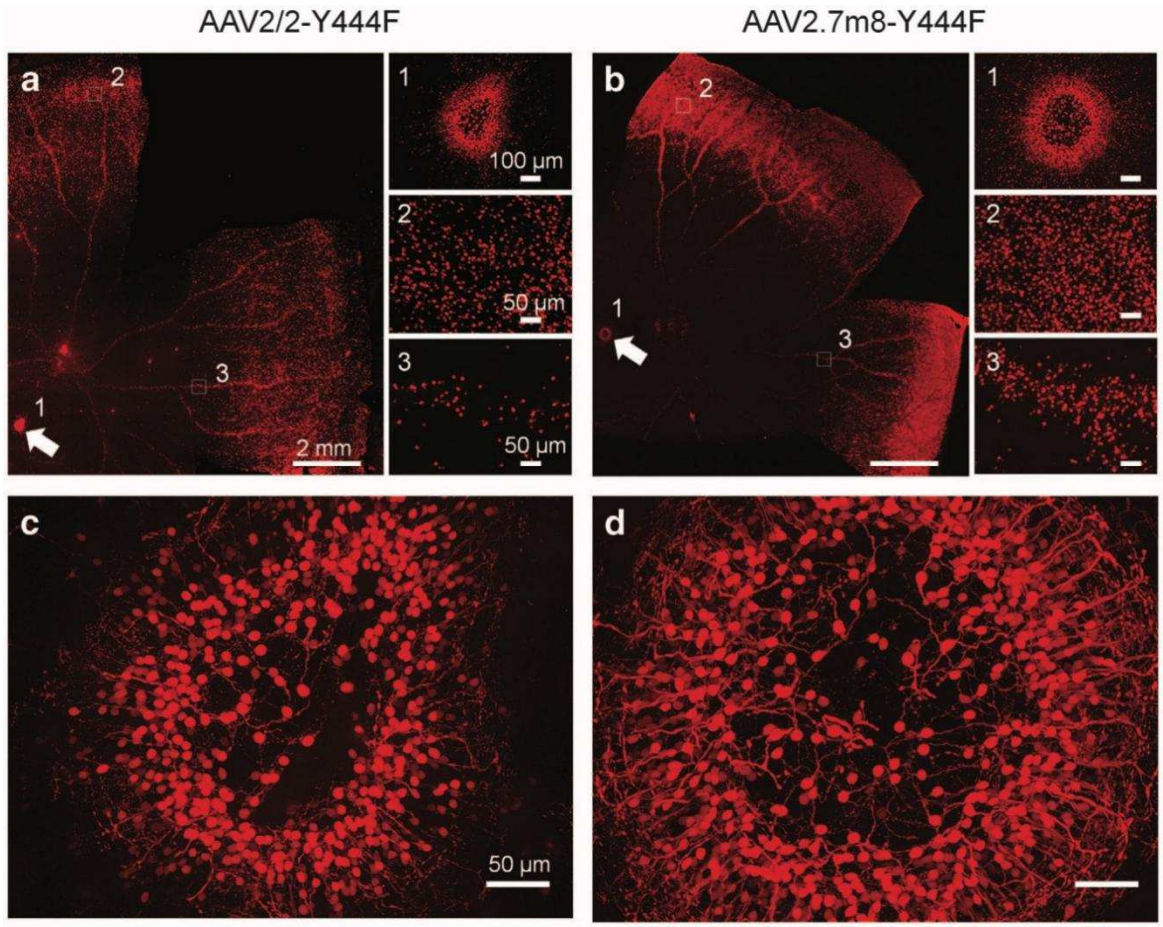

Figure 6: AAV-mediated expression patterns in the marmoset retina. The mCherry expression was driven by In4s-In3-200En-mGluR500P promoter construct with AAV2/2-Y444F mutation (a) and AAV2.7m8-Y444F mutation (b). The three panels on the right are the magnified images: 1, the fovea; 2, the representative peripheral regions of the retina; 3, the representative regions containing blood vessels. (c) The higher magnification image of the fovea in a. (d) The higher magnification image of the fovea in b. (Lu et al., 2016).

A recently published paper in our lab demonstrated that 7m8 vectors with a Y444F capsid mutation had a more robust transgene (mCherry) expression in the marmoset retina than AAV2 vectors with a Y444F capsid mutation (Figure 6). However, no one has tested the effect of multiple mutations on 7m8. In order to produce the most efficient virus vectors for improving transgene expression in RBCs, I planned to make the quadruple mutations (Y444,500,730F+T491V) on the 7m8 vectors with mGluR6 promoter, and examine the effect after one month of intravitreal injection. However, our virus vectors

could not be packaged by the Virovek company. The quadruple mutations made on the 7m8 capsid likely caused instability in capsid formation. Therefore, the experiments were discontinued.

AAV trafficking

Intracellular trafficking

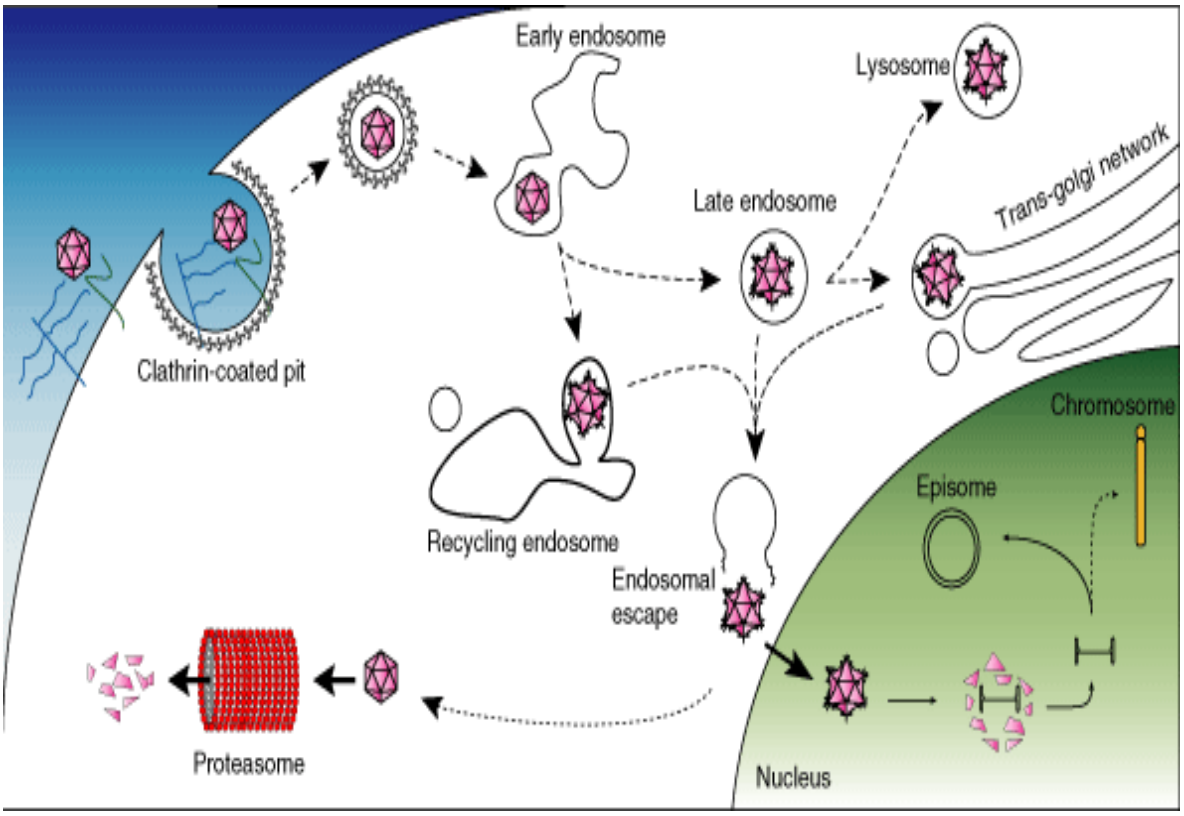

Figure 7: Schematic diagram of AAV intracellular trafficking process (Schultz and Chamberlain, 2008).

The AAV intracellular trafficking process is displayed in Figure 7. To enter a cell, AAV2 must first attach to the target cell membrane by binding to attachment receptors. Cell infection requires both primary receptors and coreceptors. Different transduction susceptibilities of various cells rely on different combinations of their receptors (Douar et al., 2001). The primary attachment receptor for AAV2 is heparan sulfate proteoglycans (HSPG), which is proved to affect AAV2 transduction efficiency directly (Summerford and

Samulski, 1998a). Human fibroblast growth factor receptor 1 (FGFR1) can work as a coreceptor for HSPG to enhance the overall efficiency of AAV2 adherence (Qing et al., 1999). There are also some other coreceptors for AAV2 such as integrin αVβ5, integrin α5β1, and hepatocyte growth factor receptor (Asokan et al., 2006; Kashiwakura et al., 2005; Summerford et al., 1999). Following attachment to the target cell, AAV2 then undergoes endocytosis through clathrin-coated vesicles (Bartlett et al., 2000). After entering the cell, the internalized vesicles become early endosomes, and then late endosomes. The mammalian cells use two sets of systems to degrade the proteins. The lysosome, which contains acid proteases and hydrolases, has long been studied for its function in breaking down endocytosed extracellular proteins. Another important system includes proteasomes, which are protein complexes that mainly function in digesting unneeded or damaged proteins. To transport the aimed protein to the proteasome, the substrate needs to be marked by ubiquitin (Lee and Goldberg, 1998). The substrate ubiquitination requires three functional proteins: activating enzyme (E1), conjugating enzyme (E2), and ubiquitin ligase (E3). Duan et al. (2000) applied E3 inhibitor dipeptides H-Leu-Ala-OH and H-His-Ala-OH with AAV vectors to the polarized human airway epithelia and showed an enhanced AAV transduction. Direct inhibition of proteasome activity shows even better effect in strengthening AAV expression; Doxorubicin and MG-132 are proteasome inhibitors that have been proved to have a dramatic AAV enhancement effect (Douar et al., 2001; Zhang et al., 2009a).

Proteasome inhibitors

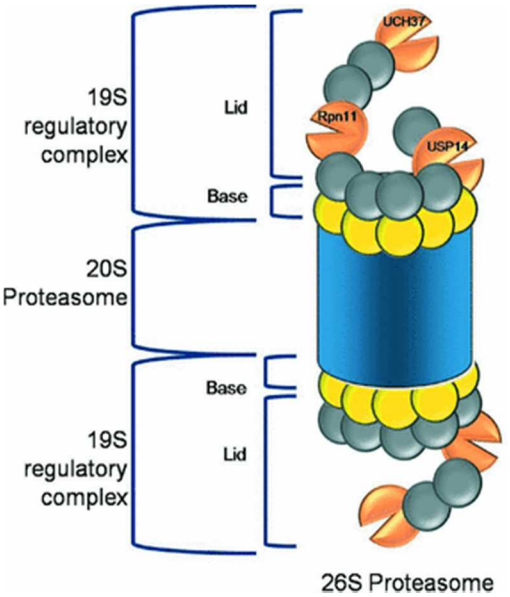

Figure 8: Schematic diagram of the 26S proteasome structure (Ventii and Wilkinson, 2008).

The classical proteasome protein degradation pathway is the ubiquitin-conjugated 26S proteasome pathway (Goldberg, 2003). The 26S proteasome is composed of a 20S core particle that catalyzes the proteolytic activity, and a 19S particle that regulates the degradation process (Figure 8). The 19S particle can recognize the ubiquitin-marked substrates, unfold them, and deliver them to the 20S core to be degraded. The 20S core is a barrel-shaped complex, with two rings of 7β subunits in the center, and two rings of 7α subunits on the outside. The two outer rings surround an opening, through which the substrate enters for degradation. Some of the β subunits inside are active proteolytic sites, taking responsibility for the chymotrypsin-like, trypsin-like, and caspase-like proteasome activities (Kish-Trier and Hill, 2013). Although most of the proteasome substrates go through this traditional pathway, some proteins are digested by the proteasome in an ubiquitin-independent manner (Erales and Coffino, 2014). In other words, these proteins are broken down by the 20S proteasome itself without the coordination of the 19S particle.

In fact, 50% of proteasomes in mammalian cells exist as the free 20S form, while only 30% of those exist as the 26S combination. Instead of dealing with the ubiquitinated polypeptides, the substrates for the 20S proteasome are damaged proteins; only the unstructured proteins can enter the narrow opening of the 20S proteasome without being unfolded by the 19S particle (Ben-Nissan and Sharon, 2014).

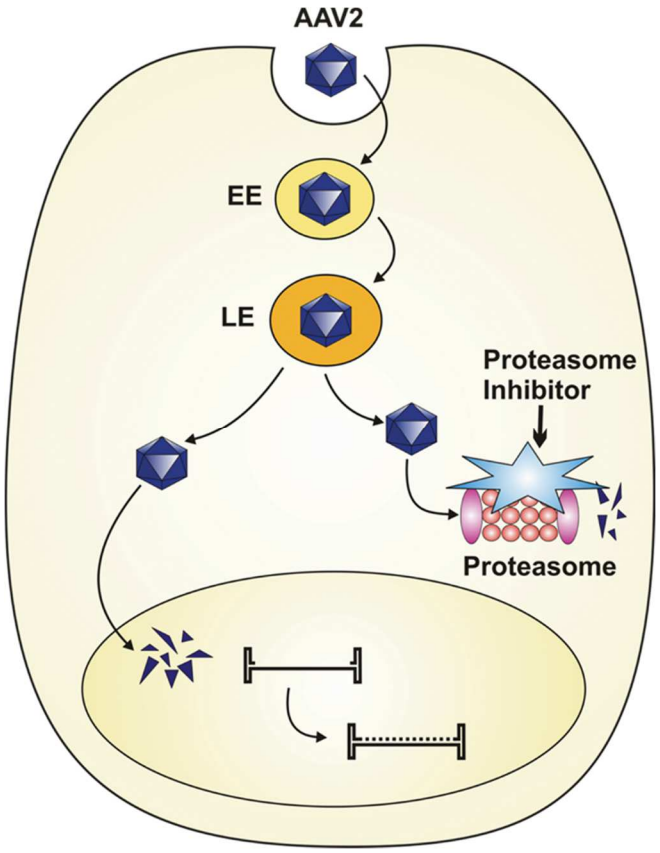

Figure 9. Schematic diagram of the effect of proteasome inhibitors on AAV2 transduction in a cell.

Proteasome inhibitors have been reported to increase transduction of various types of AAVs (AAV serotype 1-8) to different tissues (Chaanine et al., 2014), as well as to alleviate the immune responses against AAV capsids (Karman et al., 2012). The working mechanism of proteasome inhibitors on improving AAV transduction is displayed in Figure

9. Normally after AAV2 virus vectors enter a cell, they are processed by the early endosome and late endosome and are then transported to the proteasome for degradation. With the application of proteasome inhibitors, the digestive function of proteasome is blocked, which allows the AAV vectors to enter the cell nucleus and express the transgene they carried. MG132 is the first synthesized proteasome inhibitor; it is a tripeptidyl aldehyde derived from the substrates of the chymotrypsin-like active site (most important site for protein degradation). Further, bortezomib was produced by replacing the aldehyde with a boronate head in addition to some modifications in the peptide backbones (Goldberg, 2012). Bortezomib is the first U.S.FDA approved proteasome inhibitor to be tested in clinics (Chen et al., 2011). Both the MG132 and bortezomib bind with the 20S core β-subunit, inhibiting primarily the chymotrypsin-like proteasome activity, but also the caspase-like activity when the concentrations are high (Goldberg, 2012; Yan et al., 2004). Doxorubicin and aclarubicin are nonpeptide proteasome inhibitors that are also used clinically as anthracycline anticancer drugs; similar to the bortezomib, they block the chymotrypsin-like proteolytic activity of the proteasome (Yan et al., 2004). MG132, bortezomib, doxorubicin and aclarubicin have all been proven to have a dramatic effect in enhancing AAV transduction in either cultured cell lines or small animal models (Douar et al., 2001; Mitchell and Samulski, 2013; Monahan et al., 2010; Yan et al., 2004; Zhang et al., 2009a). However, no one has evaluated these drugs in the retina for improvement of AAV-mediated transgene expression. I hypothesize that with the help of these proteasome inhibitors, less AAV2 vectors will be degraded by proteasomes in the RBCs and the AAV-mediated transgene expression level will be remarkably increased. I examined the effects of MG132,

doxorubicin, and aclarubicin by co-injecting them with rAAV2 virus in the vitreous space of C57BL/6J mouse eyes.

Pharmacokinetics of doxorubicin

Hu et al., 2006 examined the pharmacokinetics of doxorubicin in the rabbit eye following intravitreal injection. They did dissection of the rabbit eyes at 0.167, 0.5, 1.0, 1.5, 2.0, 3.0, 4.0, 5.0, 6.0, 8.0, and 12.0 hours after intravitreal injection of 5 μg doxorubicin. They reported that doxorubicin could not be detected in all ocular tissues (including vitreous body, iris, retina/choroids, and sclera) 12 hours after injection. Moreover, doxorubicin was not detectable in the retina 8 hours after injection (Hu et al., 2007). In order to determine an optimal delivery protocol for doxorubicin in the mouse eye, I tested the efficacy of doxorubicin on AAV-mediated mCherry expression in the retinal bipolar cells by administrating doxorubicin twice with an 8-hour interval. The results are presented in Chapter 2 Figure 13.

Cytotoxicity of doxorubicin

Doxorubicin as an anthracycline chemotherapy regimen was well known to cause cardiotoxicity in cancer patients (Chatterjee et al., 2010; Kumar et al., 2012). Doxorubicin also works as a nonpeptide proteasome inhibitor, and was previously reported to induce neurotoxicity to rat cortical neurons (Lopes et al., 2008). The mechanisms of anthracycline-induced cytotoxicity involve iron-dependent and iron-independent mechanisms (Menna et al., 2007). The intracellular iron levels are physiologically regulated by ferritin and transferrin receptor; the transcription of the genes coding for ferritin and transferrin receptor levels are regulated by iron regulatory proteins—IRP-1 and IRP-2. IRPs regulate the levels of ferritin and transferrin receptor by binding to the

conserved iron regulatory elements (IRE) in the ferritin and transferrin mRNAs (Cairo and Pietrangelo, 2000). Doxorubicin is able to switch the cytoplasmic aconitase enzyme into IRP-1, which facilitates iron uptake to the cell and increases the intracellular free iron levels. This process is highly toxic to the cells (Minotti et al., 2001). Another mechanism of doxorubicin-induced cell damage is the formation of the drug-iron complex which catalyzes the formation of hydroxyl radical and causes DNA damage (Muindi et al., 1984). Dexrazoxane (Zinecard) is a FDA-approved drug that is used to reduce the anthracycline-induced cytotoxicity. The active form of dexrazoxane is similar to EDTA, which chelates iron and limits the formation of anthracycline-iron complexes, and therefore reduces the generation of free radicals and the subsequent oxidative damage to cells (Ichikawa et al., 2014; Langer, 2014). Previous studies on the antidote effect of dexrazoxane are mainly limited to the anthracycline-induced cardiotoxicity (Ichikawa et al., 2014; Langer, 2014; Swain et al., 1997b). However, the effect of dexrazoxane has not been tested on retinal neurons treated with doxorubicin.

Arsenic trioxide

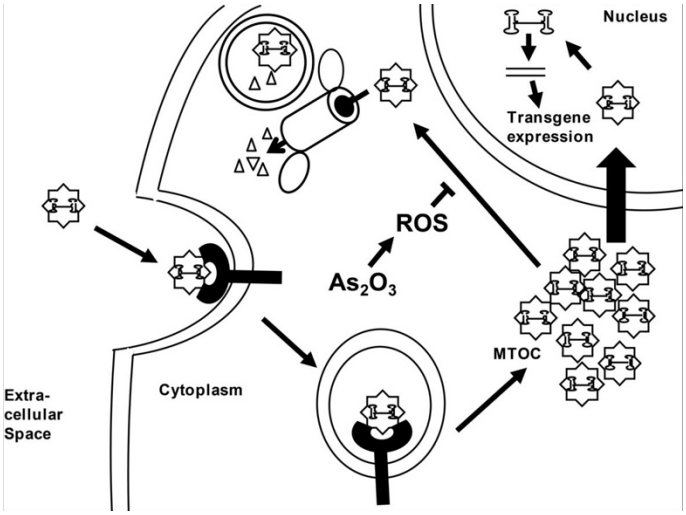

Figure 10: Role of arsenic trioxide on AAV transduction (Mitchell et al., 2013).

Before trafficking to the nucleus, AAV particles first move to the perinuclear region and accumulate there. This region is the microtubule-organizing center (MTOC); the AAV virions are enclosed in late endosomal or lysosomal compartments. They arrive at the MTOC by travelling along the microtubules (Nicolson and Samulski, 2014; Xiao and Samulski, 2012). If the viruses cannot enter the nucleus, they will eventually be degraded by the proteasomes. Arsenic trioxide (As_2O_3) is a FDA-approved chemotherapeutic agent that was shown to enhance AAV transduction by stabilizing the virus accumulation at the perinuclear region. More viruses were preserved to escape from the MTOC and continued a productive nuclear trafficking with the treatment of As_2O_3 both in vitro and in vivo (Mitchell et al., 2013). Mitchell et al. claimed the drug effect of As_2O_3 was dependent on formation of reactive oxygen species (ROS) (Figure 10). They also reported the transduction efficiency could be increased by As_2O_3 in multiple AAV serotypes, including rAAV2, rAAV6, rAAV8, rAAV9, and self-complementary rAAV2. However, the effect of arsenic trioxide on AAV-mediated transgene expression has never been tested in neural cells. Therefore, I co-injected arsenic trioxide and AAV2 virus (with a bipolar cell-specific promoter carrying mCherry transgene) to examine the efficacy of arsenic trioxide on AAV transduction in the mouse retinal bipolar cells. My result showed that the mCherry expression level had no difference among retinas treated with 500 μM As_2O_3, 1mM As_2O_3, and control (data not shown). Therefore, the virus accumulation effect of arsenic trioxide at the perinuclear region couldn't be proven to increase AAV2 transduction efficiency in RBCs, at least at concentrations up to 1mM.

Nuclear trafficking

The nucleus entry process is slow and inefficient, leaving most of the AAV accumulating in the perinuclear area, while only a small fraction of virus particles passes the nuclear membrane in cultured cells (Bartlett et al., 2000). The viral particles that are not entering the nucleus will be finally degraded by the proteasomes. Although there is lack of a well-defined mechanism, it was suggested the rAAV2 utilizes parts of the canonical nuclear import pathway to enter the nucleus. After entering the nucleus, the AAV particles need to remove their outer capsids. Then the single strand AAV DNA must synthesize a second strand for subsequent transcription, which constitutes an important rate-limiting step. Zhong et al. (2007) presented that the cellular chaperone protein FK506-binding protein 52 (FKBP52) plays an inhibiting role on AAV2 second strand DNA synthesis, whose tyrosine residues are phosphorylated by the epidermal growth factor receptor protein tyrosine kinase (EGFR-PTK). Srivastava's lab reported that dephosphorylation of FKBP52 protein at tyrosine residues by heat-shock protein 90 (HSP90) and T-cell protein tyrosine phosphatase (TC-PTP), as well as dephosphorylation at serine/threonine residues by protein phosphatase 5 (PP5) were able to augment AAV second strand synthesis and in consequence enhance AAV transduction in HeLa cells (Jayandharan et al., 2008; Qing et al., 2003; Zhong et al., 2004). Perturbing EGFR-PTK signaling by using a specific inhibitor-tyrphostin-23 can also increase AAV transduction efficiency (Zhong et al., 2007). Hydroxyurea was also reported to increase AAV transduction; it mobilizes virus vectors into the nucleoplasm, which likely facilitates uncoating and subsequent gene expression (Johnson and Samulski, 2009). In my preliminary study, I tested the effects of tyrphostin 23 and hydroxyurea on rAAV2-

mediated transgene expression in RBCs, but the results suggested no difference between treated retinas and control (data not shown).

Self-complementary AAV

As I mentioned before, one of the AAV transduction rate-limiting steps is the conversion of the single-stranded DNA (ssDNA) to double-stranded DNA (dsDNA) after translocation of AAV to the nucleus. There are two mechanisms for AAV to generate a complementary double strand DNA structure. The conventional one requires a secondary strand synthesis: the ITR sequences at each end of the genome form hairpin structures, which act as replication primers to extend a new complementary strand with the assistance of host cell DNA polymerases (McCarty, 2008). Another alternative mechanism is the strand annealing (SA), or interstrand base pairing of two matched strands from different viruses (Nakai et al., 2000). Despite the coexistence of two mechanisms, conventional DNA second strand synthesis makes the most contribution to AAV transduction (McCarty, 2008; Zhong et al., 2008c). No matter which mechanism is preferable, the need for dsDNA transformation becomes an obstacle for AAV transduction efficiency. Utilizing self-complementary AAV (scAAV) may avoid the limiting factors associated with second strand synthesis. In the scAAV vector, both of the two base-paired DNA strands are packaged as a whole and stabilized by deleting the resolution site sequence from one terminal repeat (McCarty et al., 2003; Wang et al., 2003). This design can substantially enhance the transgene expression regardless of the DNA synthesis and vector doses (McCarty, 2008; McCarty et al., 2001). Furthermore, the single stranded virus genome is stable only within the protection of the capsid shell; while the built-in double stranded genome in scAAV makes it more stable (Thomas et al., 2004). However,

the base-paired DNA construct also limits the gene carrying capability because the length of dsDNA has to be reduced by half for packaging (McCarty, 2008). Even with this limitation, injection of scAAV serotype 2 to mouse eyes has shown rapid expression in RPE cells and photoreceptor cells via subretinal delivery, and widespread RGC expression via intravitreal delivery (Yokoi et al., 2007). scAAV2/2, scAAV2/5, and scAAV2/8 also yielded higher and faster transgene expression, with different transduction selectivity and efficiency accordingly (Natkunarajah et al., 2008). In addition, scAAV vectors can be modified with Tyr-Phe mutations; scAAV2 Y444F and scAAV8 Y733F are two potent mutants that have revealed high efficiency for cell targeting (Petrs-Silva et al., 2009). Given the information on how scAAV may help to increase AAV expression, in my preliminary study, I tested scAAV vectors with mGluR500P promoter carrying mCherry transgene to target RBCs. My results showed that the mCherry expression was minimally enhanced with the application of self-complementary AAV (data not shown). Since the small increase of the transduction efficiency of the sc-construct is at the cost of a shorter virus construct, which will limit the length of the gene it carries, I did not further develop newer scAAV vectors.

1.4 Hypotheses

Targeting ChR2 in bipolar cells is one of the promising approaches for restoring vision. AAV-mediated targeting of ChR2 to RBCs has been achieved using mGluR6 promoter constructs. However, the AAV transduction efficiency in bipolar cells is low. The goal of my project is to improve AAV trafficking efficiency in bipolar cells. I tested my hypotheses that poor virus accessibility to bipolar cells and virus degradation during intracellular trafficking are two main barriers for the efficient AAV transduction to bipolar cells. I used

mCherry as the transgene instead of ChR2 to examine the AAV transduction efficiency.

Hypothesis 1: Proteasome inhibitors would improve AAV transduction efficiency in retinal neurons.

Hypothesis 2: Enzymatic digestion of inner limiting membrane would increase the number of AAV-transduced retinal neurons.

CHAPTER 2: EVALUATION OF THE EFFECT OF PROTEASOME INHIBITORS ON AAV-MEDIATED TRANSDUCTION EFFICIENCY IN RETINAL BIPOLAR CELLS

2.1 Hypothesis

Proteasome inhibitors would improve AAV transduction efficiency in retinal neurons.

2.2 Rationale

Adeno-associated virus (AAV) has been the most widely used and effective gene delivery vehicle in retinal gene therapy (Buch et al., 2008; Dalkara and Sahel, 2014; Vandenberghe and Auricchio, 2012). However, the AAV-mediated transduction efficiency in retinal bipolar cells is generally low (Lu et al., 2016). One of the limiting factors is the virus degradation by proteasomes during AAV intracellular trafficking (Nonnenmacher and Weber, 2012). Therefore, I hypothesized that application of proteasome inhibitors would assist the AAV virus to escape the capsid protein degradation activity of the proteasome. In this way, more AAV viruses can be available for nuclear entry, thus improving gene expression. In this study, I tested the effect of three proteasome inhibitors, doxorubicin, aclarubicin, and MG132, on AAV-mediated transduction efficiency in retinal bipolar cells. In order to compare the AAV-mediated transgene expression in the retinal bipolar cells, AAV virus vectors with a bipolar cell-specific promoter carrying an mCherry sequence were used via intravitreal injection.

2.3 Experimental design and method

Animals and materials

C57BL/6J mice were purchased from Jackson Laboratory (Bar Harbor, ME, USA). Experiments and procedures were approved by the Institutional Animal Care and Use Committee (IACUC) at Wayne State University and were in accordance with the NIH Guide for the Care and Use of Laboratory Animals.

Viral vectors were packaged at Virovek (Hayward, CA, USA), with the construct AAV2 (Y444F)-intro4&3-Grm6En-mGluR500P-mCherry-hGHpA. Proteasome inhibitors were purchased from commercially available sources: doxorubicin (Thermo Fisher Scientific, Waltham, MA), aclarubicin (Santa Cruz Biotech, Dallas, TX), and MG132 (Cayman Chemical, Ann Arbor, MI).

Virus injection

Virus injections were performed in C57BL/6J mice at the age of about one month. Briefly, mice were anesthetized by intraperitoneal injection of a mixture of 120 mg/kg ketamine and 15 mg/kg xylazine. Under a dissecting microscope, a small perforation was made in the temporal sclera region with a sharp needle. Viral vectors at a concentration of ~5 x 10^{12} vg/mL were co-injected with saline or proteasome inhibitor solutions into the intravitreal space through the perforation with a 10 µl Hamilton syringe with a 32-gauge blunt-point needle. Each eye was injected bout 1.5 µl injection solution. In the control group, AAV virus was co-injected with saline only. The injection solution preparation containing AAV virus and different proteasome inhibitors is listed in Table 1. To eliminate the selection bias, each mouse was given 2 different treatments at the same time--virus with one dose of the drug was injected in the left eye, and another dose was injected in the right eye. The dose ranges of the drugs were chosen based on previous research (Yan et al., 2002; Yan et al., 2004; Zhang et al., 2009a).The expression was examined about 1 month and 3 months after the viral injection.

Quantitative fluorescence and cell density measurements

Mice were deeply anesthetized with CO2 asphyxiation followed by decapitation. Eyecups were fixed in 4% paraformaldehyde in 0.1 M phosphate buffer (PB) for 20

minutes. Retinas were dissected in PB solution, flat mounted on slides, and coverslipped. Images were acquired using a Zeiss Axio Imager 2 microscope with an Apotome 2 oscillating grating to reduce out-of-focus stray light (Apotome; Carl Zeiss Microscopy GmbH, Jena, Germany). Image projections were constructed by collapsing individual z-stacks of optical sections onto a single plane in ZEN software (Carl Zeiss). Since transgene expression was not always evenly distributed throughout the retina (peripheral area better than center area), images taken from the peripheral area (~2 mm from the optic disc) were used for comparison. In each retina, 8-10 images (at 40X magnification) were taken under the Zeiss Axio Imager 2 microscope. For the purpose of comparing the mCherry transgene expression in the retinal bipolar cells, images were taken from whole-mount retina at the inner nuclear layer without mCherry antibody enhancement under the same fixed exposure time.

Quantifications for fluorescent intensity and cell density were performed using ImageJ software (NIH). The fluorescent intensity was measured as optical density. The 'Image – Adjust – Auto Threshold' function of the software was used to select the cells (the method "mean" was used to set the auto threshold). The 'Analyze – Measure' function was used to obtain the Area of the cells (total area of the cells in each image, measured in square pixels) and the Integrated Density (IntDen). The average fluorescence intensity was calculated as IntDen/Area (Zhao et al., 2014). The fluorescence intensity was displayed as the mean ± SD of the average fluorescence intensity of all measured cells. The number of retinas examined was displayed as "n" on each column in the histogram. The plot profile figures were generated from ImageJ software. The bipolar cell density

was compared as the mean ± SD of the cell number within an image region of 0.0369 mm^2 (at inner nuclear layer, 40X magnification).

Immunohistochemistry

For immunostaining of whole-mount retinas, the retinas were incubated for 2 hrs in a block solution containing 5% ChemiBLOCK (Millipore Corp., Bedford, MA, USA), 0.5% Triton X-100 and 0.05% sodium azide (Sigma-Aldrich, St. Louis, MO, USA). The primary antibody used in this study was goat anti-mCherry (1:2000; Biorbyt, Cambridge, UK). The secondary antibody was conjugated to Alexa 555 (1:1000). The primary antibody was diluted in the same solution and applied for two days at room temperature (RT). The retinas were then washed several times, followed by incubation in the secondary antibody for one day at RT.

MIXED SOLUTION: EACH MOUSE EYE WAS INJECTED WITH 1.5 μL				
AAV virus [C] in the mixed solution: $5x10^{12}$ vg/mL				
Proteasome inhibitor	**Dose 1 in the mixed solution (μM)**	**Dose 2 in the mixed solution (μM)**	**Dose 3 in the mixed solution (μM)**	**Dose 4 in the mixed solution (μM)**
Doxorubicin	200	300	500	800
Aclarubicin	50	100		
MG132	100	200	500	

Table 1: Preparation of the injection solutions containing AAV virus and proteasome inhibitors

2.4 Results

I examined three proteasome inhibitors, doxorubicin, aclarubicin, and MG132, on AAV-mediated transduction efficiency in retinal bipolar cells in C57BL/6J mice. I first examined the effect of the proteasome inhibitors on the expression level of mCherry in bipolar cells one month after virus injection. My results show that doxorubicin at the

concentration of 300-800 μM improved the expression of mCherry with the most effective concentration at 300 μM (Figure 11a-e). At the concentration of 300 μM, 500 μM, and 800 μM, doxorubicin increased the intensity of mCherry by 68.2%, 32.4%, and 31.7%, respectively (Figure 11u). On the other hand, no significant effect was observed for aclarubicin (50 μM, 100 μM) and MG132 (100 μM, 200 μM, 500 μM) (Figure 11f-j, u). Figure 11k-t are the plot profiles of Figure11a-j. Interestingly, the single cells that represent the maximum mCherry expression level in each group treated with doxorubicin 200-800 μM actually displayed similar pixel intensities (Figure 11l-o). The differences of the mean fluorescence intensities in these groups (Figure 11b-e, u) seemingly correlate with the number of bipolar cells that have high mCherry expression levels (Figure 11l-o). Therefore, I counted the number of bipolar cells that have a mCherry expression level above 0.05 RFU/pixel^2 within an image region of 0.0369 mm^2 in retinas 1 month after being treated with AAV virus with or without different proteasome inhibitors. I set 0.05 RFU/pixel^2 as the threshold according to the maximum single cell fluorescence intensity in the control. For example, in Figure 11k, the fluorescence intensity of the best-expressing cell is between 0.05-0.10 RFU/pixel^2; therefore, a threshold of 0.05 can just include the cells that have high expression. My results show that the density of bipolar cells with a mCherry expression above 0.05 RFU/pixel^2 in retinas treated with AAV and 300, 500, or 800 μM doxorubicin was 24.3, 15.8, or 10.4 times higher compared with that in retinas treated with AAV alone; while retinas treated with AAV and 200 μM doxorubicin did not show a statistical difference (Figure 11v). Since doxorubicin is a fluorescent molecule (Motlagh et al., 2016), I also injected 4 eyes with 300 μM doxorubicin only for

control, and the result showed that red fluorescence was not due to the effect of doxorubicin itself (Figure 12).

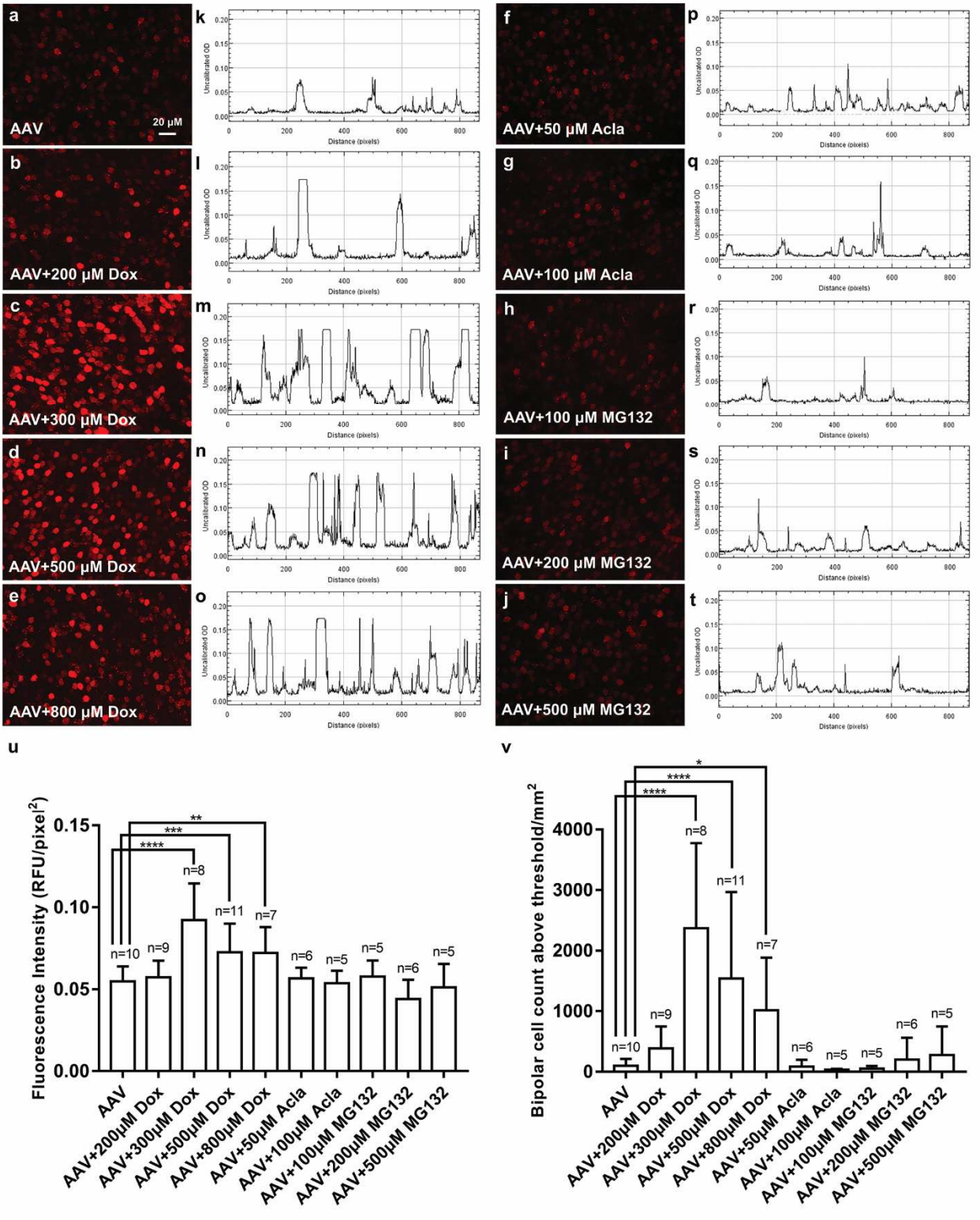

Figure 11: Comparison of AAV-mediated transduction efficiency in the mouse retinas 1 month after being treated with AAV virus with or without proteasome inhibitors. (a-j) whole-mount fluorescence images acquired at the INL without immunofluorescence enhancement. (k-t) plot profiles of image a-j. The plot profile displays a two-dimensional graph of the intensities of pixels along a random horizontal line across the image. The x-axis represents distance (in pixels) along the line, and the y-axis is the pixel intensity. (u) comparison of fluorescence intensities of the mCherry-expressing retinal bipolar cells treated with AAV virus with or without proteasome inhibitors. (v) cell densities of the retinal bipolar cells that have an mCherry expression level above 0.05 RFU/pixel^2. The data is shown as mean ± SD. The n represents the number of retinas being examined. The asterisk indicates statistically significant differences with *p<0.05, **p<0.01, ***p<0.001, ****p<0.0005 (one-way ANOVA).

Figure 12: whole-mount fluorescence image acquired at the INL in the retina 1 month after being treated with 300 µM doxorubicin.

1st injection		2nd injection (8 hours after 1st injection)	
Injection solution contains AAV virus and doxorubicin; each mouse eye was injected with 1.5 µL		Injection solution contains doxorubicin; each mouse eye was injected with 1.5 µL	
AAV virus [C] in the injection solution	$5x10^{12}$vg/mL	Doxorubicin [C] in the injection solution	500 µM
Doxorubicin [C] in the injection solution	500 µM		

Table 2: Schedule of the one-time and two-time injection of 500 µM doxorubicin

Since doxorubicin was cleared from the retinas within 8 hours after intravitreal injection in the rabbit eyes (Hu et al., 2007), I injected doxorubicin in the mouse eyes twice with an 8-hour interval to examine its effect in improving AAV-mediated transduction

efficiency in the retina (Table 2). There was no observable damage to the mouse eyes with two injections with an 8-hour interval. The fluorescence intensity was increased by 32.4% and 43.1% after injection of 500 μM doxorubicin and after adding a booster dose of 500 μM doxorubicin compared to the control (Figure 13a-c, g). There is no statistical difference between the fluorescence intensity in retinas treated with one-time and two-time 500 μM doxorubicin (Figure 13g). Figure 13d-f are the plot profiles of Figure13a-c. Figure13h shows the number of bipolar cells that have a mCherry expression level above 0.05 RFU/pixel^2 within an image region of 0.0369 mm^2 in retinas 1 month after being treated with AAV virus alone, AAV with one-time 500 μM doxorubicin, and AAV with two-time 500 μM doxorubicin. The density of bipolar cells with a mCherry expression above 0.05 RFU/pixel^2 in retinas treated with AAV with one-time 500 μM doxorubicin and AAV with two-time 500 μM doxorubicin was 15.8 and 12.6 times higher than that in retinas treated with AAV alone (Figure 13h). The two treatment groups have no statistical difference with each other in terms of the bipolar cell density (Figure 13h).

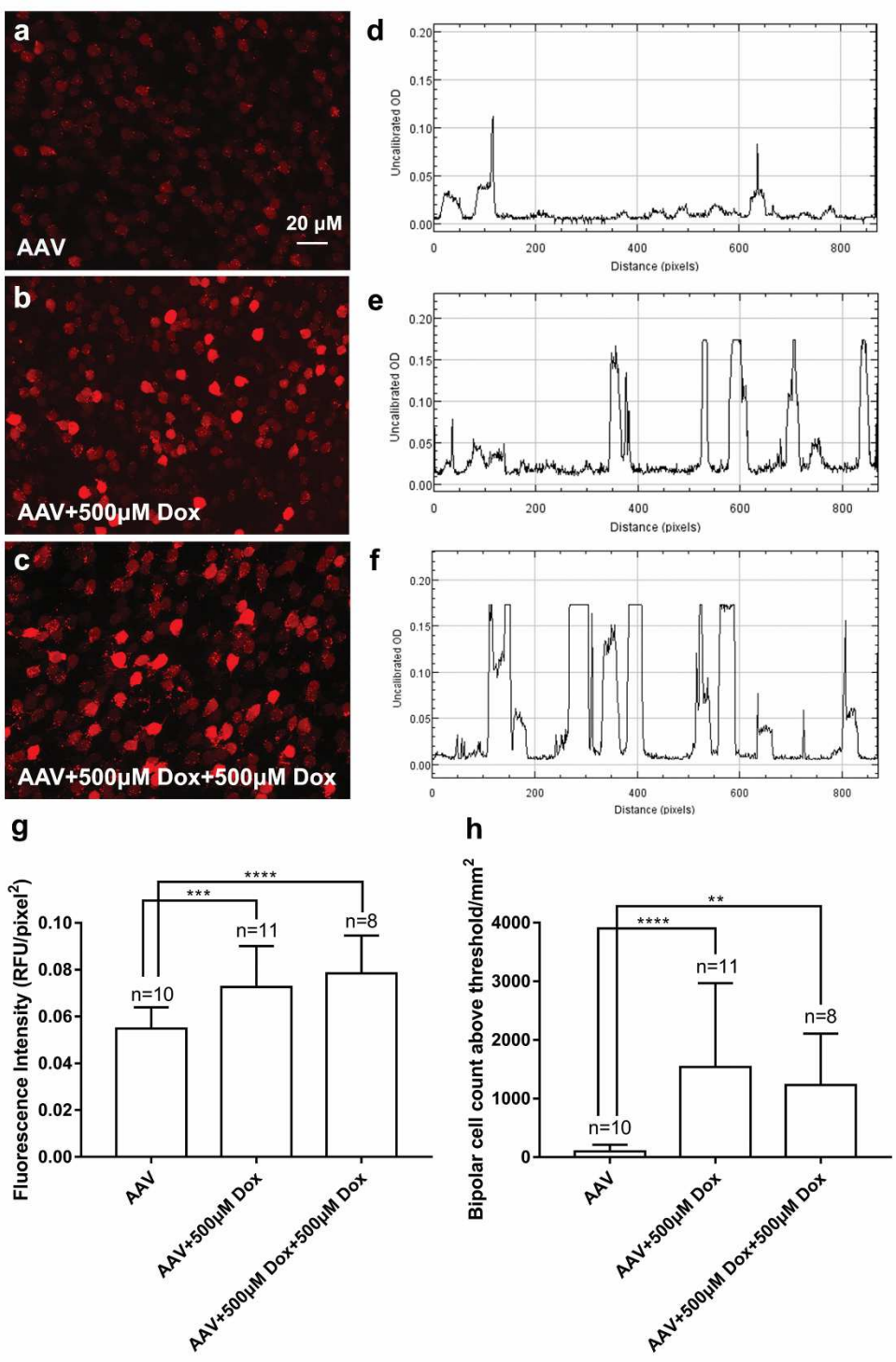

Figure 13: Comparison of AAV-mediated transduction efficiency in the mouse retinas 1 month after being treated with AAV virus with or without a booster dose of 500 μM doxorubicin. (a-c) whole-mount fluorescence images acquired at the INL without immunofluorescence enhancement. (d-f) plot profiles of image a-c. The plot profile displays a two-dimensional graph of the intensities of pixels along a random horizontal line across the image. The x-axis represents distance (in pixels) along the line, and the y-axis is the pixel intensity. (g) comparison of fluorescence intensities of the mCherry-expressing retinal bipolar cells treated with AAV virus with or without a booster dose of 500 μM doxorubicin. (h) cell densities of the retinal bipolar cells that have an mCherry expression level above 0.05 RFU/pixel^2. The data is shown as mean ± SD. The n represents the number of retinas being examined. The asterisk indicates statistically significant differences with **p<0.01, ***p<0.001, ****p<0.0005 (one-way ANOVA).

Furthermore, I tested the effect of doxorubicin three months after virus injection. The results showed that doxorubicin maintained its effect on enhancing the AAV transduction efficiency in retinal bipolar cells in the 3-month duration in a dose dependent manner (Figures 14a-d). At the concentration of 200 μM, 300 μM, and 500 μM, doxorubicin increased the mCherry intensity by 25.8%, 40.2%, and 47.9%, respectively (Figure 14i). Figures 14e-h represent the plot profiles of Figures 14a-d. Figure14j shows the number of bipolar cells that have a mCherry expression level above 0.05 RFU/pixel^2 within an image region of 0.0369 mm^2 in retinas 3 months after being treated with AAV virus with or without different doses of doxorubicin. After co-administration of AAV virus with 300 μM and 500 μM doxorubicin, the density of bipolar cells with a mCherry expression above 0.05 RFU/pixel^2 was 2.2 and 3.0 times higher than administration of AAV alone (Figure 14j).

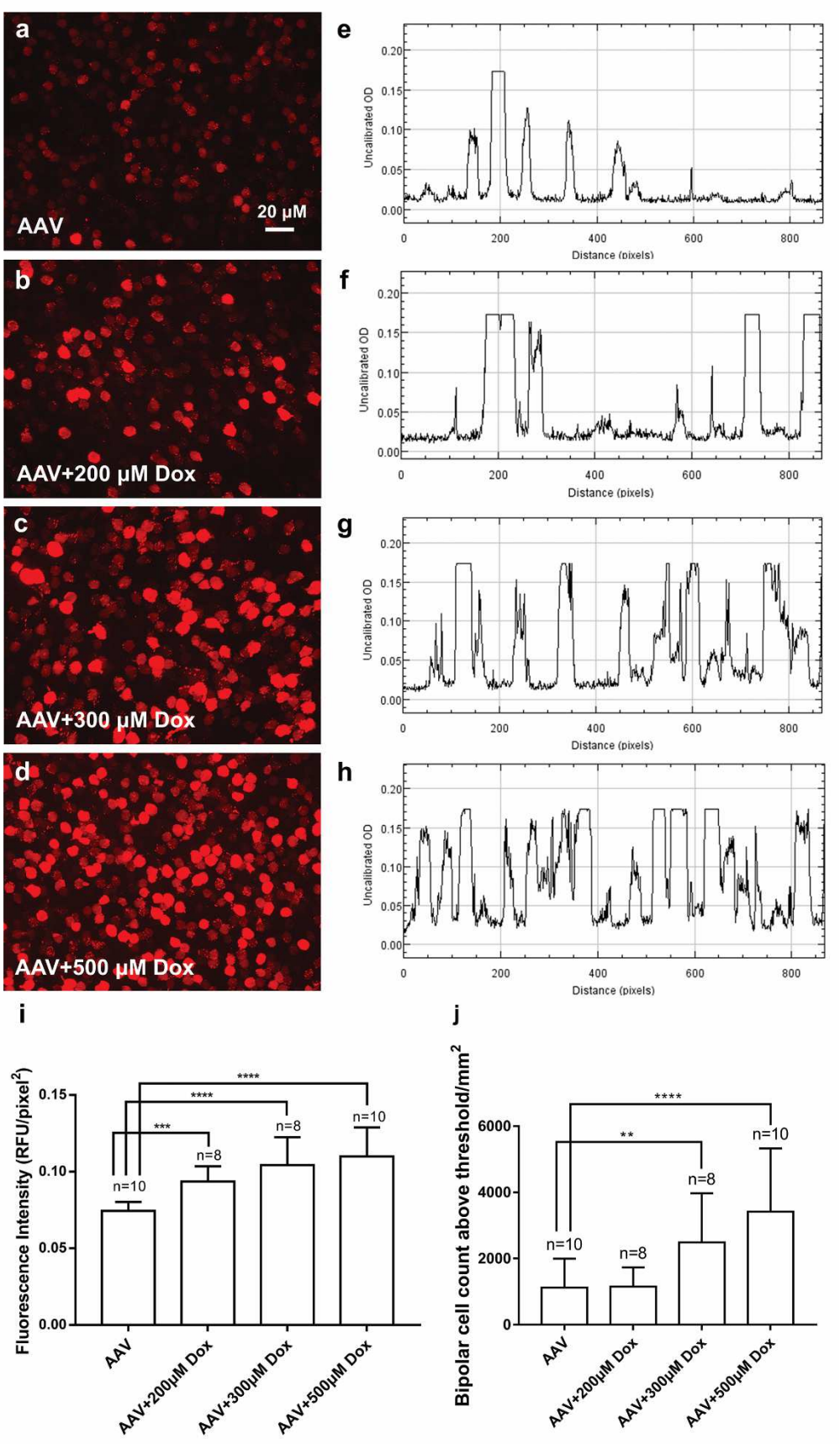

Figure 14. Comparison of AAV-mediated transduction efficiency in the mouse retinas 3 month after being treated with AAV virus with or without doxorubicin. (a-d) whole-mount fluorescence images acquired at the INL without immunofluorescence enhancement. (e-h) plot profiles of image a-d. The plot profile displays a two-dimensional graph of the intensities of pixels along a random horizontal line across the image. The x-axis represents distance (in pixels) along the line, and the y-axis is the pixel intensity. (i) comparison of fluorescence intensities of the mCherry-expressing retinal bipolar cells treated with AAV virus with or without doxorubicin. (j) cell densities of the retinal bipolar cells that have an mCherry expression level above 0.05 RFU/pixel^2. The data is shown as mean ± SD. The n represents the number of retinas being examined. The asterisk indicates statistically significant differences with **p<0.01, ***p<0.001, ****p<0.0005 (one-way ANOVA).

As stated above, doxorubicin can increase the number of bipolar cells that have a high transgene expression level. However, whether doxorubicin could affect the number of all the AAV-transduced bipolar cells is unknown. Therefore, I counted all the transduced bipolar cells within an image region of 0.0369 mm^2 in retinas 1 month and 3 months after being treated with AAV virus with or without different doses of doxorubicin. To better display all the mCherry-expressing bipolar cells, the retinas were immunostained with antibody against mCherry (images are not shown). The results show that the application of doxorubicin did not alter the density of the transduced bipolar cells (Figure 15a-b).

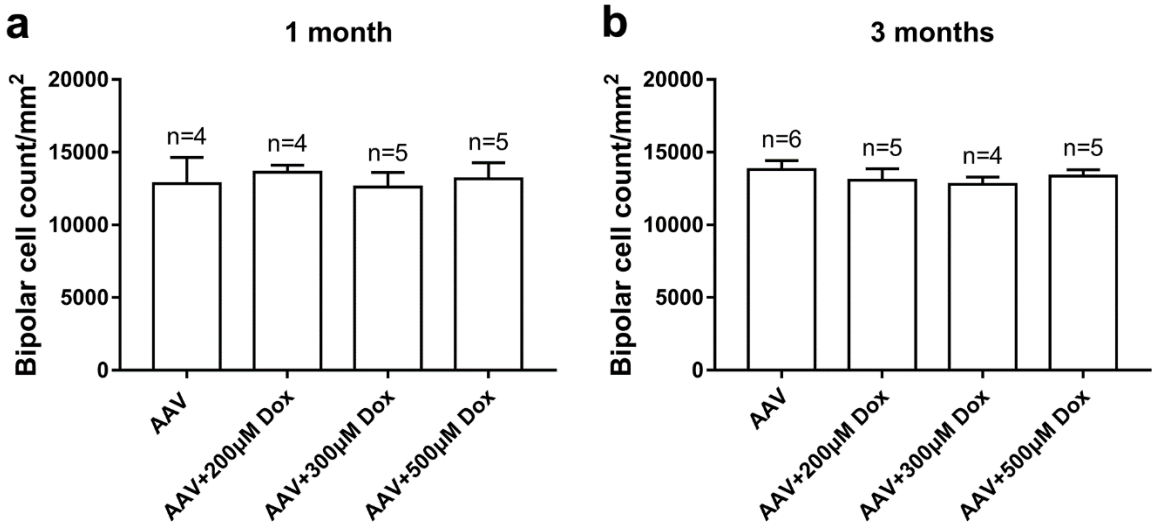

Figure 15. Comparison of bipolar cell densities in the mouse retinas 1 month and 3 months after being treated with AAV virus with or without doxorubicin. (a) comparison of AAV-transduced bipolar cell densities in the mouse retinas 1 month after being treated with AAV virus with or without doxorubicin. (b) comparison of AAV-transduced bipolar cell densities in the mouse retinas 3 months after being treated with AAV virus with or without doxorubicin. The data is shown as mean ± SD. The n represents the number of retinas being examined. The transduced bipolar cells with mCherry expression were immunostained with antibody against mCherry before counting.

2.5 Discussion

In this study, I evaluated the effect of three proteasome inhibitors, doxorubicin, aclarubicin and MG132 on AAV-mediated transduction efficiency in retinal bipolar cells in mice. Consistent with previous studies performed both in non-neuronal cells as well as in neuronal cells *in vitro* and *in vivo* (Yan et al., 2004; Zhang et al., 2009a), my results show that doxorubicin can also enhance AAV-mediated transduction efficiency in retinal bipolar cells *in vivo* (Figure 11u). Thus, this study suggests the potential value for the use of doxorubicin for facilitating the AAV-mediated transduction efficiency in retinal gene therapy. On the other hand, surprisingly, I failed to observe such an effect for aclarubicin and MG132 in retinal bipolar cells (Figure 11u) although both aclarubicin and MG132 were reported to augment AAV2 transduction in non-neuronal cells. However, it should be noted that neither aclarubicin nor MG-132 have been previously evaluated in neuronal cells. Therefore, the lack of effect of aclarubicin and MG132 could be due to a difference between neuronal and non-neuronal cells. It might also be due to a drug metabolism issue in the mouse eye. Further studies would be interesting to investigate the underlying mechanism for such a discrepancy.

Although the dose-dependent effect of doxorubicin was reported in neuronal cell lines and primary neuron cultures (Zhang et al., 2009a), in this study I examined the dose-dependent effect of doxorubicin in retinal neurons *in vivo*. My results show that the ability

of doxorubicin to enhance the AAV transgene expression in retinal bipolar cells appears to be both dose-dependent and time-dependent. Specifically, the transgene expression level peaked at the concentration of 300 μM in the short-term (1 month after treatment) and 300-500 μM in the long-term (3 months after treatment) (Figure 11u and 14i). The mCherry expression level in retinas treated with AAV alone or with 200 μM or 500 μM doxorubicin 3 months after injection was increased compared with that in retinas treated with same regimen 1 month after injection; while the mCherry expression level in retinas treated with 300 μM doxorubicin had no significant difference between 1 month and 3 months after virus injection (Figure 11u and 14i). It is likely that the AAV transgene expression in retinal bipolar cells did not reach its maximum level 1 month after viral delivery, which explains that in the control group (AAV alone), the mCherry expression level 3 months after injection was higher than 1 month after injection. Since there is no statistic difference between the mCherry intensities in retinas treated with 300 μM and 500 μM doxorubicin 3 months after virus injection (Figure 14i), suggesting that the effect of doxorubicin has reached the maximum level; the lack of increase in mCherry intensity in retinas treated with 300 μM doxorubicin from 1 month to 3 months after virus injection might be due to the effect of doxorubicin already reached the maximum level 1 month after virus injection.

Figures 11k-o and Figures 14e-h are the plot profiles of Figures11a-e and Figures14a-d, respectively. The single cells that represent the maximum mCherry expression level in each group treated with AAV with or without doxorubicin actually displayed similar pixel intensities (Figures 11k-o, Figures 14e-h). Consistent with the mean fluorescence intensities (Figure 11u, Figure 14i), the density of bipolar cells with a

mCherry expression above 0.05 RFU/pixel^2 was increased in retinas treated with 300 μM, 500 μM, and 800 μM doxorubicin 1 month after virus injection (Figure 11v), and was increased in retinas treated with 300 μM and 500 μM doxorubicin 3 months after virus injection (Figure 14j). These results suggest that doxorubicin increased the AAV transduction efficiency in retinal bipolar cells by increasing the number of cells that are able to reach high transgene expression level. Moreover, Figure 15 showed that application of doxorubicin did not alter the density of the AAV-transduced bipolar cells 1 month and 3 months after virus injection. Together, my results indicate that doxorubicin increased AAV transduction efficiency not by increasing the number of cells transduced by AAV virus, but by increasing transgene expression in the transduced bipolar cells. These results are consistent with the working mechanism of doxorubicin, which facilitates the AAV virus intracellular trafficking process, while has no effect in changing the AAV virus cell entry process.

In conclusion, my results indicate that doxorubicin but not aclarubicin and MG132 is effective in enhancing AAV transduction efficiency in retinal bipolar cells in mice. Since doxorubicin is a proteasome inhibitor that blocks the intracellular degradation of virus vectors, my experimental results validate my hypothesis that virus degradation during intracellular trafficking is one of major limiting factors for the low AAV transduction efficiency in retinal bipolar cells.

CHAPTER 3. EVALUATION OF THE DOXORUBICIN-INDUCED TOXICITY TO THE MOUSE EYES

3.1 Hypothesis

Doxorubicin-mediated free radical generation would cause toxicity to the mouse retina and lens following intravitreal injection.

3.2 Rationale

Doxorubicin was previously reported to induce neurotoxicity to rat cortical neurons (Lopes et al., 2008). One mechanism of doxorubicin-induced cell damage is the formation of the drug-iron complex which catalyzes the formation of hydroxyl radical and causes DNA damage (Muindi et al., 1984). Dexrazoxane (Zinecard) is a FDA-approved drug that is used to reduce the anthracycline-induced cytotoxicity. The active form of dexrazoxane is similar to EDTA, which chelates iron and limits the formation of anthracycline-iron complexes, and therefore reduces the generation of free radicals and the subsequent oxidative damage to cells (Ichikawa et al., 2014; Langer, 2014). Therefore, I also tested the short-term and long-term cytotoxicity that doxorubicin induced in the retina, as well as the antidote effect of dexrazoxane on retinal neurons treated with doxorubicin.

3.3 Experimental design and method

Animals and materials

Described in chapter 2.2 except the following. Dexrazoxane was purchased from Abcam, Cambridge, MA.

Virus injection

Described in chapter 2.2 except the following. The injection solution preparation containing AAV virus, doxorubicin, and dexrazoxane is listed in Table 3.

Immunohistochemistry

Described in chapter 2.2 except the following. The primary antibodies used in this study were: goat anti-mCherry (1:2000; Biorbyt, Cambridge, UK), mouse anti-PKC (1:500; Santa Cruz, Dallas, Texas, USA). The secondary antibodies were conjugated to Alexa 555 (1:1000), or Alexa 488 (1:500). The primary antibodies were diluted in the same solution and applied for two days at room temperature (RT). The retinas were then washed several times, followed by incubation in the secondary antibodies for one day at RT. Nuclei were stained with DAPI (1: 2.8ml; Sigma-Aldrich, St. Louis, MO); the retinas were incubated for 30 min in the DAPI solution.

For immunostaining of retinal vertical sections, the retinas were cryoprotected in graded sucrose (10%, 20%, and 30% wt/vol, respectively, in PB) and cut at 16 µm. The following primary antibodies were used in this study: goat anti-mCherry (1:2000; Biorbyt, Cambridge, UK), mouse anti-PKC (1:500; Santa Cruz, Dallas, Texas, USA). The secondary antibodies were conjugated to Alexa 555 (1:1000), or Alexa 488 (1:500). The retinal sections were incubated for 1 hr in the block solution. The primary antibodies were diluted in the same solution and applied overnight at RT, followed by incubation for 2 hrs in the secondary antibodies. Nuclei were stained with DAPI (1: 2.8ml; Sigma-Aldrich, St. Louis, MO); the retinal sections were incubated for 3 min in the DAPI solution.

Quantitative fluorescence and cell density measurements

Described in chapter 2.2. For measurement of the cell density, 12 images (at 20X magnification) were taken evenly throughout each retina at the ganglion cell layer (GCL). The cell density at the GCL was compared as the mean ± SD of the cell number within an image region of 0.1476 mm² (at 20X magnification).

MIXED SOLUTION: EACH MOUSE EYE WAS INJECTED WITH 1.5 μL				
AAV virus [C] in the mixed solution: $5x10^{12}$ vg/mL				
	Doxorubicin		Dexrazoxane	
	[C] in the mixed solution (μM)	[C] in the mixed solution (mg/mL)	[C] in the mixed solution (mg/mL)	[C] in the mixed solution (μM)
Dose 1	200	0.12	1.12	3336
Dose 2	300	0.17	1.74	5245
Dose 3	500	0.29	2.90	8741

Table 3: Preparation of the injection solutions containing AAV virus, doxorubicin, and dexrazoxane.

3.4 Results

3.4.1 Higher doses of doxorubicin lead to long-term cytotoxicity in the retina

Previous studies reported that doxorubicin could induce neurotoxicity to rat cortical neurons (Lopes et al., 2008). Therefore, I went on to examine whether the co-application of doxorubicin could produce cytotoxicity to the retinal neurons. I first evaluated the dose-dependent effect of doxorubicin on the survival of the cells at the GCL by measuring their density one and three months after co-injection of AAV2 virus vectors and doxorubicin. My results showed that the density of the cells as labeled by DAPI remained unchanged 1 month after virus injection with doxorubicin treatment (Figure 16), but decreased by 28.5% and 29.9% 3 months after the treatment with 300 and 500 doxorubicin, respectively (Figure 17).

I also evaluated the effect of doxorubicin and its potential toxicity to other retinal neurons by measuring the thickness of the outer nuclear layer (ONL) and the inner nuclear layer (INL) together with the inner plexiform layer (IPL) 3 months after doxorubicin treatment. For this purpose, the retinas were stained with DAPI (blue color) and rod

bipolar cells were labeled with antibody against PKC (green color). My results show that the thickness of the ONL did not change significantly (Figure 18a-e). In contrast, the thickness of the INL+IPL decreased by 19.0% and 30.8% 3 months after exposure to 300 and 500 μM doxorubicin, respectively (Figure 18a-d, and f). The thickness of the INL+IPL in retinas exposed to 500 μM doxorubicin decreased by 14.5% compared with those exposed to 300 μM doxorubicin (Figure 18f). Together, these results indicate that doxorubicin at higher concentrations (≥300 μM) is toxic to inner retinal neurons in the long term.

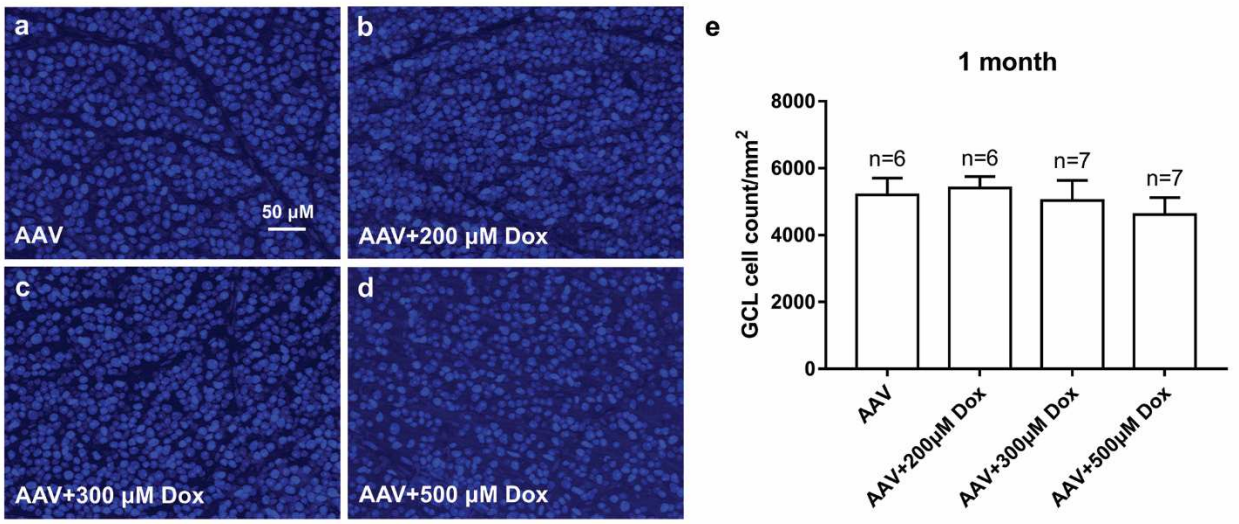

Figure 16. Comparison of the cell densities in the GCL 1 month after being treated with AAV virus with or without doxorubicin. (a-d) whole-mount images acquired at the GCL with DAPI staining. (e) comparison of cell densities in the mouse retinal GCL 1 month after being treated with AAV virus with or without doxorubicin. The data is shown as mean ± SD. The n represents the number of retinas being examined.

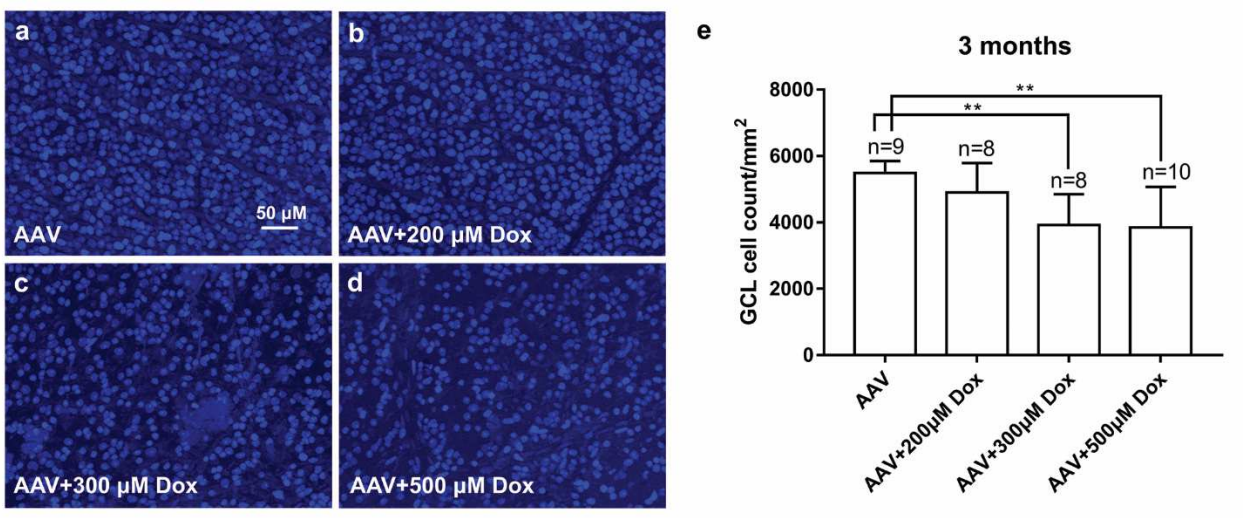

Figure 17. Comparison of the cell densities in the GCL 3 months after being treated with AAV virus with or without doxorubicin. (a-d) whole-mount images acquired at the GCL with DAPI staining. (e) comparison of cell densities in the mouse retinal GCL 3 months after being treated with AAV virus with or without doxorubicin. The data is shown as mean ± SD. The n represents the number of retinas being examined. The asterisk indicates statistically significant differences with **p<0.01 (one-way ANOVA).

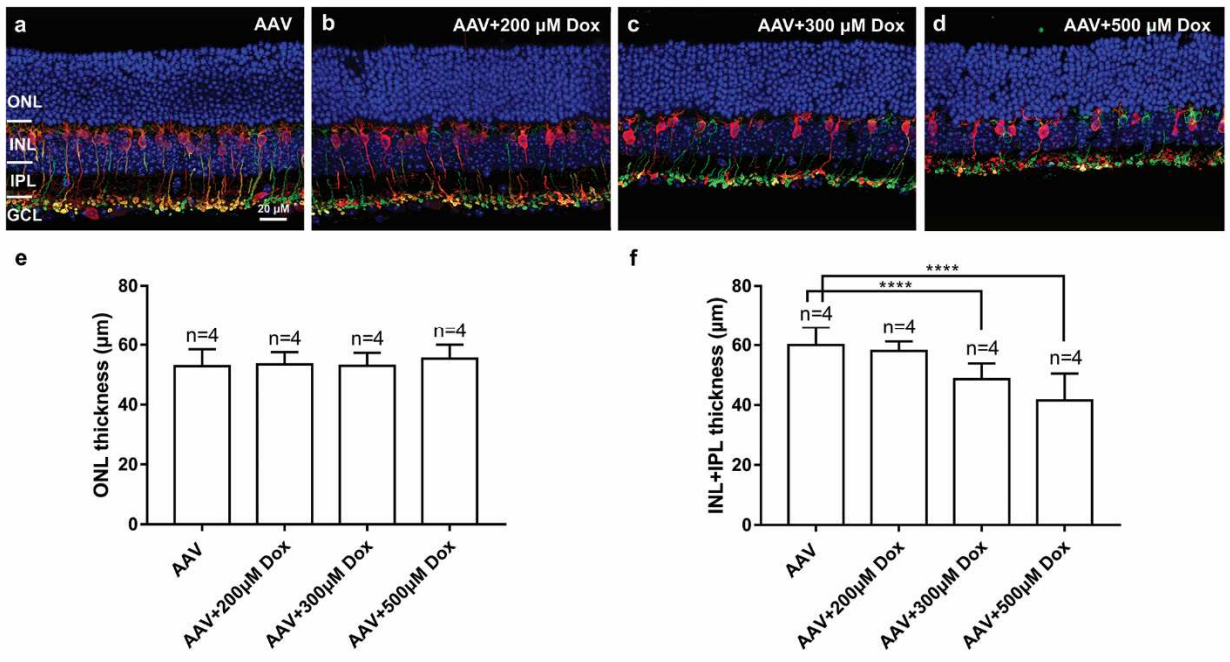

Figure 18. Comparison of ONL and INL+IPL thickness in the mouse retinas 3 months after being treated with AAV virus with or without doxorubicin. (a-d) retinal vertical sections with DAPI staining and immunostaining with antibodies against mCherry and PKC. (e) comparison of ONL thickness and (f) INL+IPL thickness in the mouse retinas 3 months after being treated with AAV virus with or without doxorubicin. The data is shown as mean ± SD. The n represents the number of retinas being examined. The asterisk indicates statistically significant differences with ****p<0.0005 (one-way ANOVA). ONL: outer nuclear layer; INL: inner nuclear layer; IPL: inner plexiform layer; GCL: ganglion cell layer.

3.4.2 Co-administration of dexrazoxane and doxorubicin prevented the doxorubicin-induced neurotoxicity

Next, I went on to examine the possible effect of dexrazoxane against the doxorubicin-induced neurotoxicity in retinal neurons. For this purpose, AAV vectors were co-injected with doxorubicin and dexrazoxane. The dosage ratio of dexrazoxane to doxorubicin is 10:1, as suggested by the previous studies in mice (Imondi et al., 1996). AAV vectors co-injected with dexrazoxane served as control. My results show that the cell density of the GCL was not changed 1 month after co-injection of AAV and dexrazoxane with or without doxorubicin (Figure 19). However, there was a slight decrease (15.7%) in the cell density 3 months after co-injection of AAV and dexrazoxane with 500 μM doxorubicin (Figure 20). The thickness of the ONL and the INL+IPL remained unchanged 3 months after the co-administration of dexrazoxane (Figure 21). Additionally, there was no statistical difference in terms of the cell density of the GCL and the thickness of the ONL and the INL+IPL between retinas treated with AAV vectors alone and those co-administered with dexrazoxane (Figure 16-21). Together, these results indicate that the doxorubicin-mediated cytotoxicity was mitigated by dexrazoxane.

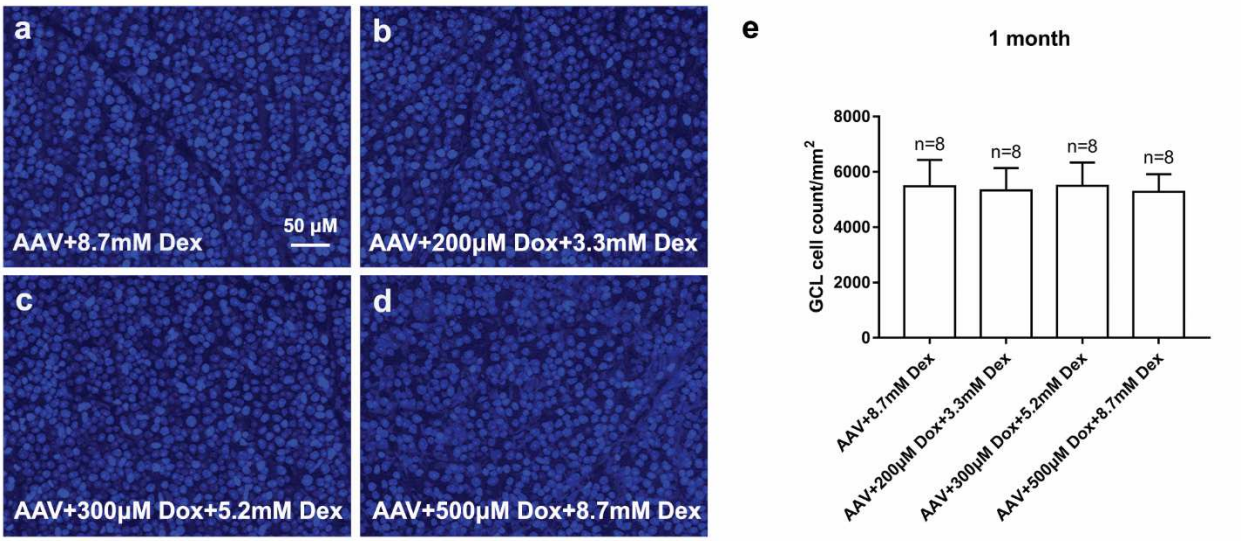

Figure 19. Comparison of the cell densities in the GCL 1 month after being treated with AAV virus and dexrazoxane with or without doxorubicin. (a-d) whole-mount images acquired at the GCL with DAPI staining. (e) comparison of cell densities in the mouse retinal GCL 1 month after being treated with AAV virus and dexrazoxane with or without doxorubicin. The data is shown as mean ± SD. The n represents the number of retinas being examined.

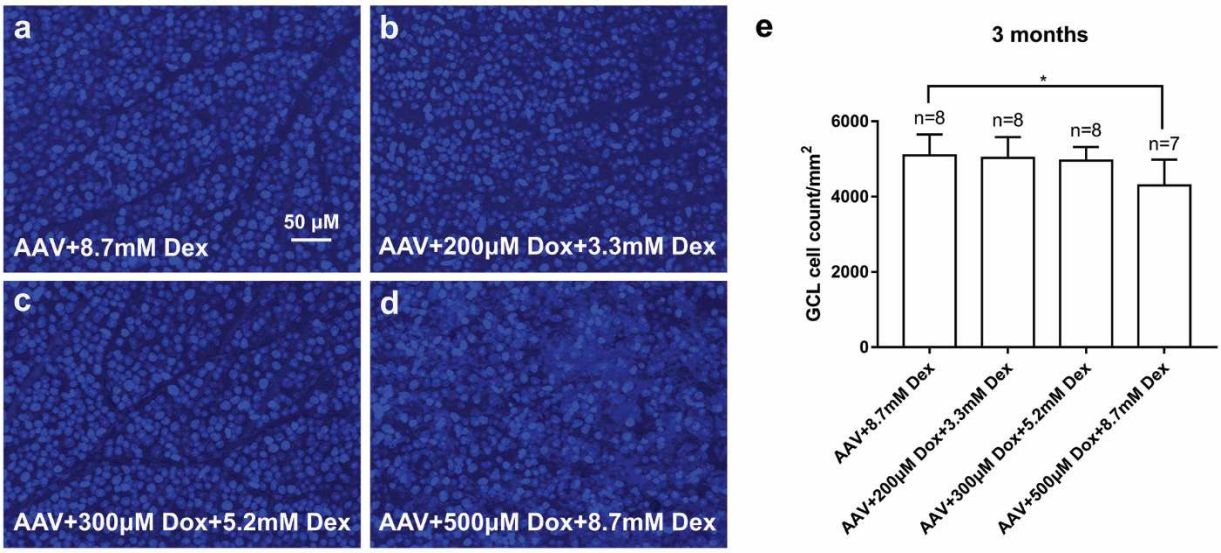

Figure 20. Comparison of the cell densities in the GCL 3 months after being treated with AAV virus and dexrazoxane with or without doxorubicin. (a-d) whole-mount images acquired at the GCL with DAPI staining. (e) comparison of cell densities in the mouse retinal GCL 3 months after being treated with AAV virus and dexrazoxane with or without doxorubicin. The data is shown as mean ± SD. The n represents the number of retinas being examined. The asterisk indicates statistically significant differences with *p<0.05 (one-way ANOVA).

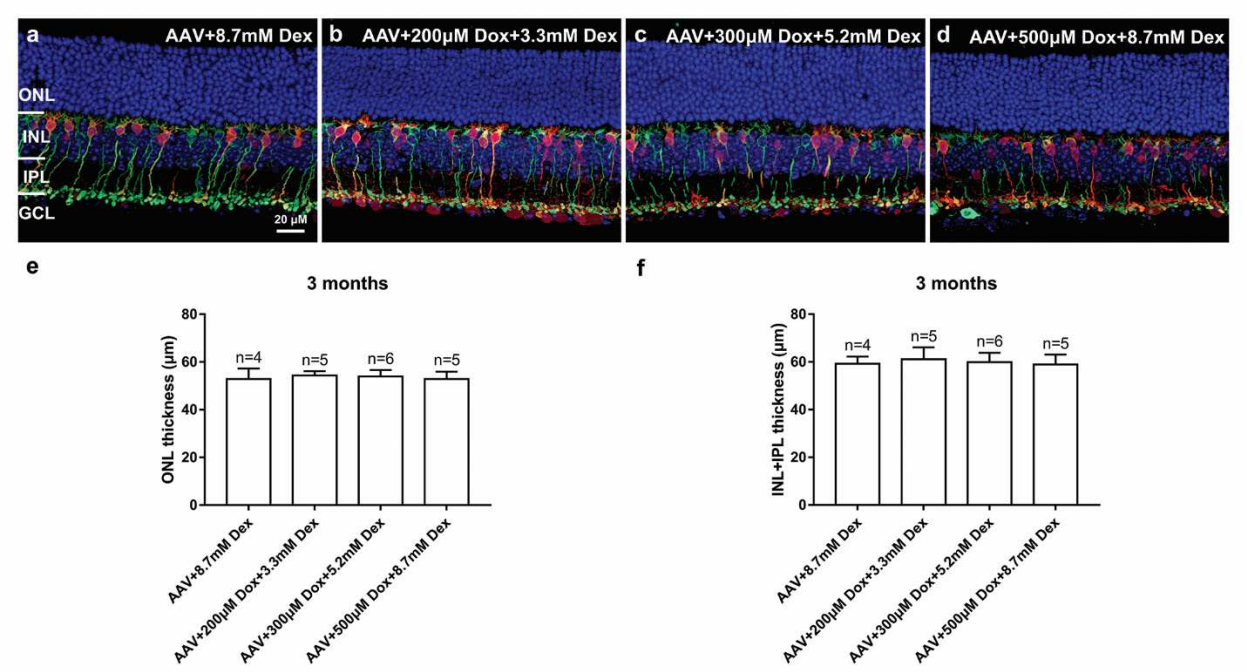

Figure 21. Comparison of ONL and INL+IPL thickness in the mouse retinas 3 months after being treated with AAV virus and dexrazoxane with or without doxorubicin. (a-d) retinal vertical sections with DAPI staining and immunostaining with antibodies against mCherry and PKC. (e) comparison of ONL thickness and (f) INL+IPL thickness in the mouse retinas 3 months after being treated with AAV virus and dexrazoxane with or without doxorubicin. The data is shown as mean ± SD. The n represents the number of retinas being examined. ONL: outer nuclear layer; INL: inner nuclear layer; IPL: inner plexiform layer; GCL: ganglion cell layer.

3.4.3 Co-administration of dexrazoxane and doxorubicin improves AAV-mediated mCherry expression

I then examined whether doxorubicin co-administered with dexrazoxane can still improve AAV-mediated transduction efficiency in bipolar cells. Again, the expression of mCherry was examined 1 month and 3 months after virus injection (Figure 22-23). The mCherry expression level in retinas treated with 200 μM, 300 μM, and 500 μM doxorubicin together with dexrazoxane was increased by 24.3%, 19.4%, and 18.9% 1 month after injection, and 48.3%, 55.1%, and 38.9% 3 months after injection, compared to that in retinas treated with dexrazoxane (Figure 22i and 23i). Interestingly, compared with injection of AAV alone, co-administration of AAV and dexrazoxane was shown to increase

mCherry expression level by 25.55% 1 month after injection (Figures 11u and 22i), while decrease mCherry expression level by 13.7% 3 months after injection (Figures 14i and 23i). Importantly, however, compared to that in retinas treated with AAV alone, the mCherry expression with the application of 200 μM, 300 μM, and 500 μM doxorubicin together with dexrazoxane was still increased by 56.1%, 49.85, and 49.26 1 month after injection, and increased by 27.9%, 33.8%, and 19.9% 3 months after injection (Figures 11u, 14i, 22i, and 23i). Another noticeable thing is that 3 months after co-injection of AAV and 500 μM doxorubicin together with dexrazoxane decreased the mCherry expression level by 19.0% compared with the regimen without dexrazoxane (Figures 14i and 23i).

Figures 22e-h and 23e-h represent the plot profiles of Figure 22a-d and 23a-d. Figures 22j and 23j show the number of bipolar cells that have a mCherry expression level above 0.05 RFU/pixel2 within an image region of 0.0369 mm^2 in retinas 1 month and 3 months after being treated with AAV virus and dexrazoxane with or without different doses of doxorubicin. 1 month after co-administration of AAV virus and dexrazoxane with 200 μM and 500 μM doxorubicin, the density of bipolar cells with a mCherry expression above 0.05 RFU/pixel2 was 7.2 and 6.0 times higher than administration of AAV with dexrazoxane (Figure 22j); again, the result was not compared with that treated with AAV alone. 3 months after co-administration of AAV virus and dexrazoxane with 200 μM and 300 μM doxorubicin, the density of bipolar cells with a mCherry expression above 0.05 RFU/$pixel^2$ was 5.0 and 7.2 times higher than administration of AAV with dexrazoxane; 3 months after co-administration of AAV virus and dexrazoxane with 500 μM doxorubicin, the density of bipolar cells with a mCherry expression above 0.05 RFU/$pixel^2$ was 1.2 times higher than administration of AAV alone (Figure 23j). Also, consistent with the

mCherry expression level, 3 months after co-administration of AAV and dexrazoxane was shown to decrease the density of bipolar cells with a mCherry expression above 0.05 RFU/pixel^2 compared with injection of AAV alone (Figure 23j).

To make sure that co-administration of dexrazoxane and doxorubicin would not change the number of AAV-transduced bipolar cells. I counted all the transduced bipolar cells within an image region of 0.0369 mm^2 in retinas 1 month and 3 months after being treated with AAV virus and dexrazoxane with or without different doses of doxorubicin. To better display all the mCherry-expressing bipolar cells, the retinas were immunostained with antibody against mCherry (images are not shown). The results show that the application of doxorubicin and dexrazoxane did not alter the density of the transduced bipolar cells (Figure 24a-b).

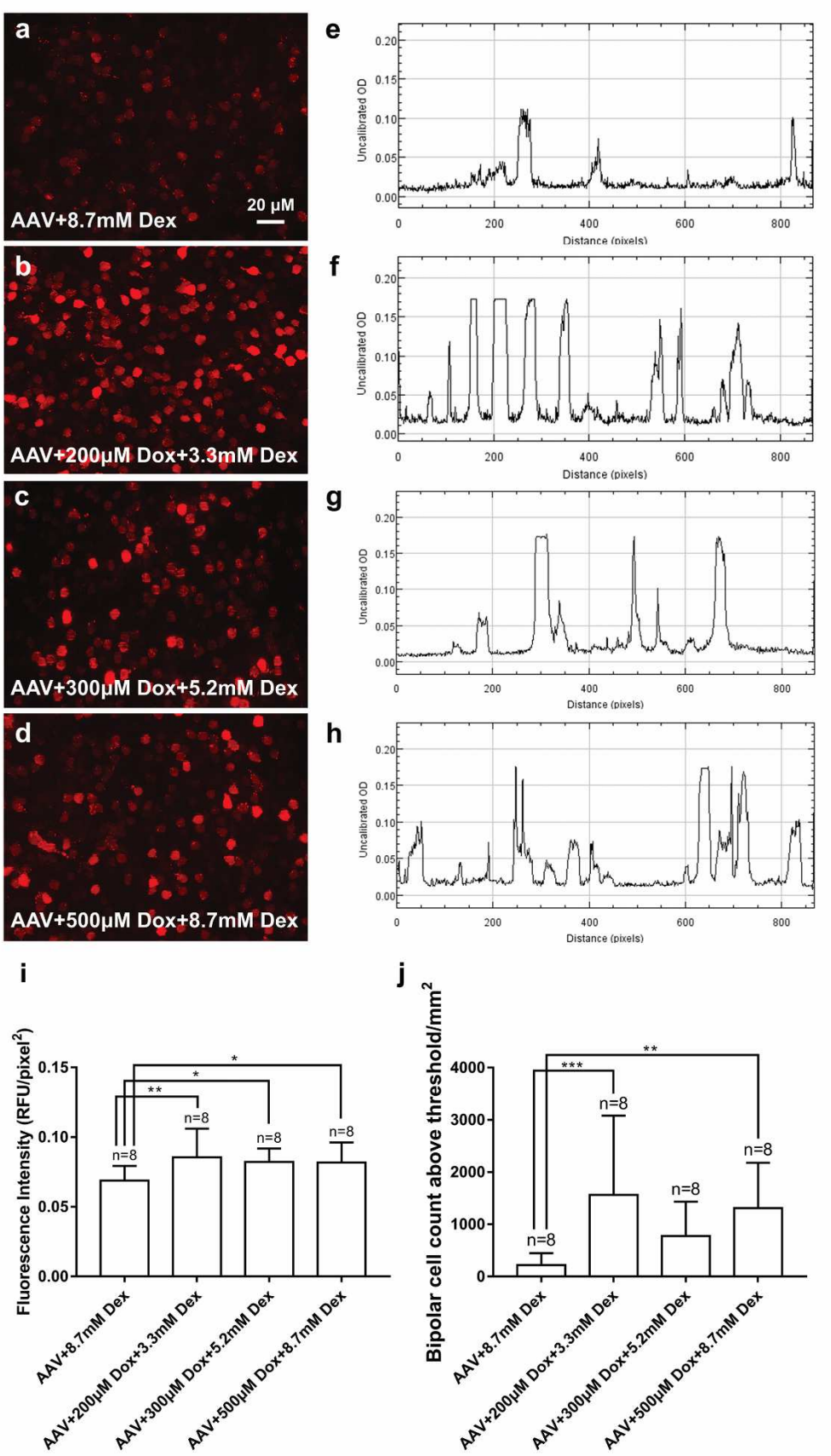

Figure 22. Comparison of AAV-mediated transduction efficiency in the mouse retinas 1 month after being treated with AAV virus and dexrazoxane with or without doxorubicin. (a-d) whole-mount fluorescence images acquired at the INL without immunofluorescence enhancement. (e-h) plot profiles of image a-d. The plot profile displays a two-dimensional graph of the intensities of pixels along a random horizontal line across the image. The x-axis represents distance (in pixels) along the line, and the y-axis is the pixel intensity. (i) comparison of fluorescence intensities of the mCherry-expressing retinal bipolar cells treated with AAV virus and dexrazoxane with or without doxorubicin. (j) cell densities of the retinal bipolar cells that have an mCherry expression level above 0.05 RFU/pixel^2. The data is shown as mean ± SD. The n represents the number of retinas being examined. The asterisk indicates statistically significant differences with *p<0.05, **p<0.01, ***p<0.001 (one-way ANOVA).

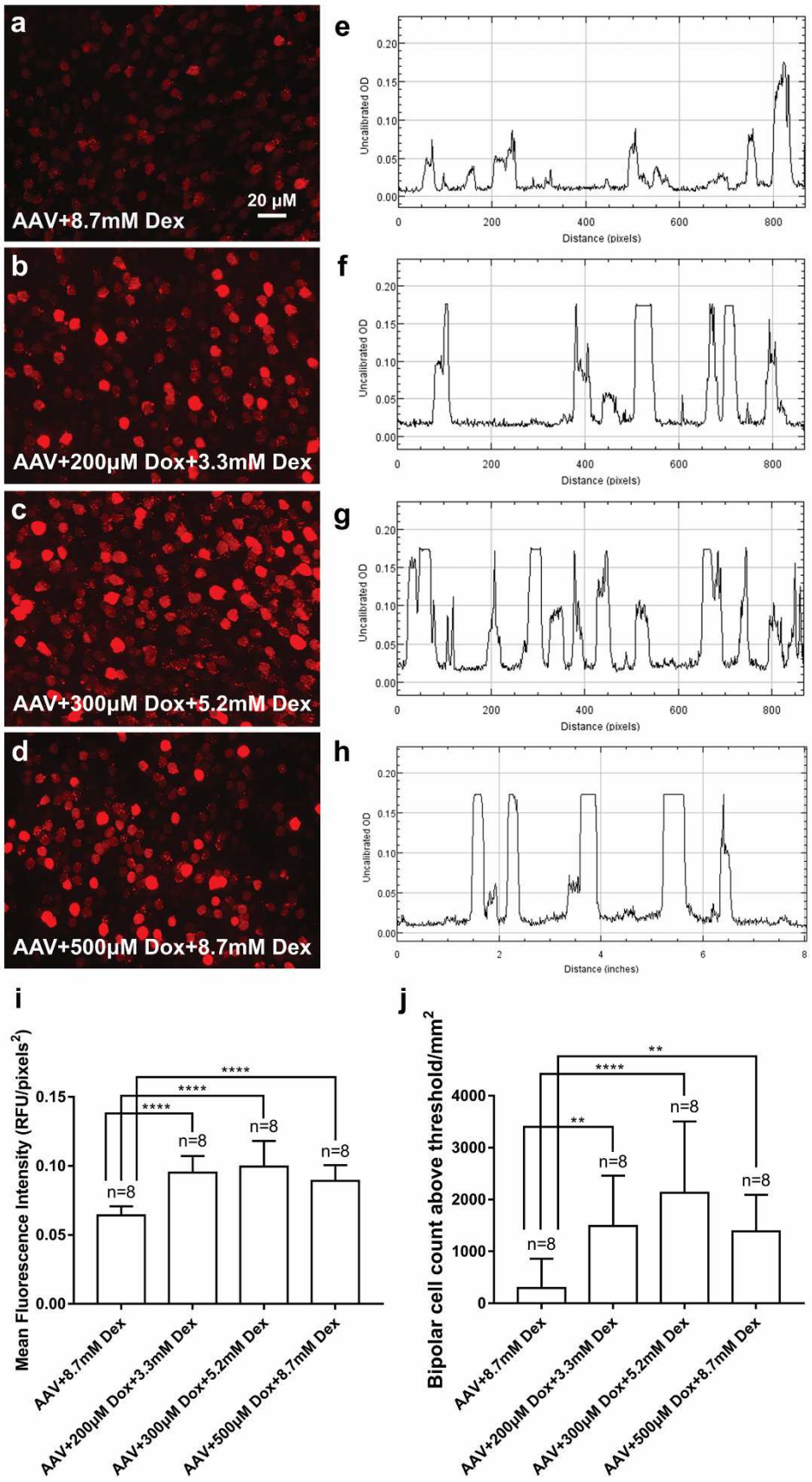

Figure 23. Comparison of AAV-mediated transduction efficiency in the mouse retinas 3 months after being treated with AAV virus and dexrazoxane with or without doxorubicin. (a-d) whole-mount fluorescence images acquired at the INL without immunofluorescence enhancement. (e-h) plot profiles of image a-d. The plot profile displays a two-dimensional graph of the intensities of pixels along a random horizontal line across the image. The x-axis represents distance (in pixels) along the line, and the y-axis is the pixel intensity. (i) comparison of fluorescence intensities of the mCherry-expressing retinal bipolar cells treated with AAV virus and dexrazoxane with or without doxorubicin. (j) cell densities of the retinal bipolar cells that have an mCherry expression level above 0.05 RFU/pixel^2. The data is shown as mean ± SD. The n represents the number of retinas being examined. The asterisk indicates statistically significant differences with **p<0.01, ****p<0.0005 (one-way ANOVA).

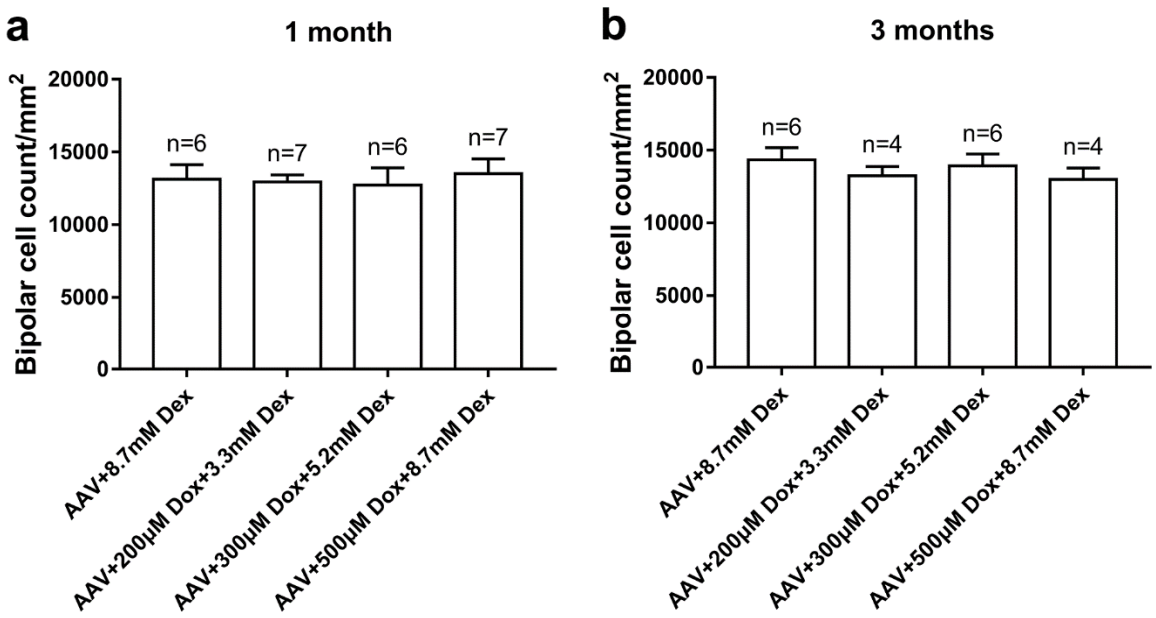

Figure 24. Comparison of bipolar cell densities in the mouse retinas 1 month and 3 months after being treated with AAV virus and dexrazoxane with or without doxorubicin. (a) comparison of AAV-transduced bipolar cell densities in the mouse retinas 1 month after being treated with AAV virus and dexrazoxane with or without doxorubicin. (b) comparison of AAV-transduced bipolar cell densities in the mouse retinas 3 months after being treated with AAV virus and dexrazoxane with or without doxorubicin. The data is shown as mean ± SD. The n represents the number of retinas being examined. The transduced bipolar cells with mCherry expression were immunostained with antibody against mCherry before counting.

3.4.4 Intravitreal injection of doxorubicin caused lens opacity in the mouse eyes

Previous research reported that intravitreal injection of doxorubicin in rabbit eyes could cause lens cataract within 2-3 months (Phylactos and Unger, 1998). To investigate

whether intravitreal injection of doxorubicin would cause lens cataract in our mouse model, I observed the mouse lens 1 month and 3 months after injection of virus with or without doxorubicin. At the end of one month following intravitreal injection of high-dose doxorubicin (500 μM), lens opacity in three out of eight mouse eyes was observed (Table 4), which started to appear around 1-2 weeks after intravitreal injection. At the end of three months following intravitreal injection, even lower doses of doxorubicin started to show lens opacity. Two out of eight mouse eyes injected with 200 μM doxorubicin appeared to have mild lens opacity, while five out of eight and nine out of ten mouse eyes injected with 300 μM and 500 μM doxorubicin showed mature lens opacity, respectively (Table 4). The slit lamp image of the lens opacity is shown in Figure 25. Since the mechanism of doxorubicin-induced cataract is due to the generation of oxygen radicals (Phylactos and Unger, 1998), and dexrazoxane was reported to reduce the production of free radicals by doxorubicin-iron complex (Langer, 2014), co-injection of doxorubicin and dexrazoxane could possibly alleviate doxorubicin-induced lens cataract. My results showed that with co-administration of dexrazoxane, three out of eight mouse eyes showed lens opacity 1 month after treatment of 500 μM doxorubicin; six out of eight mouse eyes showed lens opacity 3 months after treatment of 500 μM doxorubicin, and the mouse eyes treated with 200 μM and 300 μM doxorubicin did not have lens opacity at all 3 months after injection (Table 4).

Figure 25. Slit lamp image of the mouse eye 3 months after being treated with high concentration of doxorubicin.

1 month	Total # of eyes	# of eyes with cataract	cataract/ normal ratio	3 months	Total # of eyes	# of eyes with cataract	cataract/ normal ratio
AAV+saline	8	0	0	AAV+saline	10	0	0
AAV+Dox 200 μM	8	0	0	AAV+Dox 200 μM	8	2 (mild)	25%
AAV+Dox 300 μM	8	0	0	AAV+Dox 300 μM	8	5	62.5%
AAV+Dox 500 μM	8	3	37.5%	AAV+Dox 500 μM	10	9	90%
AAV+Dex	8	0	0	AAV+Dex	8	0	0
AAV+Dox 200μM+Dex	8	0	0	AAV+Dox 200μM+Dex	8	0	0
AAV+Dox 300μM+Dex	8	0	0	AAV+Dox 300μM+Dex	8	0	0
AAV+Dox 500μM+Dex	8	3	37.5%	AAV+Dox 500μM+Dex	8	6	75%

Table 4: Number of mouse eyes with lens opacity 1 month and 3 months after being treated with AAV virus with or without doxorubicin and dexrazoxane.

3.5 Discussion

Since doxorubicin was reported to induce neurotoxicity (Lopes et al., 2008), I evaluated both the short-term (1 month after treatment) and the long-term (3 months after treatment) doxorubicin-induced cytotoxicity in the mouse retina. I found that doxorubicin at a relatively high concentration (300 – 500 μM) could lead to cytotoxicity to retinal neurons in the long term. The cytotoxic effects include reducing the cell density of the GCL and the thickness of the INL and IPL. Since the INL of the mouse retina contains bipolar cells, amacrine cells, horizontal cells, and Muller cells (Jeon et al., 1998), and the cell density of bipolar cells did not change 3 months after injection of high-dose (500 μM) doxorubicin (Figure 15b), the thinning of the INL together with the IPL is likely due to the loss of the other types of cells. In harlequin (Hq) mutant mice (a mouse model with oxidative stress-mediated neurodegeneration), retinal ganglion cells, horizontal cells, and amacrine cells were found to be positive for 8-OHdG (8-hydroxydeoxyguanosine, a principal component of oxidatively damaged DNA) (Klein et al., 2002), which suggested the susceptibilities of those cell types to oxidative damage. A possible reason could be the expression of different subsets of UPS (ubiquitin proteasome system) components among different retinal cell types (Plafker et al., 2012). The susceptibilities of horizontal cells and amacrine cells to oxidative damage may explain the decreased thickness of the INL and IPL. Interestingly, no apparent cell loss was observed for photoreceptors because the thickness of the ONL was not found to be altered after the treatment with doxorubicin. Photoreceptor cells are located farther from the injection site, thus less exposed to the doxorubicin. Moreover, they were not found to be positive for 8-OHdG

(Klein et al., 2002), therefore might be less susceptible to the doxorubicin-induced oxidative damage.

The late-onset doxorubicin-induced cytotoxicity has been reported in cardiac tissue when doxorubicin was used as an antitumor drug clinically (Kumar et al., 2012; Steinherz et al., 1991). The mechanism of causing cell death could be due to the fact that doxorubicin-induced reactive oxygen species (ROS) formation mutates the mitochondria DNA and damages the membrane lipid structure and respiratory chain proteins (Singal and Iliskovic, 1998). The mitochondrial injury after acute doxorubicin exposure then accumulates over time without further doxorubicin exposure, which is also referred to as “dose memory”(Lebrecht et al., 2003).

Dexrazoxane (Zinecard) is a FDA-approved drug that has been used to reduce anthracycline (doxorubicin)-induced cytotoxicity. Our results show that co-injection of dexrazoxane with doxorubicin can mitigate the doxorubicin-induced cytotoxicity, while still maintaining the effect of doxorubicin. Under our experimental conditions, the optimal dose of doxorubicin if used in combination with dexrazoxane is 200-300 μM, as it showed no long-term neurotoxicity (Figure 20 and 21) and the AAV-mediated transgene expression in bipolar cells was significantly improved (Figure 23). On the other hand, there was no statistically significant difference in the cell density of the GCL between retinas treated with 500 μM doxorubicin with/without co-administration of dexrazoxane (Figure 17 and 20). This suggests that co-administration of dexrazoxane could not completely abrogate the doxorubicin-induced cytotoxicity, especially when the dose of doxorubicin was high. Consistent with the results in clinic, dexrazoxane does not completely eliminate the risk of doxorubicin-induced cardiotoxicity(Hensley et al., 2009). There was no statistically

significant difference in the mCherry intensity among retinas treated with 200 μM, 300 μM, and 500 μM doxorubicin and dexrazoxane after virus injection (Figure 23). When comparing the mCherry expression level between retinas treated with 200-500 μM doxorubicin with and without dexrazoxane, we found that there was a decrease in retinas treated with 500 μM doxorubicin and dexrazoxane compared to those without dexrazoxane (Figure 14 and Figure 23). This is possibly because the anti-ROS effect of dexrazoxane might also reduce part of the efficacy of doxorubicin, since ROS has been reported to augment AAV transduction efficiency (Sanlioglu and Engelhardt, 1999). We also observed a slight decrease in the mCherry expression level in retinas treated with AAV and dexrazoxane compared to retinas treated with AAV alone (Figure 23).

Currently, the application of dexrazoxane is limited in reducing doxorubicin-induced cytotoxicity. However, dexrazoxane is also a mammalian DNA topoisomerase II inhibitor (Hasinoff et al., 1995). The adverse effects of dexrazoxane when used intravenously include myelosuppression, secondary malignancies, and embryo-fetal toxicity (Hensley et al., 2009). However, since the retinal neurons are non-dividing cells, it is less likely for dexrazoxane to affect normal cell function as a DNA topoisomerase II inhibitor. Furthermore, no known research has evaluated the effect of dexrazoxane on AAV transduction. Further studies need to be done to determine whether the iron-chelating effect or any other possible effects of dexrazoxane could interrupt AAV transduction.

It is worth pointing out that, in clinical practice, dexrazoxane is only used when patients received a cumulative doxorubicin dose of 300 mg/m^2; it is not used concomitantly with the initial doses of doxorubicin to avoid interfering with the anticancer effect of doxorubicin (Hensley et al., 2009; Swain et al., 1997a). In addition, dexrazoxane

is given before the administration of doxorubicin (within 30 minutes) (Hensley et al., 2009). Since the higher doses of doxorubicin were shown to cause toxicity to the retina and we only did a one-time intravitreal injection, it would make it necessary for the concomitant use of dexrazoxane. Therefore, in this study we delivered the two drugs together with the AAV virus via co-injection. Certainly, further studies on the pharmacodynamics and pharmacokinetics of the two drugs in the eye may help to develop an optimal protocol for drug delivery for clinical applications.

It was reported that intravitreal injection of doxorubicin in rabbit eyes could cause lens cataract within 2-3 months; the underlying mechanism is due to the oxygen radicals generated from doxorubicin (Phylactos and Unger, 1998). Cataractogenesis was reported even when doxorubicin was given intraperitoneally in rats, with the histopathologic findings showing nuclei retention in the central lens fibers and cortical lens fiber-cell swelling with liquefaction (Bayer et al., 2005). My results showed that three out of eight mouse eyes were observed to have cataract at the end of one month following intravitreal injection of high-dose doxorubicin (500 μM). At the end of three months following intravitreal injection, two out of eight mouse eyes treated with 200 μM doxorubicin were observed to have mild lens opacity, five out of eight mouse eyes treated with 300 μM doxorubicin and nine out of ten mouse eyes treated with 500 μM doxorubicin showed mature lens opacity, respectively (Table 4). With co-administration of dexrazoxane, three out of eight mouse eyes showed lens opacity 1 month after treatment with 500 μM doxorubicin; six out of eight mouse eyes showed lens opacity 3 months after treatment with 500 μM doxorubicin, and the mouse eyes treated with 200 μM and 300 μM doxorubicin did not have lens opacity at all 3 months after injection (Table 4). According

to my results on the long-term (3 months) effect of doxorubicin and dexrazoxane on the mouse lens, the lens cataracts caused by intravitreal injection of lower doses of doxorubicin (200 μM and 300 μM) could be totally prevented by co-injection of doxorubicin and dexrazoxane; while the incidence of lens cataracts caused by intravitreal injection of high dose doxorubicin (500 μM doxorubicin) was reduced, with the ratio of number of lens cataracts/total number of mouse eyes decreased from 9/10 to 6/8. This indicated that doxorubicin-induced lens cataracts in the mouse eyes after intravitreal injection could be due to the generation of oxygen radicals, and that with the addition of an oxygen radical reducing drug (dexrazoxane), the incidence of lens cataracts was markedly reduced.

In conclusion, my results suggest that the co-application of doxorubicin and dexrazoxane could be a potential adjuvant regimen to AAV-mediated gene therapy. Further studies on the mechanism of doxorubicin and dexrazoxane interaction may help to further improve the regimen to keep the effect of facilitating AAV transduction while simultaneously reducing the toxicity to both the retinas and the lenses.

CHAPTER 4: TO TEST THE HYPOTHESIS THAT ILM ACTS AS A BARRIER FOR AAV TRANSDUCTION IN RETINAL BIPOLAR CELLS

4.1 Hypothesis

Enzymatic digestion of inner limiting membrane would increase the number of AAV-transduced retinal neurons.

4.2 Rationale

The bipolar cell layer is located in the middle of the retina, which means that it is difficult for viruses to access bipolar cells with either intravitreal or subretinal delivery. For our purpose, we prefer to inject virus through the vitreous space; hence a second barrier shows up: the inner limiting membrane. The inner limiting membrane (ILM) is a basement membrane that resides between the vitreous body and the retina as a boundary. Removal of ILM would allow more AAV virus to access to the retinal neurons. Therefore, enzymatic digestion of the ILM may increase the number of retinal neurons transduced by AAV virus. Plasmin is a trypsin-like serine protease; it can dissolve laminin and fibronectin in ILM, as well as facilitate extracellular matrix degradation (Liotta et al., 1981). In this study, I co-injected AAV2 virus with different doses of plasmin to evaluate the effect of plasmin on improving AAV transduction efficiency in the retinal bipolar cells.

4.3 Experimental design and method

Animals and materials

Described in chapter 2.2 except the following. Plasmin was purchased from Sigma-Aldrich (St. Louis, MO, USA).

Virus injection

Described in chapter 2.2 except the following. The plasmin injection solutions are listed in Table 5.

Quantitative fluorescence and cell density measurements

Described in chapter 2.2.

PLASMIN STOCK SOLUTION: 0.5 IU/μL AAV VIRUS STOCK SOLUTION: $2X10^{13}$ VG/ML		
MIXED SOLUTION: EACH MOUSE EYE WAS INJECTED WITH 1.5 μL		
	Plasmin [C] in the mixed solution (IU/μl)	AAV virus [C] in the mixed solution (vg/ml)
H	0.25	$5x10^{12}$
M	0.0625 (H:4)	$5x10^{12}$
L	0.015625 (M:4)	$5x10^{12}$

Table 5. The preparation of plasmin injection solutions. H, high concentration; M, middle concentration; L, low concentration.

4.4 Results

My results showed that injection of different concentrations of plasmin with AAV virus did not improve the AAV-mediated mCherry expression in the retinal bipolar cells throughout the retina, including the center region (Figure 26a-d, i), middle region (Figure 27a-d, i), and peripheral retinal region (Figure 28a-d, i). Figure 26e-h and, 27e-h, and 28e-h represent the plot profiles of Figure 26a-d, 27a-d, and 28a-d. Figure26j, 27j, and 28j show the number of bipolar cells that have a mCherry expression level above 0.05 RFU/pixel^2 within an image region of 0.0369 mm^2 in center, middle, and peripheral retina. The result is consistent with the mCherry expression level.

In terms of the density of all the AAV-transduced bipolar cells, injection of middle concentration of plasmin increased the cell density in the center area of the retina (Figure 29a), and injection of both low and middle concentration of plasmin increased the cell density in the middle area of the retina (Figure 29b). While in the peripheral area of the retina, high concentration of plasmin actually decreased the cell density (Figure 29c).

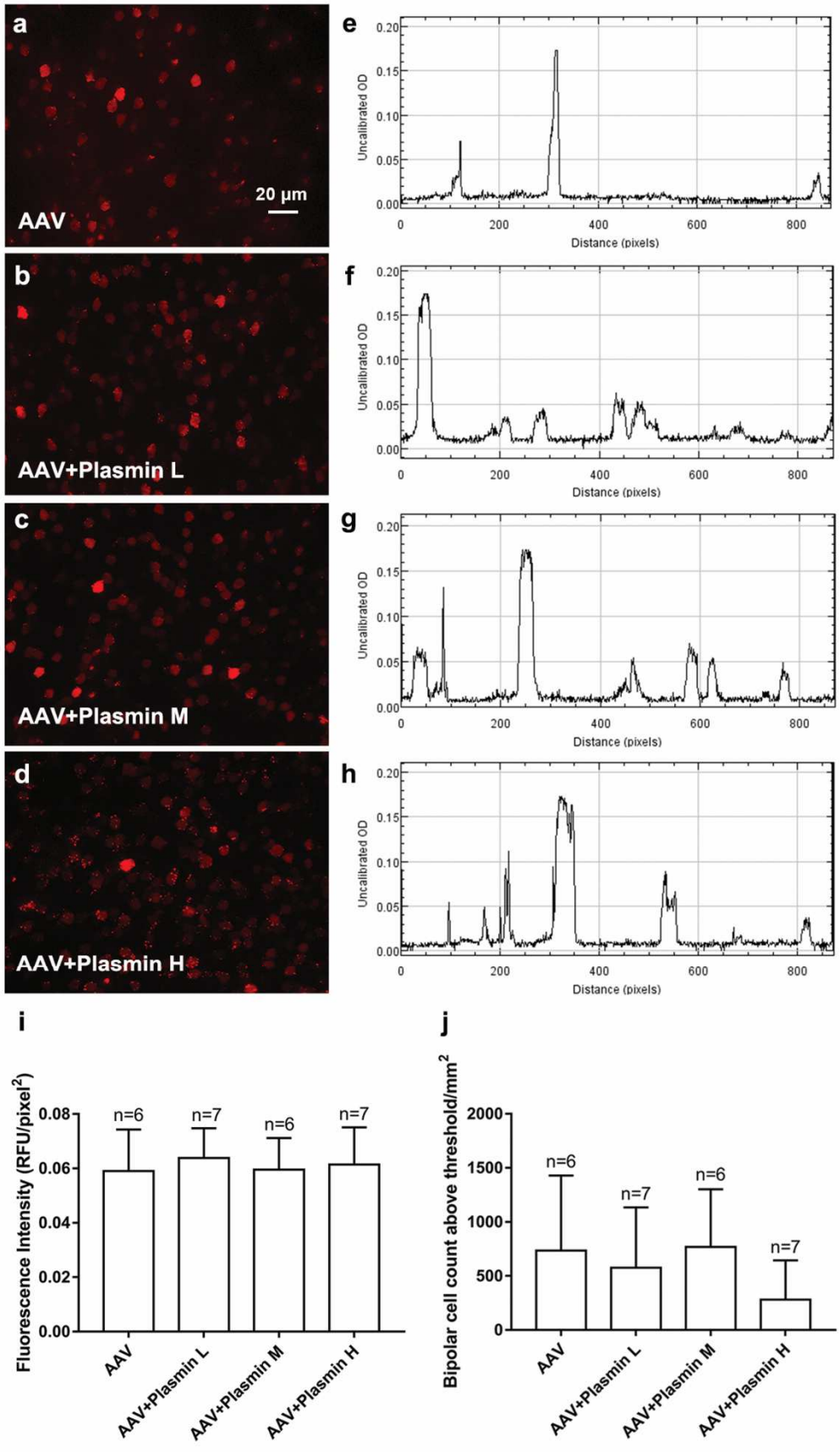

Figure 26. Comparison of AAV-mediated transduction efficiency and bipolar cell densities in the center area of the mouse retinas 1 month after being treated with AAV virus with or without plasmin. (a-d) whole-mount fluorescence images acquired at the INL without immunofluorescence enhancement. (e-h) plot profiles of image a-d. The plot profile displays a two-dimensional graph of the intensities of pixels along a random horizontal line across the image. The x-axis represents distance (in pixels) along the line, and the y-axis is the pixel intensity. (i) comparison of fluorescence intensities of the mCherry-expressing retinal bipolar cells treated with AAV virus with or without plasmin. (j) cell densities of the retinal bipolar cells that have an mCherry expression level above 0.05 RFU/pixel^2. The data is shown as mean ± SD. The n represents the number of retinas being examined.

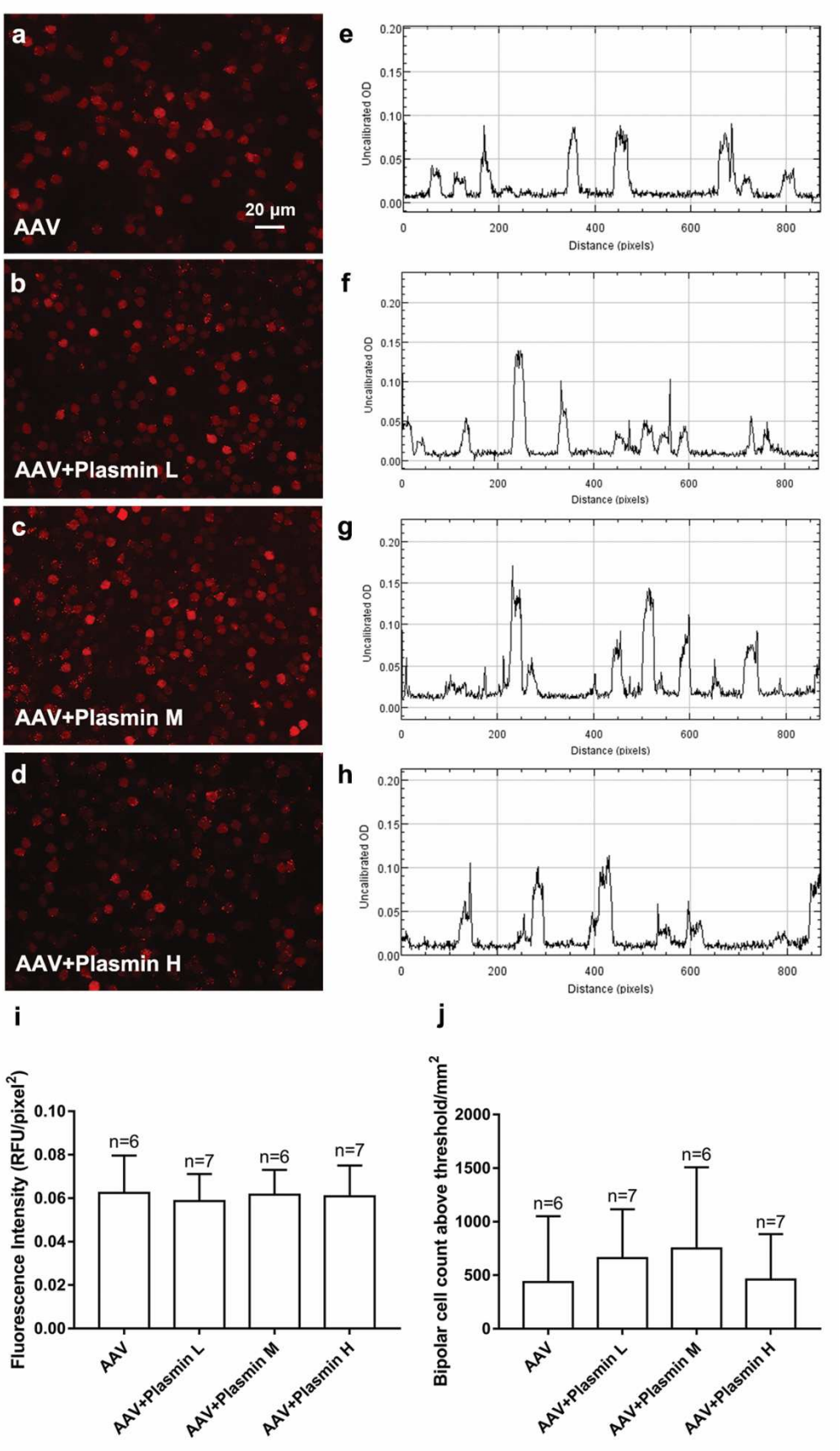

Figure 27. Comparison of AAV-mediated transduction efficiency and bipolar cell densities in the middle area of the mouse retinas 1 month after being treated with AAV virus with or without plasmin. (a-d) whole-mount fluorescence images acquired at the INL without immunofluorescence enhancement. (e-h) plot profiles of image a-d. The plot profile displays a two-dimensional graph of the intensities of pixels along a random horizontal line across the image. The x-axis represents distance (in pixels) along the line, and the y-axis is the pixel intensity. (i) comparison of fluorescence intensities of the mCherry-expressing retinal bipolar cells treated with AAV virus with or without plasmin. (j) cell densities of the retinal bipolar cells that have an mCherry expression level above 0.05 RFU/pixel^2. The data is shown as mean ± SD. The n represents the number of retinas being examined.

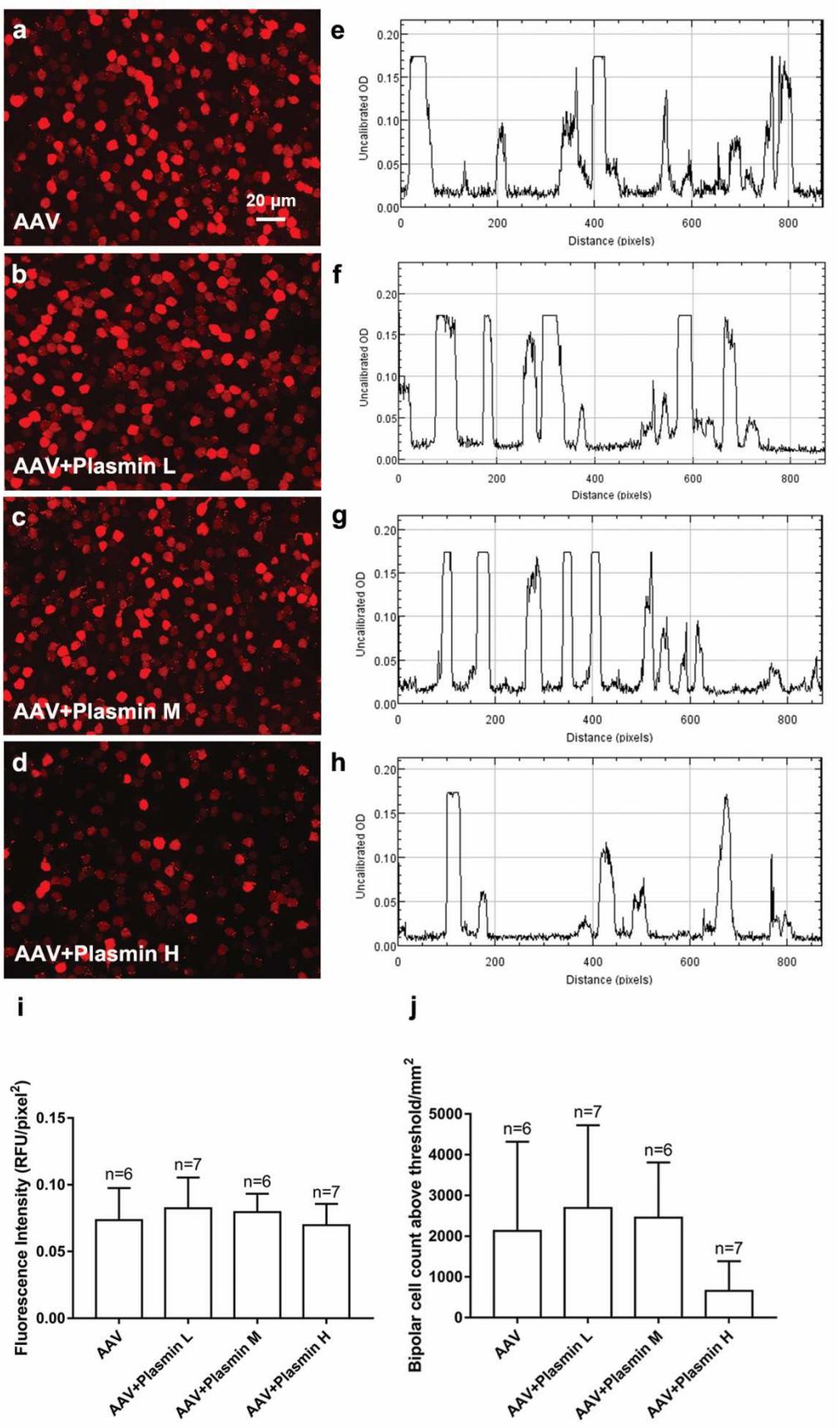

Figure 28. Comparison of AAV-mediated transduction efficiency and bipolar cell densities in the peripheral area of the mouse retinas 1 month after being treated with AAV virus with or without plasmin. (a-d) whole-mount fluorescence images acquired at the INL without immunofluorescence enhancement. (e-h) plot profiles of image a-d. The plot profile displays a two-dimensional graph of the intensities of pixels along a random horizontal line across the image. The x-axis represents distance (in pixels) along the line, and the y-axis is the pixel intensity. (i) comparison of fluorescence intensities of the mCherry-expressing retinal bipolar cells treated with AAV virus with or without plasmin. (j) cell densities of the retinal bipolar cells that have an mCherry expression level above 0.05 RFU/pixel^2. The data is shown as mean ± SD. The n represents the number of retinas being examined.

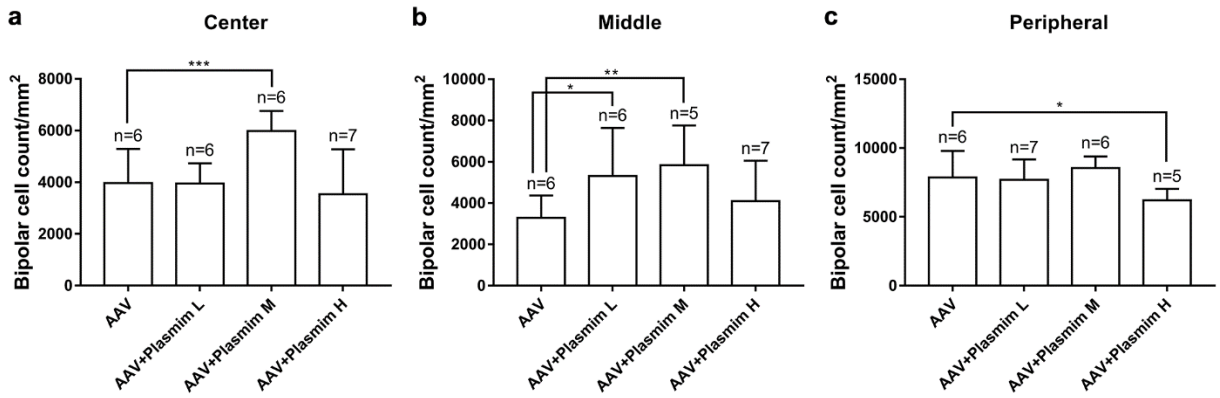

Figure 29. Comparison of bipolar cell densities in the center/middle/peripheral area of the mouse retinas 1 month after being treated with AAV virus with or without plasmin. (a) comparison of AAV-transduced bipolar cell densities in the center area of the mouse retinas. (b) comparison of AAV-transduced bipolar cell densities in the middle area of the mouse retinas. (c) comparison of AAV-transduced bipolar cell densities in the peripheral area of the mouse retinas. The data is shown as mean ± SD. The n represents the number of retinas being examined. The asterisk indicates statistically significant differences with *p<0.05, **p<0.01, ***p<0.001 (one-way ANOVA).

4.5 Discussion

There are mainly two ways to remove the ILM. One method is enzyme digestion, the other is direct surgical removal. Previous research has reported that intravitreal AAV-mediated gene transduction in the inner retina was improved by surgical peeling of the ILM in cynomolgus monkeys (Takahashi et al., 2017). However, damage of the Muller cell processes following the surgical removal of the ILM was revealed (Nakamura et al., 2003). Therefore, we investigated using enzyme digestion.

In this study, I examined the effect of 3 different doses of plasmin in improving AAV transduction efficiency in the retinal bipolar cells. My results showed no improvement in AAV-mediated mCherry expression level in the retina after intravitreal injection of AAV2 virus and plasmin. However, the density of all the AAV-transduced retinal bipolar cells was increased in the center and middle area of the retina following co-injection of AAV2 virus and middle and/or low concentration of plasmin.

Previous research reported that intravitreal co-injection of AAV5 with a proteolytic enzyme Pronase E leads to a marked enhancement of AAV5 transduction in various retinal cell types in rats. They also found that in contrast to AAV2, AAV5 did not have attachment sites at the vitreoretinal junction. Enzymatic digestion of the ILM removed the barrier for the AAV serotype 5 to reach the retina (Dalkara et al., 2009a). The primary receptors for different AAV serotypes are different. AAV5 requires a terminal sialic acid for binding and transduction (Kaludov et al., 2001), while AAV2 uses HSPG (Summerford and Samulski, 1998b). Since sialic acid is absent in the ILM (Cho et al., 2002), sialic acid-dependent AAV serotype 5 is unable to accumulate at the vitreoretinal junction (Dalkara et al., 2009b) and thus can possibly explain the lack of transduction efficiency of AAV5 virus vectors following intravitreal injection (Hellström et al., 2008). AAV2 virus, in contrast, is the most efficient one among other serotypes of AAV virus after intravitreal injection (Hellström et al., 2008). Therefore, removal of the ILM may have a much stronger influence on the AAV5 transduction efficiency in the retina compared to the AAV2 transduction efficiency. As indicated in my results, enzymatic digestion of the ILM by plasmin did not make a difference on the AAV2 transduction efficiency in the retina following intravitreal injection. Another enzyme, microplasmin, has been demonstrated to

disrupt the border between the ILM and vitreous body in macaque, resulting in an increased transduction similar to the effect of pronase E on rodents (Yin et al., 2011). Although the ILM of the rodent retina is relatively homogeneous, the thickness of the ILM can also vary among different regions of the retina, given the fact that the AAV transduction efficiency (represented by the mCherry expression level) was higher in the peripheral area of the retina than that in the center and middle areas of the retina. My results also demonstrated that the cell density in the center area of the retina was increased after treatment with the middle concentration of plasmin, and the cell density in the middle area of the retina was also increased after treatment with both the low and middle concentrations of plasmin. However, the cell density in the peripheral area of the retina was not influenced by either the low or middle concentration of plasmin. This indicated that modest digestion of ILM may allow more AAV viral vectors to access the retina and infect more retinal bipolar cells. Nevertheless, there was no improvement in the expression level of AAV-meditated mCherry in the retina after intravitreal injection of AAV2 virus and plasmin. Since the ILM is much thicker in primates and human than that in rodents (Matsumoto et al., 1984), therefore, removal of the ILM in primates could play a more important role in improving AAV transduction efficiency in the retina than removal of the ILM in rodents. Further studies may need to be done in primate models in order to better evaluate the effect of plasmin on improving AAV transduction efficiency in the retina following intravitreal injection.

CHAPTER 5: CONCLUSION AND FUTURE DIRECTIONS

Optogenetic therapy is one of the most promising developing therapies for vision restoration. Targeting retinal bipolar cells with AAV viral vectors has been drawing increasing interest. However, the AAV transduction efficiency in bipolar cells is low. In this study, I tested my hypotheses that virus degradation during intracellular trafficking and poor virus accessibility to bipolar cells are two main barriers for the efficient AAV transduction to bipolar cells.

To test my first hypothesis, I evaluated the effect of three proteasome inhibitors, doxorubicin, aclarubicin and MG132 on AAV-mediated transduction efficiency in retinal bipolar cells in mice. My results show that doxorubicin, but not aclarubicin and MG132, can improve the AAV transduction efficiency in retinal bipolar cells. Moreover, the way of doxorubicin to improve AAV transduction efficiency is by increasing the number of cells that are able to reach high transgene expression level, not by increasing the number of cells transduced by AAV virus. The effective doses of doxorubicin after long-term evaluation (3 months after treatment) are 200 – 500 μM. Since doxorubicin was reported to induce neurotoxicity, I also evaluated the doxorubicin-induced toxicity in the mouse retina. My results show that doxorubicin at a relative high concentration (300 – 500 μM) could lead to cytotoxicity to retinal neurons in the long-term (3 months after treatment). The cytotoxic effects include reducing the cell density of the GCL and the thickness of the INL and IPL. Lens opacity was also observed in the mouse eyes. Dexrazoxane (Zinecard) is a FDA-approved drug that has been used to reduce the doxorubicin-induced cytotoxicity. Our results show that co-injection of dexrazoxane with doxorubicin can mitigate the doxorubicin-induced cytotoxicity, while still maintaining the effect of

doxorubicin. Under our experimental conditions, the optimal dose of doxorubicin if used in combination with dexrazoxane is 200-300 μM, as it showed no long-term neurotoxicity and the AAV-mediated transgene expression in bipolar cells was significantly improved. With 500 μM doxorubicin however, the cell density of the GCL was still not brought back to normal after co-administration of dexrazoxane, and the lens opacity was still observed in the mouse eyes. This suggests that co-administration of dexrazoxane could not completely abrogate the doxorubicin-induced cytotoxicity, especially when the dose of doxorubicin was high.

To test my second hypothesis, I examined the effect of 3 different doses of plasmin in improving AAV transduction efficiency in the retinal bipolar cells. My results show that the density of the AAV-transduced retinal bipolar cells was increased in the center and middle area of the retina following co-injection of AAV2 virus and middle and/or low concentration of plasmin. However, there was no improvement in the AAV-mediated transgene expression level in the retina after intravitreal injection of AAV2 virus and plasmin. The relatively remarkable effect of plasmin in the center and middle areas of the retina is probably due to the ILM is thicker in those areas. Since the ILM of the primates and human is much thicker than that in rodents, removal of the ILM in primates might play a more important role in improving AAV transduction efficiency in the retina than removal of the ILM in rodents.

Further studies may need to be done in the following areas:

1. Improve the drug delivery protocol of the doxorubicin-dexrazoxane regimen. Multiple combinations of drug delivery could be tested. For example, one-time doxorubicin injection followed by multiple dexrazoxane injections at different time points, or

dexrazoxane injection given prior to doxorubicin injection. More studies on the pharmacodynamics and pharmacokinetics of doxorubicin and dexrazoxane in the eye will help to develop an optimal protocol for drug delivery.

2. Evaluate the toxicity of plasmin in the retina. The hyperosmolarity of high dose plasmin may cause transient retinal detachment. Digestion of the extracellular matrix by high dose plasmin may also cause structural/functional abnormality of the retina.
3. Examine a combined regimen containing of doxorubicin, dexrazoxane, plasmin, and a more potent viral vector such as 7m8. This combined regimen may further improve the gene delivery efficiency in the retina. A therapeutic gene such as ChR2 can also be tested with this regimen in a retinal degenerative disease model. Electrophysiology and behavior studies can be done to evaluate the therapeutic gene delivery efficiency of this combined regimen in disease models.
4. Evaluate the effect of plasmin in primate models. Intravitreal injection of AAV virus and plasmin in primates might lead to a more prominent effect in improving AAV transduction efficiency in the retina because of the thickness of the primate ILM.

REFERENCES

Anasagasti, A., Irigoyen, C., Barandika, O., Lopez de Munain, A., and Ruiz-Ederra, J. (2012). Current mutation discovery approaches in Retinitis Pigmentosa. Vision research *75*, 117-129.

Aslanidi, G.V., Rivers, A.E., Ortiz, L., Song, L., Ling, C., Govindasamy, L., Van Vliet, K., Tan, M., Agbandje-McKenna, M., and Srivastava, A. (2013). Optimization of the capsid of recombinant adeno-associated virus 2 (AAV2) vectors: the final threshold? PloS one *8*, e59142.

Asokan, A., Hamra, J.B., Govindasamy, L., Agbandje-McKenna, M., and Samulski, R.J. (2006). Adeno-associated virus type 2 contains an integrin alpha5beta1 binding domain essential for viral cell entry. Journal of virology *80*, 8961-8969.

Auricchio, A. (2003). Pseudotyped AAV vectors for constitutive and regulated gene expression in the eye. Vision research *43*, 913-918.

Bartlett, J.S., Wilcher, R., and Samulski, R.J. (2000). Infectious entry pathway of adeno-associated virus and adeno-associated virus vectors. .pdf. Journal of virology *74*, 2777-2785.

Bayer, A., Evereklioglu, C., Demirkaya, E., Altun, S., Karslioglu, Y., and Sobaci, G. (2005). Doxorubicin-induced cataract formation in rats and the inhibitory effects of hazelnut, a natural antioxidant: a histopathological study. Medical science monitor : international medical journal of experimental and clinical research *11*, Br300-304.

Ben-Nissan, G., and Sharon, M. (2014). Regulating the 20S Proteasome Ubiquitin-Independent Degradation Pathway. Biomolecules *4*, 862-884.

Bi, A., Cui, J., Ma, Y.P., Olshevskaya, E., Pu, M., Dizhoor, A.M., and Pan, Z.H. (2006).

Ectopic expression of a microbial-type rhodopsin restores visual responses in mice with photoreceptor degeneration. Neuron *50*, 23-33.

Boyden, E.S., Zhang, F., Bamberg, E., Nagel, G., and Deisseroth, K. (2005). Millisecond-timescale, genetically targeted optical control of neural activity. Nature neuroscience *8*, 1263-1268.

Brandstatter, J.H., Koulen, P., and Wassle, H. (1998). Diversity of glutamate receptors in the mammalian retina. Vision research *38*, 1385-1397.

Buch, P.K., Bainbridge, J.W., and Ali, R.R. (2008). AAV-mediated gene therapy for retinal disorders: from mouse to man. Gene therapy *15*, 849-857.

Cairo, G., and Pietrangelo, A. (2000). Iron regulatory proteins in pathobiology. Biochemical Journal *352*, 241-250.

Casaroli-Marano, R.P., Alforja, S., Giralt, J., and Farah, M.E. (2014). Epimacular brachytherapy for wet AMD: current perspectives. Clinical ophthalmology *8*, 1661-1670.

Chaanine, A.H., Nonnenmacher, M., Kohlbrenner, E., Jin, D., Kovacic, J.C., Akar, F.G., Hajjar, R.J., and Weber, T. (2014). Effect of bortezomib on the efficacy of AAV9.SERCA2a treatment to preserve cardiac function in a rat pressure-overload model of heart failure. Gene therapy *21*, 379-386.

Chatterjee, K., Zhang, J., Honbo, N., and Karliner, J.S. (2010). Doxorubicin Cardiomyopathy. Cardiology *115*, 155-162.

Chen, D., Frezza, M., Schmitt, S., Kanwar, J., and Dou, Q.P. (2011). Bortezomib as the first proteasome inhibitor anticancer drug- current status and future perspectives.pdf. Curr Cancer Drug Targets.

Cho, E.Y., Choi, H.L., and Chan, F.L. (2002). Expression pattern of glycoconjugates in rat retina as analysed by lectin histochemistry. The Histochemical journal *34*, 589-600.

Cideciyan, A.V., Aleman, T.S., Boye, S.L., Schwartz, S.B., Kaushal, S., Roman, A.J., Pang, J.J., Sumaroka, A., Windsor, E.A., Wilson, J.M.*, et al.* (2008). Human gene therapy for RPE65 isomerase deficiency activates the retinoid cycle of vision but with slow rod kinetics. Proceedings of the National Academy of Sciences of the United States of America *105*, 15112-15117.

Cronin, T., Vandenberghe, L.H., Hantz, P., Juttner, J., Reimann, A., Kacso, A.E., Huckfeldt, R.M., Busskamp, V., Kohler, H., Lagali, P.S.*, et al.* (2014). Efficient transduction and optogenetic stimulation of retinal bipolar cells by a synthetic adeno-associated virus capsid and promoter. EMBO molecular medicine *6*, 1175-1190.

Curcio, C.A., and Hendrickson, A.E. (1991). Organization and Development of the Primate Photoreceptor Mosaic. Progress in Retinal Research *10*.

Dalkara, D., Kolstad, K.D., Caporale, N., Visel, M., Klimczak, R.R., Schaffer, D.V., and Flannery, J.G. (2009a). Inner limiting membrane barriers to AAV-mediated retinal transduction from the vitreous. Molecular therapy : the journal of the American Society of Gene Therapy *17*, 2096-2102.

Dalkara, D., Kolstad, K.D., Caporale, N., Visel, M., Klimczak, R.R., Schaffer, D.V., and Flannery, J.G. (2009b). Inner Limiting Membrane Barriers to AAV-mediated Retinal Transduction From the Vitreous. Molecular Therapy *17*, 2096-2102.

Dalkara, D., and Sahel, J.A. (2014). Gene therapy for inherited retinal degenerations. Comptes rendus biologies *337*, 185-192.

Dalkara, D.B.L., Klimczak RR, Visel M, Yin L, Merigan WH, Flannery JG, Schaffer DV

(2013). In Vivo–Directed Evolution of a New Adeno-Associated Virus for Therapeutic Outer Retinal Gene Delivery from the Vitreous.pdf. Sci Transl Med.

Doroudchi, M.M., Greenberg, K.P., Liu, J., Silka, K.A., Boyden, E.S., Lockridge, J.A., Arman, A.C., Janani, R., Boye, S.E., Boye, S.L., *et al.* (2011). Virally delivered channelrhodopsin-2 safely and effectively restores visual function in multiple mouse models of blindness. Molecular therapy : the journal of the American Society of Gene Therapy *19*, 1220-1229.

Douar, A.M., Poulard, K., Stockholm, D., and Danos, O. (2001). Intracellular trafficking of adeno-associated virus vectors: routing to the late endosomal compartment and proteasome degradation. Journal of virology *75*, 1824-1833.

Erales, J., and Coffino, P. (2014). Ubiquitin-independent proteasomal degradation. Biochimica et biophysica acta *1843*, 216-221.

Goldberg, A.L. (2003). Protein degradation and protection against misfolded or damaged proteins.pdf. Nature *426*, 895-899.

Goldberg, A.L. (2012). Development of proteasome inhibitors as research tools and cancer drugs. The Journal of cell biology *199*, 583-588.

Halfter, W., Dong, S., Dong, A., Eller, A.W., and Nischt, R. (2008). Origin and turnover of ECM proteins from the inner limiting membrane and vitreous body. Eye *22*, 1207-1213.

Hasinoff, B.B., Kuschak, T.I., Yalowich, J.C., and Creighton, A.M. (1995). A QSAR study comparing the cytotoxicity and DNA topoisomerase II inhibitory effects of bisdioxopiperazine analogs of ICRF-187 (dexrazoxane). Biochemical Pharmacology *50*, 953-958.

Hellström, M., Ruitenberg, M.J., Pollett, M.A., Ehlert, E.M.E., Twisk, J., Verhaagen, J., and Harvey, A.R. (2008). Cellular tropism and transduction properties of seven adeno-associated viral vector serotypes in adult retina after intravitreal injection. Gene therapy *16*, 521.

Hensley, M.L., Hagerty, K.L., Kewalramani, T., Green, D.M., Meropol, N.J., Wasserman, T.H., Cohen, G.I., Emami, B., Gradishar, W.J., Mitchell, R.B.*, et al.* (2009). American Society of Clinical Oncology 2008 Clinical Practice Guideline Update: Use of Chemotherapy and Radiation Therapy Protectants. Journal of Clinical Oncology *27*, 127-145.

Hermonat, P.L., and Muzyczka, N. (1984). Use of adeno-associated virus as a mammalian DNA cloning vector- Transduction of neomycin resistance into mammalian tissue culture cells. Proc Natl Acad Sci U S A *81*, 6466-6470.

Hu, T., Le, Q., Wu, Z., and Wu, W. (2007). Determination of doxorubicin in rabbit ocular tissues and pharmacokinetics after intravitreal injection of a single dose of doxorubicin-loaded poly-beta-hydroxybutyrate microspheres. Journal of pharmaceutical and biomedical analysis *43*, 263-269.

Ichikawa, Y., Ghanefar, M., Bayeva, M., Wu, R., Khechaduri, A., Naga Prasad, S.V., Mutharasan, R.K., Naik, T.J., and Ardehali, H. (2014). Cardiotoxicity of doxorubicin is mediated through mitochondrial iron accumulation. The Journal of clinical investigation *124*, 617-630.

Imondi, A.R., Della Torre, P., Mazue, G., Sullivan, T.M., Robbins, T.L., Hagerman, L.M., Podesta, A., and Pinciroli, G. (1996). Dose-response relationship of dexrazoxane for prevention of doxorubicin-induced cardiotoxicity in mice, rats, and dogs. Cancer

research *56*, 4200-4204.

Ivanova, E., Hwang, G.S., Pan, Z.H., and Troilo, D. (2010). Evaluation of AAV-mediated expression of Chop2-GFP in the marmoset retina. Investigative ophthalmology & visual science *51*, 5288-5296.

Ivanova, E., and Pan, Z.H. (2009). Evaluation of the adeno-associated virus mediated long-term

expression of channelrhodopsin-2 in the mouse retina. Molecular Vision.

Jager, R.D., Mieler, W.F, and Miller, J.W (2008). age related macular degeneration .pdf. N Engl J Med.

James W.B. Bainbridge, P.D., F.R.C.Ophth., Alexander J. Smith, Ph.D., Susie S. Barker, Ph.D., Scott Robbie, M.R.C.Ophth., Robert Henderson, M.R.C.Ophth., Kamaljit Balaggan, M.R.C.Ophth., Ananth Viswanathan, M.D., F.R.C.Ophth., Graham E. Holder, Ph.D., Andrew Stockman, Ph.D., Nick Tyler, Ph.D., Simon Petersen-Jones, Ph.D., Shomi S. Bhattacharya, Ph.D., Adrian J. Thrasher, Ph.D., M.R.C.P., F.R.C.P., Fred W. Fitzke, Ph.D., Barrie J. Carter, Ph.D., Gary S. Rubin, Ph.D., Anthony T. Moore, F.R.C.Ophth., and Robin R. Ali, Ph.D. (2008). Effect of gene therapy on visual function in Leber's congenital amaurosis..pdf. N Engl J Med.

Jayandharan, G.R., Zhong, L., Li, B., Kachniarz, B., and Srivastava, A. (2008). Strategies for improving the transduction efficiency of single-stranded adeno-associated virus vectors in vitro and in vivo. Gene therapy *15*, 1287-1293.

Jeon, C.-J., Strettoi, E., and Masland, R.H. (1998). The Major Cell Populations of the Mouse Retina. The Journal of Neuroscience *18*, 8936-8946.

Johnson, J.S., and Samulski, R.J. (2009). Enhancement of adeno-associated virus

infection by mobilizing capsids into and out of the nucleolus. Journal of virology *83*, 2632-2644.

Jones, B.W., and Marc, R.E. (2005). Retinal remodeling during retinal degeneration. Experimental eye research *81*, 123-137.

Kaludov, N., Brown, K.E., Walters, R.W., Zabner, J., and Chiorini, J.A. (2001). Adeno-associated virus serotype 4 (AAV4) and AAV5 both require sialic acid binding for hemagglutination and efficient transduction but differ in sialic acid linkage specificity. Journal of virology *75*, 6884-6893.

Karman, J., Gumlaw, N.K., Zhang, J., Jiang, J.L., Cheng, S.H., and Zhu, Y. (2012). Proteasome inhibition is partially effective in attenuating pre-existing immunity against recombinant adeno-associated viral vectors. PloS one *7*, e34684.

Kashiwakura, Y., Tamayose, K., Iwabuchi, K., Hirai, Y., Shimada, T., Matsumoto, K., Nakamura, T., Watanabe, M., Oshimi, K., and Daida, H. (2005). Hepatocyte growth factor receptor is a coreceptor for adeno-associated virus type 2 infection. Journal of virology *79*, 609-614.

Kay, C.N., Ryals, R.C., Aslanidi, G.V., Min, S.H., Ruan, Q., Sun, J., Dyka, F.M., Kasuga, D., Ayala, A.E., Van Vliet, K.*, et al.* (2013). Targeting photoreceptors via intravitreal delivery using novel, capsid-mutated AAV vectors. PloS one *8*, e62097.

Kish-Trier, E., and Hill, C.P. (2013). Structural biology of the proteasome. Annual review of biophysics *42*, 29-49.

Klein, J.A., Longo-Guess, C.M., Rossmann, M.P., Seburn, K.L., Hurd, R.E., Frankel, W.N., Bronson, R.T., and Ackerman, S.L. (2002). The harlequin mouse mutation downregulates apoptosis-inducing factor. Nature *419*, 367.

Kolomiets, B., Dubus, E., Simonutti, M., Rosolen, S., Sahel, J.A., and Picaud, S. (2010). Late histological and functional changes in the P23H rat retina after photoreceptor loss. Neurobiology of disease *38*, 47-58.

Kumar, S., Marfatia, R., Tannenbaum, S., Yang, C., and Avelar, E. (2012). Doxorubicin-Induced Cardiomyopathy 17 Years after Chemotherapy. Texas Heart Institute Journal *39*, 424-427.

Lagali, P.S., Balya, D., Awatramani, G.B., Munch, T.A., Kim, D.S., Busskamp, V., Cepko, C.L., and Roska, B. (2008). Light-activated channels targeted to ON bipolar cells restore visual function in retinal degeneration. Nature neuroscience *11*, 667-675.

Langer, S.W. (2014). Dexrazoxane for the treatment of chemotherapyrelated side effects. Cancer Manag Res.

Lanyi, J.K. (1986). Halorhodopsin- A Light-Driven Chloride Ion Pump. Annu Rev Biophys Biophys Chem.

Lebrecht, D., Setzer, B., Ketelsen, U.P., Haberstroh, J., and Walker, U.A. (2003). Time-Dependent and Tissue-Specific Accumulation of mtDNA and Respiratory Chain Defects in Chronic Doxorubicin Cardiomyopathy. Circulation *108*, 2423.

Lee, D.H., and Goldberg, A.L. (1998). Proteasome inhibitors- valuable new tools for cell biologists. Trends Cell Biol *8*, 397-403.

Liotta, L.A., Goldfarb, R.H., Brundage, R., Siegal, G.P., Terranova, V., and Garbisa, S. (1981). Effect of plasminogen activator (urokinase), plasmin, and thrombin on glycoprotein and collagenous components of basement membrane. Cancer research *41*, 4629-4636.

Lopes, M.Â., Meisel, A., Dirnagl, U., Carvalho, F.D., and Bastos, M.d.L. (2008).

Doxorubicin induces biphasic neurotoxicity to rat cortical neurons. NeuroToxicology *29*, 286-293.

Lu, B., Malcuit, C., Wang, S., Girman, S., Francis, P., Lemieux, L., Lanza, R., and Lund, R. (2009). Long-term safety and function of RPE from human embryonic stem cells in preclinical models of macular degeneration. Stem cells (Dayton, Ohio) *27*, 2126-2135.

Lu, Q., Ganjawala, T.H., Ivanova, E., Cheng, J.G., Troilo, D., and Pan, Z.H. (2016). AAV-mediated transduction and targeting of retinal bipolar cells with improved mGluR6 promoters in rodents and primates. Gene therapy *23*, 680-689.

Lu, Q., Ivanova, E., Ganjawala, T.H., and Pan, Z.H. (2013). Cre-mediated recombination efficiency and transgene expression patterns of three retinal bipolar cell-expressing Cre transgenic mouse lines. Molecular Vision *19*, 1310-1320.

Mace, E., Caplette, R., Marre, O., Sengupta, A., Chaffiol, A., Barbe, P., Desrosiers, M., Bamberg, E., Sahel, J.A., Picaud, S.*, et al.* (2015). Targeting Channelrhodopsin-2 to ON-bipolar Cells With Vitreally Administered AAV Restores ON and OFF Visual Responses in Blind Mice. Molecular therapy : the journal of the American Society of Gene Therapy *23*, 7-16.

Matsumoto, B., Blanks, J.C., and Ryan, S.J. (1984). Topographic variations in the rabbit and primate internal limiting membrane. Investigative ophthalmology & visual science *25*, 71-82.

McCarty, D.M. (2008). Self-complementary AAV vectors; advances and applications. Molecular therapy : the journal of the American Society of Gene Therapy *16*, 1648-1656.

McCarty, D.M., Fu, H., Monahan, P.E., Toulson, C.E., Naik, P., and Samulski, R.J.

(2003). Adeno-associated virus terminal repeat (TR) mutant generates self-complementary vectors to overcome the rate-limiting step to transduction in vivo.pdf. Gene therapy *10*, 2112-2118.

McCarty, D.M., Monahan, P.E., and Samulski, R.J. (2001). Self-complementary recombinant adeno-associated virus (scAAV) vectors promote efficient transduction independently of DNA synthesis.pdf. Gene therapy *8*, 1248-1254.

McClements, M.E., and MacLaren, R.E. (2013). Gene therapy for retinal disease. Translational research : the journal of laboratory and clinical medicine *161*, 241-254.

Menna, P., Recalcati, S., Cairo, G., and Minotti, G. (2007). An introduction to the metabolic determinants of anthracycline cardiotoxicity. Cardiovascular toxicology *7*, 80-85.

Mester, V., and Kuhn, F. (2000). Internal limiting membrane removal in the management of full-thickness macular holes.pdf. American journal of ophthalmology *129*, 769-777.

Minotti, G., Ronchi, R., Salvatorelli, E., Menna, P., and Cairo, G. (2001). Doxorubicin irreversibly inactivates iron regulatory proteins 1 and 2 in cardiomyocytes: evidence for distinct metabolic pathways and implications for iron-mediated cardiotoxicity of antitumor therapy. Cancer research *61*, 8422-8428.

Mitchell, A.M., Li, C., and Samulski, R.J. (2013). Arsenic trioxide stabilizes accumulations of adeno-associated virus virions at the perinuclear region, increasing transduction in vitro and in vivo. Journal of virology *87*, 4571-4583.

Mitchell, A.M., and Samulski, R.J. (2013). Mechanistic insights into the enhancement of adeno-associated virus transduction by proteasome inhibitors. Journal of virology *87*, 13035-13041.

Monahan, P.E., Lothrop, C.D., Sun, J., Hirsch, M.L., Kafri, T., Kantor, B., Sarkar, R., Tillson, D.M., Elia, J.R., and Samulski, R.J. (2010). Proteasome inhibitors enhance gene delivery by AAV virus vectors expressing large genomes in hemophilia mouse and dog models: a strategy for broad clinical application. Molecular therapy : the journal of the American Society of Gene Therapy *18*, 1907-1916.

Morimura, H., Fishman, G., Grover, S., Fulton, A., Berson, E., and Dryja, T. (1998). Mutations in the RPE65 gene in patients with autosomal recessive retinitis pigmentosa or leber congenital amaurosis. Proceedings of the National Academy of Sciences of the United States of America *95*, 3088-3093.

Motlagh, N.S., Parvin, P., Ghasemi, F., and Atyabi, F. (2016). Fluorescence properties of several chemotherapy drugs: doxorubicin, paclitaxel and bleomycin. Biomedical optics express *7*, 2400-2406.

Muindi, J.R., Sinha, B.K., Gianni, L., and Myers, C.E. (1984). Hydroxyl radical production and DNA damage induced by anthra- cycline–iron complex. FEBS letters.

Nagel, G., Szellas, T., Huhn, W., Kateriya, S., Adeishvili, N., Berthold, P., Ollig, D., Hegemann, P., and Bamberg, E. (2003). Channelrhodopsin-2, a directly light-gated cation-selective membrane channel. Proceedings of the National Academy of Sciences of the United States of America *100*, 13940-13945.

Nakai, H., Storm, T.A., and Kay, M.A. (2000). Recruitment of single-stranded recombinant adeno-associated virus vector genomes and intermolecular recombination are responsible for stable transduction of liver in vivo.pdf. Journal of virology *74*, 9451-9463.

Nakamura, T., Murata, T., Hisatomi, T., Enaida, H., Sassa, Y., Ueno, A., Sakamoto, T.,

and Ishibashi, T. (2003). Ultrastructure of the vitreoretinal interface following the removal of the internal limiting membrane using indocyanine green. Current eye research *27*, 395-399.

Natkunarajah, M., Trittibach, P., McIntosh, J., Duran, Y., Barker, S.E., Smith, A.J., Nathwani, A.C., and Ali, R.R. (2008). Assessment of ocular transduction using single-stranded and self-complementary recombinant adeno-associated virus serotype 2/8. Gene therapy *15*, 463-467.

Nicolson, S.C., and Samulski, R.J. (2014). Recombinant adeno-associated virus utilizes host cell nuclear import machinery to enter the nucleus. Journal of virology *88*, 4132-4144.

Nonnenmacher, M., and Weber, T. (2012). Intracellular transport of recombinant adeno-associated virus vectors. Gene therapy *19*, 649-658.

Ong, J.M., and da Cruz, L. (2012). A review and update on the current status of stem cell therapy and the retina. British medical bulletin *102*, 133-146.

Osakada, F., and Takahashi, M. (2015). Challenges in retinal circuit regeneration: linking neuronal connectivity to circuit function. Biological & pharmaceutical bulletin *38*, 341-357.

Parmeggiani, F., Sorrentino, F.S., Romano, M.R., Costagliola, C., Semeraro, F., Incorvaia, C., D'Angelo, S., Perri, P., De Nadai, K., Bonomo Roversi, E.*, et al.* (2013). Mechanism of inflammation in age-related macular degeneration: an up-to-date on genetic landmarks. Mediators of inflammation *2013*, 435607.

Petrs-Silva, H., Dinculescu, A., Li, Q., Deng, W.T., Pang, J.J., Min, S.H., Chiodo, V., Neeley, A.W., Govindasamy, L., Bennett, A.*, et al.* (2011). Novel properties of tyrosine-

mutant AAV2 vectors in the mouse retina. Molecular therapy : the journal of the American Society of Gene Therapy *19*, 293-301.

Petrs-Silva, H., Dinculescu, A., Li, Q., Min, S.H., Chiodo, V., Pang, J.J., Zhong, L., Zolotukhin, S., Srivastava, A., Lewin, A.S.*, et al.* (2009). High-efficiency transduction of the mouse retina by tyrosine-mutant AAV serotype vectors. Molecular therapy : the journal of the American Society of Gene Therapy *17*, 463-471.

Petrs-Silva, H., and Linden, R. (2013). Advances in gene therapy technologies to treat retinitis pigmentosa. Clinical ophthalmology.

Phelan, J.K., and Bok, D. (2000). A brief review of retinitis pigmentosa and the identified retinitis pigmentosa genes.pdf. Mol Vis *8*, 116-124.

Phylactos, A.C., and Unger, W.G. (1998). Biochemical changes induced by intravitreally-injected doxorubicin in the iris-ciliary body and lens of the rabbit eye. Documenta ophthalmologica Advances in ophthalmology *95*, 145-155.

Plafker, S.M., O'Mealey, G.B., and Szweda, L.I. (2012). MECHANISMS FOR COUNTERING OXIDATIVE STRESS AND DAMAGE IN RETINAL PIGMENT EPITHELIUM. International review of cell and molecular biology *298*, 135-177.

Qing, K., Li, W., Zhong, L., Tan, M., Hansen, J., Weigel-Kelley, K.A., Chen, L., Yoder, M.C., and Srivastava, A. (2003). Adeno-Associated Virus Type 2-Mediated Gene Transfer: Role of Cellular T-Cell Protein Tyrosine Phosphatase in Transgene Expression in Established Cell Lines In Vitro and Transgenic Mice In Vivo. Journal of virology *77*, 2741-2746.

Qing, K., Mah, C.S., Hansen, J., Zhou, S., Dwarki, V., and Srivastava, A. (1999). Human fibroblast growth factor receptor 1 is a co-receptor for infection by adeno-associated

virus 2.pdf. Nat Med *5*, 71-77.

Sahel, J.A., and Roska, B. (2013). Gene therapy for blindness. Annual review of neuroscience *36*, 467-488.

Sanlioglu, S., and Engelhardt, J.F. (1999). Cellular redox state alters recombinant adeno-associated virus transduction through tyrosine phosphatase pathways. Gene therapy *6*, 1427-1437.

Scholl, H.P., Strauss, R.W., Singh, M.S., Dalkara, D., Roska, B., Picaud, S., and Sahel, J.A. (2016). Emerging therapies for inherited retinal degeneration. Sci Transl Med *8*, 368rv366.

Schultz, B.R., and Chamberlain, J.S. (2008). Recombinant adeno-associated virus transduction and integration. Molecular therapy : the journal of the American Society of Gene Therapy *16*, 1189-1199.

Singal, P.K., and Iliskovic, N. (1998). Doxorubicin-induced cardiomyopathy. N Engl J Med *339*, 900-905.

Steinherz, L.J., Steinherz, P.G., Tan, C.C., Heller, G., and Murphy, M. (1991). Cardiac toxicity 4 to 20 years after completing anthracycline therapy. Jama *266*, 1672-1677.

Stingl, K., and Zrenner, E. (2013). Electronic approaches to restitute vision in patients with neurodegenerative diseases of the retina. Ophthalmic research *50*, 215-220.

Stone, E.M. (2007). Leber congenital amaurosis - a model for efficient genetic testing of heterogeneous disorders: LXIV Edward Jackson Memorial Lecture. American journal of ophthalmology *144*, 791-811.

Summerford, C., Bartlett, J., and Samulski, R. (1999). AlphaVbeta5 integrin- a co-receptor for adeno-associated virus type 2 infection.pdf. Nat Med *5*, 78-82.

Summerford, C., and Samulski, R. (1998a). Membrane-associated heparan sulfate proteoglycan is a receptor for adeno-associated virus type 2 virions. Journal of virology *72*, 1438-1445.

Summerford, C., and Samulski, R.J. (1998b). Membrane-associated heparan sulfate proteoglycan is a receptor for adeno-associated virus type 2 virions. Journal of virology *72*, 1438-1445.

Surace, E.M., and Auricchio, A. (2003). Adeno-associated viral vectors for retinal gene transfer. Progress in Retinal and Eye Research *22*, 705-719.

Swain, S.M., Whaley, F.S., Gerber, M.C., Ewer, M.S., Bianchine, J.R., and Gams, R.A. (1997a). Delayed administration of dexrazoxane provides cardioprotection for patients with advanced breast cancer treated with doxorubicin-containing therapy. Journal of Clinical Oncology *15*, 1333-1340.

Swain, S.M., Whaley, F.S., Gerber, M.C., Weisberg, S., York, M., Spicer, D., Jones, S.E., Wadler, S., Desai, A., Vogel, C.*, et al.* (1997b). Cardioprotection with dexrazoxane for doxorubicin-containing therapy in advanced breast cancer. Journal of Clinical Oncology *15*, 1318-1332.

Takahashi, K., Igarashi, T., Miyake, K., Kobayashi, M., Yaguchi, C., Iijima, O., Yamazaki, Y., Katakai, Y., Miyake, N., Kameya, S.*, et al.* (2017). Improved Intravitreal AAV-Mediated Inner Retinal Gene Transduction after Surgical Internal Limiting Membrane Peeling in Cynomolgus Monkeys. Molecular Therapy *25*, 296-302.

Thomas, C.E., Storm, T.A., Huang, Z., and Kay, M.A. (2004). Rapid Uncoating of Vector Genomes Is the Key to Efficient Liver Transduction with Pseudotyped Adeno-Associated Virus Vectors. Journal of virology *78*, 3110-3122.

Vandenberghe, L.H., and Auricchio, A. (2012). Novel adeno-associated viral vectors for retinal gene therapy. Gene therapy *19*, 162-168.

Ventii, Karen H., and Wilkinson, Keith D. (2008). Protein partners of deubiquitinating enzymes. Biochemical Journal *414*, 161.

Wang, Z., Ma, H., Li, J., Sun, L., Zhang, J., and Xiao, X. (2003). Rapid and highly efficient transduction by double-stranded adeno-associated virus vectors in vitro and in vivo.pdf. Gene therapy *10*, 2105-2111.

Wassle, H. (2004). Parallel processing in the mammalian retina. Nature reviews Neuroscience *5*, 747-757.

Watanabe, S., Sanuki, R., Ueno, S., Koyasu, T., Hasegawa, T., and Furukawa, T. (2013). Tropisms of AAV for subretinal delivery to the neonatal mouse retina and its application for in vivo rescue of developmental photoreceptor disorders. PloS one *8*, e54146.

Xiao, P.J., and Samulski, R.J. (2012). Cytoplasmic trafficking, endosomal escape, and perinuclear accumulation of adeno-associated virus type 2 particles are facilitated by microtubule network. Journal of virology *86*, 10462-10473.

Yan, Z., Zak, R., Luxton, G.W., Ritchie, T.C., Bantel-Schaal, U., and Engelhardt, J.F. (2002). Ubiquitination of both adeno-associated virus type 2 and 5 capsid proteins affects the transduction efficiency of recombinant vectors. Journal of virology *76*, 2043-2053.

Yan, Z., Zak, R., Zhang, Y., Ding, W., Godwin, S., Munson, K., Peluso, R., and Engelhardt, J.F. (2004). Distinct Classes of Proteasome-Modulating Agents Cooperatively Augment Recombinant Adeno-Associated Virus Type 2 and Type 5-

Mediated Transduction from the Apical Surfaces of Human Airway Epithelia. Journal of virology *78*, 2863-2874.

Yin, L., Greenberg, K., Hunter, J., Dalkara, D., Kolstad, K.D., Masella, B.D., Wolfe, R., Visel, M., Stone, D., Libby, R.T.*, et al.* (2011). Intravitreal injection of AAV2 transduces macaque inner retina. Investigative ophthalmology & visual science *52*, 2775-2783.

Yokoi, K., Kachi, S., Zhang, H.S., Gregory, P.D., Spratt, S.K., Samulski, R.J., and Campochiaro, P.A. (2007). Ocular gene transfer with self-complementary AAV vectors. Investigative ophthalmology & visual science *48*, 3324-3328.

Zhang, T., Hu, J., Ding, W., and Wang, X. (2009a). Doxorubicin augments rAAV-2 transduction in rat neuronal cells. Neurochemistry international *55*, 521-528.

Zhang, Y., Ivanova, E., Bi, A., and Pan, Z.H. (2009b). Ectopic expression of multiple microbial rhodopsins restores ON and OFF light responses in retinas with photoreceptor degeneration. The Journal of neuroscience : the official journal of the Society for Neuroscience *29*, 9186-9196.

Zhao, L., Dai, J., and Wu, Q. (2014). Autophagy-like processes are involved in lipid droplet degradation in Auxenochlorella protothecoides during the heterotrophy-autotrophy transition. Frontiers in Plant Science *5*.

Zhong, L., Li, B., Jayandharan, G., Mah, C.S., Govindasamy, L., Agbandje-McKenna, M., Herzog, R.W., Weigel-Van Aken, K.A., Hobbs, J.A., Zolotukhin, S.*, et al.* (2008a). Tyrosine-phosphorylation of AAV2 vectors and its consequences on viral intracellular trafficking and transgene expression. Virology *381*, 194-202.

Zhong, L., Li, B., Mah, C.S., Govindasamy, L., Agbandje-McKenna, M., Cooper, M., Herzog, R.W., Zolotukhin, I., Warrington, K.H., Jr., Weigel-Van Aken, K.A.*, et al.*

(2008b). Next generation of adeno-associated virus 2 vectors: point mutations in tyrosines lead to high-efficiency transduction at lower doses. Proceedings of the National Academy of Sciences of the United States of America *105*, 7827-7832.

Zhong, L., Qing, K., Si, Y., Chen, L., Tan, M., and Srivastava, A. (2004). Heat-shock Treatment-mediated Increase in Transduction by Recombinant Adeno-associated Virus 2 Vectors Is Independent of the Cellular Heat-shock Protein 90*. J Biol Chem *279*, 12714-12723.

Zhong, L., Zhao, W., Wu, J., Li, B., Zolotukhin, S., Govindasamy, L., Agbandje-McKenna, M., and Srivastava, A. (2007). A Dual Role of EGFR Protein Tyrosine Kinase Signaling in Ubiquitination of AAV2 Capsids and Viral Second-strand DNA Synthesis. Molecular Therapy *15*, 1323-1330.

Zhong, L., Zhou, X., Li, Y., Qing, K., Xiao, X., Samulski, R.J., and Srivastava, A. (2008c). Single-polarity recombinant adeno-associated virus 2 vector-mediated transgene expression in vitro and in vivo: mechanism of transduction. Molecular therapy : the journal of the American Society of Gene Therapy *16*, 290-295.

ABSTRACT

IMPROVING AAV TRANSDUCTION EFFICIENCY IN RETINAL BIPOLAR CELLS FOR OPTOGENETIC VISION

by

SHENGJIE CUI

August 2018

Advisor: Dr. Zhuo-Hua Pan

Major: Anatomy and Cell Biology

Degree: Doctor of Philosophy

Recombinant adeno-associated virus (AAV) vectors are the most promising vehicles for therapeutic gene delivery to the retina. We are developing AAV-mediated expression of optogenetic tools in surviving inner retinal neurons as a potential strategy to restoring vision after the death of photoreceptor cells in retinal degeneration. Targeting optogeneitc tools, such as channelrhodopsin-2 (ChR2), to retinal bipolar cells (RBCs) is particularly attractive. In particular, our lab has recently developed an optimized mGluR6 promoter-based virus vector that can mainly target ChR2 to rod bipolar cells. However, AAV-mediated transduction efficiency in RBCs is relatively low. The transduction efficiency could be affected by a number of factors, including the physical barrier of the retina and proteasome degradation during intracellular trafficking. In this dissertation, I evaluated the effect of proteasome inhibitors on improving AAV-mediated transduction efficiency in retinal bipolar cells. My result indicated that doxorubicin, among other proteasome inhibitors, is effective in improving AAV transduction efficiency in retinal bipolar cells in a dose-dependent manner. I then evaluated doxorubicin-induced long-term toxicity to the mouse retinas and lenses. Dexrazoxane was co-administered with doxorubicin to prevent

its long-term toxicity. The optimal regimen for long-term use was found to be 200-300 μM doxorubicin used in combination with dexrazoxane. I also examined the effect of plasmin on improving the AAV-mediated transduction efficiency in retinal bipolar cells. My results showed that plasmin did not improve the AAV transgene expression level in retinal bipolar cells in mice. However, middle and/or low concentration of plasmin increased the number of retinal bipolar cells that express mCherry transgene in the center and middle area of the retina. The studies will help to develop useful tools in improving the AAV-mediated transgene expression, potentially optogenetic light sensor expression, in retinal bipolar cells, which may further contribute to new clinical applications.

AUTOBIOGRAPHICAL STATEMENT

SHENGJIE CUI

Education and qualification:

Ph.D., Wayne State University School of Medicine, 2012-2018, Anatomy & Cell Biology

M.D., Hebei Medical University, 2007-2012

Research experience:

Graduate research assistant

- Design and execute experiments to improve AAV-mediated gene delivery in the retina
- Contribute to research project aiming at improving the optogenetic technologies for vision restoration

Abstract:

Cui, S., et al. (2016). Evaluation of Proteasome Inhibitors on AAV-Mediated Transduction Efficiency in Retinal Bipolar Cells. Molecular Therapy 24: S42-S43.

Manuscript under review:

Cui, S., et al. (2018). Effect of proteasome inhibitors on AAV-mediated transduction efficiency in retinal bipolar cells.

Patent application:

Title of Invention: Method of Enhancing Viral-Mediated Gene Delivery

Patent application number: US20170319669

Inventor: Zhuo-Hua Pan, Shengjie Cui, Gary Abrams

University service:

2016 Wayne State University Graduate Student Research Day Committee